1-15-2016 12:00 AM

Structural and functional studies of the heptose modifying enzymes that play a role in Campylobacter jejuni virulence.

Heba Soliman Barnawi
The University of Western Ontario

Supervisor
Dr. Carole Creuzenet
The University of Western Ontario

Graduate Program in Microbiology and Immunology
A thesis submitted in partial fulfillment of the requirements for the degree in Master of Science

ABSTRACT

Campylobacter jejuni is a major cause of gastroenteritis in humans. The capsule of some species contains unique modified heptoses. Heptose modification and novel epimerases and reductases were identified for *C. jejuni* NCTC11168 and 18-176. We hypothesized that heptose modifying enzymes in *C. jejuni* have specific catalytic residues that allow for substrate and product specificity. Substrate synthesis, structural modeling, point mutations, and enzymatic analysis have been applied to map the active sites. Putative catalytic residues showed substrate and/or product specificity. The epimerases structures were solved by crystallography done by our collaborator. We also hypothesized that synthesis of the modified heptoses is important for biofilm formation. *In vitro* experiment of *C. jejuni* NCTC11168 showed that the heptose modefication biosynthesis mutants have a significant reduction in biofilm formation under aerobic conditions.

This project has provided essential information about the structure and mechanism of heptose modifying enzymes. It also will emphasize their importance in some *C. jejuni* virulence properties such as biofilm formation.

Keywords: *Campylobacter jejuni*, Modified heptose, Epimerase, Reductase, Structure, binding site, Biofilm.

CO-AUTHORSHIP

The crystallography structures' PDB files for the epimerases were generated by Laura Woodward in Dr. James Naismith laboratory (St. Andrews University, UK) and the structure view was modified using PyMol software to generate the figures represented in this thesis by us. The site-directed mutagenesis of the epimerases mutants (DdahB-N121S, MlghB-N121S, H67A, Y134F) and the reductases mutants were generated by Michael Roubakha. MlghB-Y132F mutant was created, expressed and purified by Chelsea Kubinec. She was also involved in confirming the enzymatic activity of MlghB mutants using different enzymes stocks. The GDP-*manno*-heptose substrate that was used in all enzymatic activity was kindly provided by Dr. Creuzenet. The mutant strains that were used in the biofilm assay were previously generated by Anthony Wong and Dirk Lange. The work conducted by me in this project was expressing and purifying all the wild type and the mutants' enzymes. In addition, I also performed all enzymatic analyses, kinetics, homology modeling, and the first two steps of GDP-*manno*-heptose synthesis.

ACKNOWLEDGMENT

I would like to express my deepest gratitude to my supervisor, Dr. Carole Creuzenet for giving me this great opportunity to conduct this research in her lab. Special thanks for her continued guidance, support, motivation, and patience. I would also like to thank my advisory committee members, Dr. John McCormick and Dr. Gary Shaw for their helpful advice and suggestions. I also extend my thanks to the department office staff, Fernanda Russell, Kim Arts, and Fred Williams for their help with administrative matters.

I would like to thank all members of the Dr. Creuzenet lab, past and present for every help they provided to me during my studies. Special thanks to Najwa Zebian for her invaluable assistance and her continued support and kindness. Thanks to her for being such a great motivating friend and of kind assistance.

I am also grateful to the Ministry of Higher Education of Saudi Arabia, the University of Hail, and the Saudi Cultural Bureau for their financial and academic support. Without this support, I would not be able to have this great chance to pursue this MSc studies. Finally, I would like to extend my sincere gratitude to the ones who strongly supported me from the beginning to the very last moment of this journey, my family. Thanks to my father Soliman and my mother Salma for the endless prayers and support. Thanks for enduring all the difficulties of sending me abroad to achieve my goals. To my siblings Rashad, Elham**,** and the rest of my family for keeping me motivated.

TABLE OF CONTENTS

LIST OF FIGURES

LIST OF TABLES

LIST OF ABBREVIATIONS

ATP	adenosine triphosphate
C. jejuni	*Campylobacter jejuni*
CE	capillary electrophoresis
CFU	colony forming unit
CPS	capsular polysaccharide
dTDP	deoxythymidine diphosphate
E. coli	*Escherichia coli*
Gal	galactose
GalN	galactosamine
GalNAc	N-acetyl galactosamine
GBS	Guillain-Barré syndrome
GDP	guanosine diphosphate
GFS	GDP-fucose synthetase
Glc	glucose
GST	glutathione S-transferase
GTP	guanosine triphosphate
HPLC	high performance liquid chromatography
PAD	pulsed amperometric detection
kDa	kilodalton
Kdo	2-keto-3-deoxyoctonate
LOS	lipooligosaccharide
LPS	lipopolysaccharide
Me	methyl
MeOPN	phosphoramidate
MFS	Miller Fisher syndrome

MW	molecular weight
NADPH	nicotinamide adenine dinucleotide phosphate
PBS	phosphate buffered saline
PCR	polymerases chain reaction
PDB	protein data bank
PH	potency of hydrogen
S. enterica	*Salmonella enterica*
S. suis	*Streptococcus suis*
SDR	short-chain dehydrogenases/reductases
SDS-PAGE	sodium dodecyl sulfate- polyacrylamide gel electrophoresis
WT	wild type

CHAPTER 1- INTRODUCTION

1.1. *Campylobacter jejuni:*

1.1.1. History and taxonomy:

In 1886, Theodor Escherich observed non-culturable spiral bacteria in a stool sample from a patient with diarrhea (48). Since then, the same organism has been frequently observed in bovines and ovines. Two decades after Escherich's observation, McFaydean and Stockman were able to isolate vibrio-like bacteria from aborted bovines (113). In 1919, several investigations conducted by Smith and Taylor on bovines' abortions in the USA led to the isolation of spiral bacteria. After confirming that these were the same as the vibrio-like bacteria isolated by McFaydean and Stockman, they proposed the name *Vibrio fetus* (155). In 1931, Johns *et al* isolated a dysentery related bacterium that they called *Vibrio jejuni (52)*. The first human infection was reported in 1938, from an outbreak of diarrhea caused by contaminated milk that affected 355 individuals. *V. jejuni* was observed in most of the patients fecal samples (102). *V. jejuni* was then renamed as *Campylobacter jejuni*, derived from Greek word for the curved rod, in 1963 by Sebald and Ve´ron (153).

1.1.2. General characteristics:

C. jejuni is a spirally curved gram-negative bacteria 0.5 to 8 μm long and 0.2-0.5 μm wide (101). It has rapid darting and spinning motion mediated by single polar or bipolar flagella. Biochemically, *C. jejuni* is catalase and oxidase positive, and urease negative. *C. jejuni* requires microaerobic conditions for growth, nitrogen-rich atmosphere with 5% oxygen and 10% carbon dioxide (101). As a source of energy, it utilizes amino

acids, which are considered the most important source of carbon, and tricarboxylic acid cycle intermediates (100, 127, 161). The best temperature range for growth is 34-44°C, with an optimal temperature of 42°C. Under stressful conditions, such as in cases of insufficient nutrition, temperature variation, or osmotic shock, *C. jejuni* tends to transform into coccoid form. Coccoids are a viable but not culturable form of bacterial cells that are metabolically active (132). The genome of *C. jejuni* is characterized by a circular chromosome of 1.6 megabases in size with 30.6% G+C content (135).

1.2. Epidemiology and pathogenesis:

Campylobacters have been recognized as an important cause of human enteritis. Among ten species, *C. jejuni* and *C. coli* were the cause of 95% of the enteritis cases, of which 90 % were caused by *C. jejuni*. It is a major bacterial cause of food-borne gastrointestinal infection, known as campylobacteriosis. *C. jejuni* is the third most common cause of diarrhea after *E. coli* and *rotavirus* in developing countries (5). Campylobacteriosis cases in developing countries are most common in children and immune-compromised individuals. In the developed world, *C. jejuni* infections are reported to be more frequent than *Salmonella* and *Shigella* infections combined (3). The incidence of campylobacteriosis has increased over the last ten years (81). According to the Centers for Disease Control and Prevention, 56 outbreaks of 1,550 illnesses were reported between 2009 and 2010 in the United States (65). In Canada, 49.69 campylobacteriosis cases per 100,000 population were reported in the Waterloo region, Ontario, between 1990 and 2004 (85). The highest rate of campylobacteriosis incidence

within Canada was reported in the province of British Columbia with an annual average of 38 cases per 100, 000 population during 2005 and 2009 (81).

C. jejuni is naturally found as a commensal in the lumen of poultry intestine, wild birds, and cattle. A high colonization level was found in the intestinal ceca of chickens, ranging between 10^5 to 10^9 colony forming units (CFU)/g (2, 22). Infections of humans with *C. jejuni* result from the consumption of undercooked poultry meat or cross-contamination with other food during food processing (59). The infection also can be acquired through the consumption of unpasteurized milk or contaminated water (28, 149).

1.3. Clinical characteristics:

1.3.1. Induced enteritis and immune response:

C. jejuni infection induces acute inflammatory enteritis. The onset of campylobacteriosis symptoms starts one to three days following exposure to an infectious dose as low as 360-800 CFU (24). The symptoms start with abdominal pain, headache, dizziness, fever, and severe diarrhea. The patient starts having watery diarrhea, and as the disease progresses, it becomes bloody diarrhea (172). However, the infection is self-limiting, and it resolves within seven days. The severity of symptoms varies among different age groups. Infection in early childhood is more prevalent than in late childhood due to the development of immunity (24, 171, 187).

The intestinal innate immune response plays an important role in fighting against *C. jejuni* through the production of cytokines and antimicrobial peptides (190). The humoral immune response against *C. jejuni* is important in humans (24, 25, 129). Fecal

IgA and plasma IgG *C. jejuni* specific antibodies response were reported (74, 98). The cellular immune response to *C. jejuni* is not well understood. *C. jejuni* can escape killing by human monocytes and survive intracellularly (68). An *in vitro* study showed the survival of *C. jejuni* 81-176 within vacuoles inside human 28SC monocytes (68). It also found that *C. jejuni* mediates apoptosis to the infected monocytes by activating the programmed cell death pathway (68). However in avian host cells, it was shown that *C. jejuni* cannot survive within chicken's peritoneal macrophages *in vitro* (128).

1.3.2. Immunological neuromuscular disorders:

1.3.2.1. Guillain-Barre Syndrome (GBS):

An autoimmune disease known as Guillain-Barre Syndrome is one of the long-term consequences of *C. jejuni* infection, known as acute inflammatory demyelinating polyneuropathy. GBS is the most common cause of paralysis with yearly incidence up to 1.7 per 100,000 population (6). Damage to the peripheral nerves is caused by infiltration of the immune cells and anti-gangliosides antibodies (33). It has been reported that up to 60% of GBS cases have a history of bacterial infection 30 days before the onset of symptoms (64, 125). Many bacterial and viral infections can result in disease occurrence, such as *C. jejuni*, *Mycoplasma pneumonia,* and *Epstein-Barr* virus (56, 177). *C. jejuni* infection is the most common identified cause due to molecular mimicry on the lipopolysaccharide (LOS) (188). The LOS in some *C. jejuni* contains gangliosides mimic

structures, which induce the generation of antibodies that cross-react with the host gangliosides causing the disease.

1.3.2.2. Miller Fisher syndrome (MFS):

In contrast to GBS, Miller Fisher syndrome is a rare neurological disorder. It has mild clinical symptoms characterized by weakness of eye muscles and loss of full control of body movements (50). It also can be a consequence of earlier infections, such as influenza (66). The onset of MFS is often preceded by *C. jejuni* infection. A study containing 11 MFS diagnosed patients reported that 63 % of the patients have positive *C. jejuni* cultures (150).

1.4. Virulence factors:

1.4.1. Adhesion and invasion:

In an avian host, *C. jejuni* colonizes the mucus layer and the crypts of the colon and the mucosa of the cecum. When humans are infected, the bacteria adhere to the ileum and colon to facilitate invasion. *C. jejuni* adhesion to the intestinal cells is essential for disease occurrence. Greater binding ability was observed in strains isolated from patients who experienced diarrhea and fever compared to the strains isolated from patients with no symptoms (49). *C. jejuni* expresses different adhesins, some of which have been studied extensively. An outer membrane protein, known as *Campylobacter* adherence factor (CadF), has been identified as an adhesin that binds to fibronectin on the extracellular matrix of INT-407 cells (90). According to *in vivo* and *in vitro* analysis, *C.*

jejuni lacking CadF are unable to adhere to or invade intestinal cells (122). Fibronectin binding is involved in the induction of signals that activate microfilaments polymerization for cell uptake, which suggests that CadF is also important for bacterial invasion (90). Another adhesin was identified, which is the surface lipoprotein JlpA. It is involved in *C. jejuni* adherence to HEp-2 cells (76). JlpA binding results in activation of the inflammatory response in the host (77). A periplasmic amino acid transporter, Ped1, was identified as an adhesin. *Ped1*mutants showed a decrease in adhesion and colonization to the cells (137). However, since Ped1 is localized in the periplasmic space of *C. jejuni*, the mechanism of its interaction with the host is still unknown.

Intracellular *C. jejuni* have been observed in patients' samples with diarrhea and in laboratory cell lines (41). *C. jejuni* cells need microtubule or microfilament polymerization for maximal invasion (23, 41). Internalization of *C. jejuni* is activated by the functional binding of CadF to fibronectin on the cell surface (90). Some secreted proteins required for *C. jejuni* invasion were identified, such as *Campylobacter* invasion antigen B (CiaB). The *ciaB* deficient strains are able to bind host cells, but are unable to invade them (92). Other virulence factors are found to play a role in *C. jejuni* adhesion and/or invasion to host cells including the flagella, Lipooligosaccharide (LOS), and the capsular polysaccharides (CPS) (18, 41).

1.4.2. Intracellular survival:

One of the most important *C. jejuni* virulence factors is the ability to survive in macrophages in a strain dependant manner. Different studies reported that *C. jejuni* 81-

176, M129, 2964 strains can survive in human and/or murine macrophages for several days (43, 68, 86). On the other hand, NCTC11168 strain doesn't survive beyond a few hours (184). Intracellular *C. jejuni* was found to induce proinflammatory responses in human monocytes. In addition, it was found to mediate cell arrest by the production of cytolethal distending toxin (CDT) and to induce apoptosis (68, 189). Infected human monocyte apoptosis was reported to be independent of CDT (154, 189). As reported from an in vitro experiment of M129 strain, *C. jejuni* survives in the intestinal cells and results in deterioration of the cell monolayers (91) .

C. jejuni can also survive within free-living protozoa as a protective environmental host. Many studies reported the intracellular survival of *C. jejuni* in *Acanthamoeba,* which is a genus of amoeba commonly found in soil and water (29, 152, 176). In fact, a longer survival period of C. *jejuni* was observed when *C. jejuni* cells were inside amoeba compared to being in culture media alone (15, 133). It was also found to survive at lower temperatures and to replicate inside the amoeba at 37°C (14). On the other hand, studies showed that *C. jejuni* can only survive extracellularly (30, 44). The conflict in these findings could be explained by the different experimental techniques and different *C. jejuni* and *Acanthamoeba* strains used in different studies (176).

1.4.3. Biofilm formation:

C. jejuni cells can exist in biofilms to protect themselves and survive under unfavorable conditions. Biofilm formation protects the bacteria when they are out of the host, which allow their transition into another host or into food products during food

processing. The ability of *C. jejuni* to survive in the environment increases the chance of chicken colonization and food contamination, and thus human infection through consumption of this contaminated food. *C. jejuni* biofilms are found in water distribution systems and surfaces submerged in an aquatic environment (73). *C. jejuni* populations can exist in nature in different forms. They exist in biofilms, which are surface adherent bacterial populations enclosed by a matrix, known as extracellular polymeric substance (EPS) (38). The matrix composition is highly variable depending on the microbial species but it usually contains extracellular DNA, proteins, and polysaccharides (27). *C. jejuni* populations also can form aggregates that are not attached to a surface or pellicles at an air-liquid interface (80). Studies showed that *C. jejuni* can form a single species or mixed culture biofilms in the environment (73). Many factors can affect *C. jejuni* biofilm formation including a functional flagella, temperature, nutrition, or oxygen concentration (80, 145, 146). Strains with flagellar structure gene mutations showed a decrease in biofilm formation and inability to attach to surfaces (145). Other studies showed that aerobic conditions activate *C. jejuni* biofilm formation (146). Biofilm formation was proposed as a virulence factor because it provides protection for the bacterial cells from environmental stressors and from antibacterial agents (38).

1.4.4. Flagella and motility:

The polar flagella of *C. jejuni* have a critical role, not only in motility, but also in secretion, invasion, colonization, and biofilm formation (93, 107, 145). Motility is required for the bacteria to initiate infection in the host by penetrating the mucus layer in

the intestine (94). *In vivo* and *in vitro* experiments showed that non-flagellated *C. jejuni* are not motile and unable to invade cells (179). Equally important, the *C. jejuni* flagellar apparatus acts as a secretion system for virulence proteins, such as Cia proteins that are important for adhesion (93).

More than 40 genes participate in the formation and regulation of the flagellar structure, which consists of a basal body, hook, and a hollow cylindrical filament. The building units of the flagella are two structural proteins FlaA and FlaB. Both are regulated by FlgS/FlgR, a two component system, and sigma factors (σ28, σ54) (67, 105, 185). Transposon mutagenesis experiment found that σ28 and σ54 regulate the production of FlaA and FlaB respectively. Based on *in vitro* study of *flaA-flaB*+ mutants, expression of FlaA was found to be more significant for motility and invasion of intestinal cells than FlaB (61). *C. jejuni* flagellin is heavily glycosylated. This glycosylation is known to occour through an O-linked glycosylation system. O-linked glycosylation is important for flagellar filament assembly and motility (62).

1.4.5. Glycosylation:

Protein glycosylation is an essential biological process in all life domains where a particular protein is modified by the addition of sugar structures. Glycosylated proteins are essential for multiple cellular functions (121). Bacterial protein glycosylation was discovered in many organisms after it was thought to exist only in eukaryotes (169). Many prokaryotes have been found to modify proteins by adding sugars either through the hydroxyl groups of serine and threonine residues (O-linked), or the amide group of an

asparagine residue (N- linked) (121). O-linked glycosylation was observed in the pilin subunit of *Neisseria meningitides*, the surface layer proteins of *Colstridium symiosum* and *Streptococcus sanguis* as well as in the flagellin of *Pseudomonas aeruginosa* (26, 119, 120) *C. jejuni* encodes two glycosylation loci for both glycosylation types, which makes it an effective model to study bacterial protein glycosylation by constructing knockout mutants (166). The O-linked glycosylation locus is extremely variable among different strains of *Campylobacter* species. *C. jejuni* flagellin proteins are of the most heavily O-glycosylated bacterial proteins. O-linked glycosylation plays an essential role in the flagellin assembly and thus the motility of *C. jejuni* cells (62). The location of the O-linked glycans as exposed moieties on the flagellin indicates a significant potential for interaction with the host cells. Studies showed that O-linked glycosylation is important for adhesion, and invasion of the host cells (62). Unlike the O-linked glycosylation loci, N-linked glycosylation loci is highly conserved among *C. jejuni* strains and has no putative phase-variable genes (168). Disruption of the N-linked glycosylation pathway in *C. jejuni* significantly reduces adhesion, invasion and colonization of chickens (78, 165).

1.4.6. Lipooligosaccharide (LOS):

The lipooligosaccharide (LOS) and lipopolysaccharide (LPS) are important virulence factors found in the outer membrane of mucosal gram-negative bacteria (140). LPS are high molecular weight (High M_r) glyco-lipids composed of oligosaccharide core attached to lipid A, in addition to surface-exposed repeating units of polysaccharide, O-antigen. On the other hand, LOS are low molecular weight (low M_r) with the same main

structure of LPS, except that it lacks the O-antigen. Two decades ago, *C. jejuni* was considered to contain both LPS and LOS (141). The discovery of the capsular gene cluster proved that *C. jejuni*'s high molecular weight polysaccharide is in fact capsule (84, 135). *C. jejuni* LOS structure has been extensively studied. Lipid A, the hydrophobic membrane anchor, has a conserved structure among Gram-ngative bacteria. It consists of two phosphorylated D-glucosamines in (1-6) linkage and attached acyl chains (104, 126, 142). The oligosaccharide chain has been divided into inner and outer core, based on the different sugar composition. The inner core structure is conserved among various strains, containing a backbone of 2-keto-3-deoxyoctulosonic acid (Kdo), two L-*glycero*-D-*manno*-heptoses (L, D-Hep), D-galactose (D-Gal), and terminal D-glucose (D-Glc) (123, 160). The outer core is structurally diverse among *C. jejuni* strains. To date, the structure of more than ten *C. jejuni* serostrains LOS outer core have been identified (10-12, 58, 160, 167). LOS is an important structure for bacterial transition across the intestinal epithelial cells, and for immune evasion (106, 109). A remarkable feature in the *C. jejuni* LOS is that it possesses structures that mimic humans' peripheral nerves gangliosides. This mimicry contributes to autoimmune neurological disorders upon infection, such as GBS and MFS (57, 58, 72, 124, 125).

1.4.7. Capsule polysaccharide (CPS):

Like many other Gram-negative bacteria, *C. jejuni* possesses capsular polysaccharide surface structure. The capsular polysaccharide (CPS) is made of high molecular weight polysaccharides, organized in repeated units of carbohydrates called K-

antigen. This K-antigen is attached to the outer membrane by a phospholipid anchor. CPS structures are extremely diverse, not only between different species but also between different strains within the same species (82). The highly diverse structure makes them a major component of the classical Penner serotyping system (84). The variation is attributed to different genetic components and extensive phase variable modifications in favor of evading the host immune response (148).

C. jejuni CPS acquire unique modifications as different strains express heptoses of unusual configuration such as, D-*altro*-, L-*gluco*-, *ido*- heptoses (9, 111, 160). Further heptoses modifications can be acquired in *C. jejuni* CPS by C6 dehydration to generate 6-deoxy-heptose found in 81-176 strain (110). In addition, an *O*-methyl phosphoramidate group (MeOPN), which is a rare labile phosphorylated structure, is found attached to the modified heptose and to different sugar components in multiple strains (114-116).

The K-antigen backbone structures of different *C. jejuni* strains have been identified. *C. jejuni* 81-176 contains repeated units of β-D-N-acetylglucosamine (β-D-GlcNAc), α-D-galactose (α-D-Gal), and the modified heptose 6-deoxy-D-*altro*-heptose. On the other hand, *C. jejuni* NCTC 11168 CPS backbone contains repeated units of β-D-Ribofuranose (D-Rib*f*), β-D-2-acetamido-2-deoxy-β-D-galactofuranose (β-D-Gal*f*NAc), -D-glucuronic acid (α-D-Glc*p*A) with 2-amino-2-deoxyglycerol (GroN), and a modified heptose 3,6-OMe-L-*gluco*-heptose (9, 160).

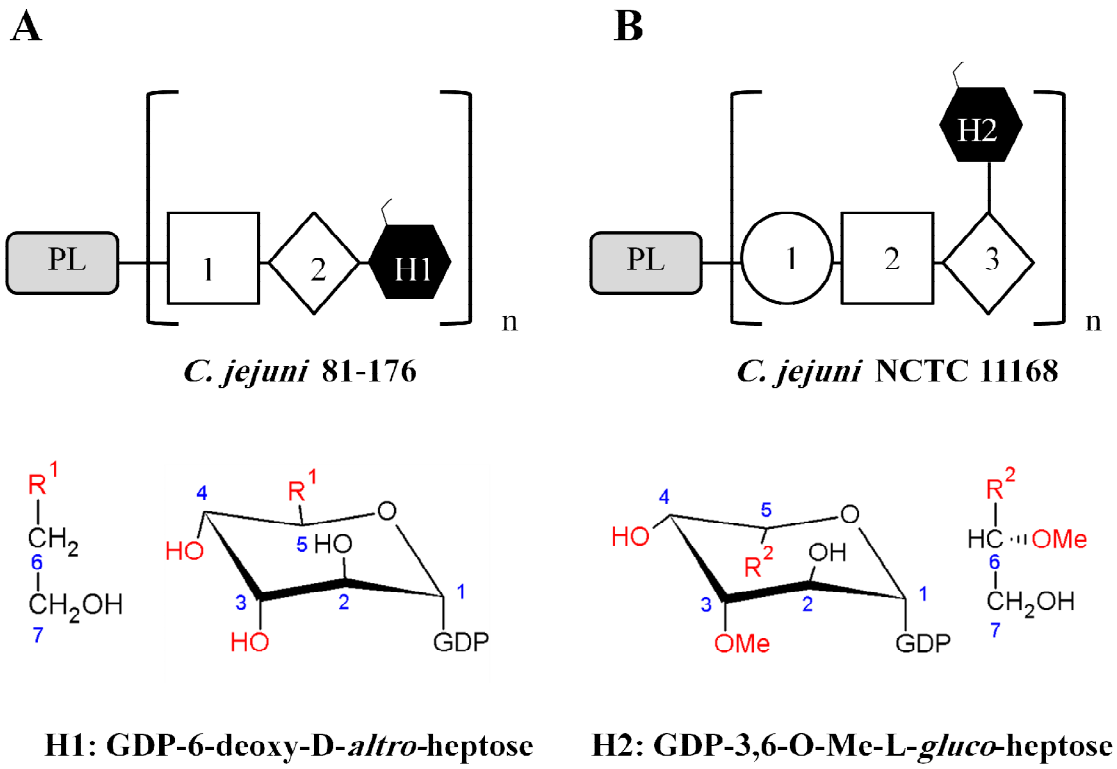

H1: GDP-6-deoxy-D-*altro*-heptose **H2: GDP-3,6-O-Me-L-*gluco*-heptose**

Figure 1: Schematic representation comparing the CPS structure and the modified heptoses of *C. jejuni* 81-176 and NCTC 11168. A. the CPS of *C. jejuni* 81-176 contains phospholipid anchor (PL) and attached repeated units of D-GlcNAc (1), D-Gal (2), and the modified heptose 6-deoxy-D-altro-heptose (H1), represented in chemical structure underneath. B. the CPS of *C. jejuni* NCTC 11168 contains repeated units of D-Rib*f* (1), D-Gal*f*NAc (2), D-GlcpA (3), and a side branch of modified heptose 3,6-O-Me-L-gluco-heptose (H2), represented in chemical structure underneath.

1.4.7.1. CPS genetics:

CPS has been recently classified in *E. coli* into four groups based on genetic and synthetic properties (181). *C. jejuni* CPS resemble both group II and III enterobacterial capsules. Both groups corresponding gene clusters are characterized by two conserved regions containing genes involved in assembly and transport (region 1, 3), flanking a major biosynthetic region (region 2) (Figure 2). Region 2 is the strain-specific region that includes genes encoding the various sugar nucleotide synthetases for the K-antigen (148). In group III CPS, four conserved genes belong to region 1, *kpsE*, *kpsT*, *kpsM*, and *kpsD*. While in *C. jejuni* there is a fifth gene, *kpsF*, which could have a regulatory role in the export of the capsule chain (35, 36). KpsE and KpsD play a role in the translocation of the polysaccharide chain across the periplasmic space to the outer membrane (8). While KpsM and KpsT are ABC-transporters involved in transporting the polysaccharide across the inner membrane to the periplasmic area (131, 139). Region 3 contains two genes, *kpsS* and *kpsC* (84). Homologues *kpsS* and *kpsC* genes in group II CPS in *E. coli* are involved in attaching the Kdo, which is synthesized by KpsU, to the phosphatidic acid and subsequently to the polysaccharide's reducing end (183). However, the lack of *kpsU* in *C. jejuni* suggests that the K-antigen is not linked to the phospholipid via Kdo. Therefore, *kpsS* and *kpsC* could be encoding proteins that are involved in attaching the polysaccharide into the phospholipid anchor.

In *C. jejuni* NCTC 11168, the capsular genes cluster was identified in 2000 by a complete genome sequencing (83, 84). After this discovery, several studies were dedicated to investigate the function of the genes in CPS biosynthesis and structural

diversity. The biosynthetic region (region 2) of six *C. jejuni* strains was studied and compared to the sequenced strain NCTC 11168 (82). The study revealed that the structural diversity is related to variation in region 2 of the capsular cluster. Despite the variations, several genes involved in particular sugar synthesis or modifications were conserved between several strains, including the heptose synthesis genes, *cjj1423c* (*hddC), cjj1424c (gmhA2),* and *cjj1425c* (hddA). Genes involved in heptose modifications were identified in *C. jejuni* 81-176, cjj1425 (*wcaG*), *cjj1426* (*ddahA*), *cjj1427* (*ddahC*), and *cjj1430* (*ddahB*), as well as in NCTC 11168 strain *cj1426, cj1427* (*wcaG*), *cj1428* (*mlghC*), and *cj1430* (*mlghB*) (82, 111). MeOPN synthesis genes (*cj1415c* - *cj1418c*), and two genes (*cj1421c* and *cj1422c*) encode transferases for the addition of MeOPN to D-Gal*f*NAc and D-α-L-*gluco*Hep*p,* respectively. In addition, *cj1426c* (*mlghD*) is reported to methylate the 3,6-O-Me-L-*gluco*-heptose at O6, while *cj1419c* could be responsible for the methylation at O3 (Creuzenet lab, unpublished) (111, 164) (Figure 3).

1.4.7.2. CPS synthesis:

The synthesis of the capsule has been extensively studied in *E. coli* for the three groups. Since *C. jejuni* capsule resembles group II and III, the synthesis mechanism of these groups only will be explained in this section (Figure 2). CPS synthesis starts in the cytoplasm where the phosphosugar nucleotide precursors are polymerized prior to being exported to the periplasmic space. There, specific surface translocation reactions take place to export CPS to the cell surface (162).

While the initiation mechanism of the polysaccharide synthesis remain unknown, the synthesis process has been shown to take place on the cytoplasmic face of the plasma membrane (181). A membrane-bound complex, consisting of glycosyltransferases (KfiA-D) and Kps proteins, is believed to be the origin of the synthesis process (147). The elongation of the polysaccharide chain is carried out by the glycosyltransferases at the non-reducing end in a sequential pattern. The growing polysaccharide chain is then transported across the inner membrane to the periplasmic space. The Kdo attachment to the reducing end of the polysaccharide in group II CPS is believed to occur before the export step. This fact was concluded from the accumulation of the polysaccharides lacking Kdo in the cytoplasm due to mutations in KpsC and KpsS (148). However in group III and *C. jejuni* CPS where there is no Kdo, it is believed that KpsC and KpsS are involved in attaching the polysaccharide chain to the phospholipid (84). The translocation of the capsule to the cell surface occurs through periplasmic scaffolds. These scaffolds are areas where the cell plasma membrane and the outer membrane are in proximity forming structures called Bayer junctions (182). The ABC transporter, KpsM and KpsT, form a functional transporter dimer that binds directly to the polysaccharide and exports it through an export channel. KpsD, which is a transporter protein in the periplasmic space, could be involved in joining the membranes closely to facilitate the export to the outer membrane (8).

The regulation of CPS expression in *C. jejuni* is not fully understood. There is no experimental evidence of transcriptional regulatory patterns in CPS gene cluster. However, some findings suggest that some genes are regulated differently depending on

the growth conditions. High iron growth conditions are found to up-regulate the expression of four genes in region 2 in *C. jejuni* NCTC 11168 (134). Furthermore, down-regulation of three biosynthesis genes and four transport genes was reported after serial passage of *C. jejuni* NCTC 11168 or 81-176 with HCT-8 human intestinal cells (37).

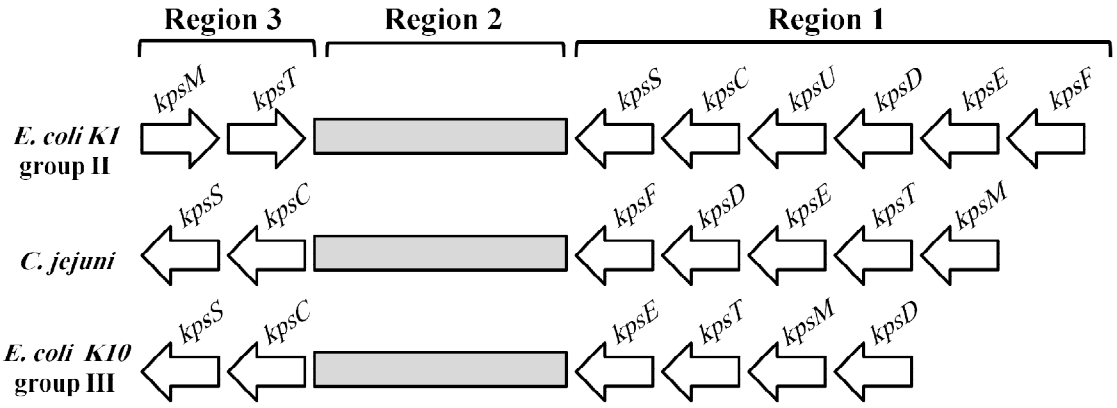

Figure 2: Schematic representation of CPS cluster regions. *E. coli* group II and III CPS regions compared to *C. jejuni* NCTC 11168 CPS cluster.

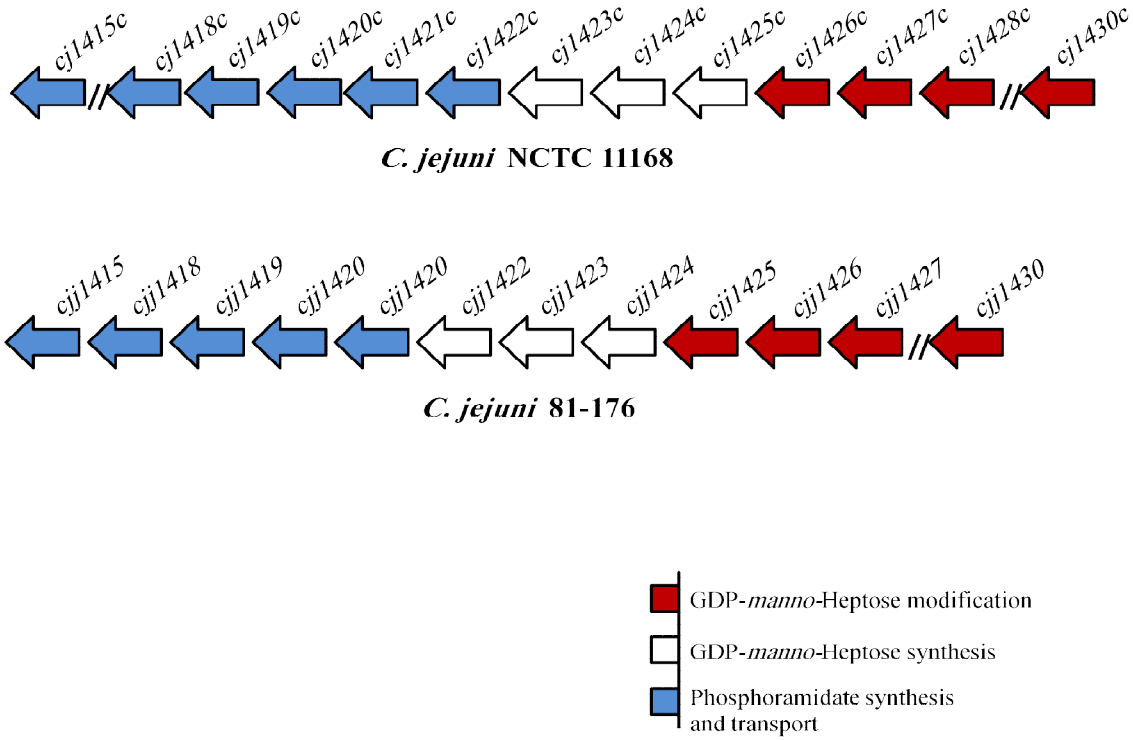

Figure 3: Schematic representation of region 2 of both *C. jejuni* NCTC 11168 and 81-176 strains. The genes involved in GDP-*manno*-heptose synthesis and modification, as well as the phosphoramidate synthesis and transfer genes.

1.4.7.3. Biological role in virulence:

CPSs are an essential part of the bacterial cell as they are involved in many different functions. They provide protection from environmental conditions and host defenses. Most importantly, they play an important role in bacterial pathogenesis and virulence (170). The involvement of the capsule in *C. jejuni* virulence is strain dependant.

Multiple studies conducted on different strains of a capsule less mutant (KpsM) revealed different results. In *C. jejuni* 81-176 strain, the KpsM mutant showed inability to colonize or to invade cells. In a ferret model, as well as in intestinal cells, the KpsM mutant of *C. jejuni* 81-176 strain exhibits decreased invasion levels (18, 109). However in NCTC 11186 strain, although the KpsM mutants showed a significant reduction in the colonization of chicken intestine, it was more adhesive and invasive to the epithelial cells *in vitro* than the wild type (78, 184).

CPS also protects *C. jejuni* from the innate immune system mediators, such as serum complements, and cationic antimicrobial peptides (109). Indeed, KpsM mutant in NCTC 11186 strain showed high susceptibility to serum, bile salt and phagocytosis (184). It is also believed that the extensive structural variation of CPS within *C. jejuni* strains protects the bacteria from bacteriophages and helps in evading the host immune response (71, 84). However, the complete mechanisms of these phase variable modifications in virulence still unknown.

1.5. GDP-*manno*-heptose synthesis:

Heptose sugar is a natural component of the LOS and LPS of most Gram-negative bacteria. They are producing ADP-L-*glycero*-D-*manno*-heptose as a component of the core oligosaccharide by a single synthesis pathway (88, 95, 175). Interestingly, some strains of *C. jejuni* possess additional heptose biosynthesis pathway to produce GDP-D-*glycero*-α-D-*manno*-heptose (GDP-*manno*-heptose). An identical pathway was identified in *Aneurinibacillus thermoaerophilus* and the enzymes have been used for an *in vitro* synthesis of GDP-*manno*-heptose for biochemical analyses (31, 87) (Figure 4). The genes involved in the synthesis of GDP-*manno*-heptose in *C. jejuni* are encoded in region 2 of the capsular cluster (Figure 3). The synthesis pathway starts by the conversion of D-sedoheptulose-7-phosphate (sedoheptulose-7P) into D-*glycero*-α-D-*manno*-heptose-7-phosphate (heptose-7P) by the phosphosugar isomerases GmhA. The kinase HddA then adds a phosphate group to generate D-*glycero*-α-D-*manno*-heptose-1,7-biphosphate (heptose-1,7P). One phosphate is removed by GmhB giving D-*glycero*-α-D-*manno*-heptose-1-phosphate. Lastly, HddC acts to add a guanine nucleotide from a Guanine triphosphate molecule (GTP) to generate the activated end product GDP-D-*glycero*-α-D-*manno*-heptose (82, 175). In some *C. jejuni* strains, this heptose is further modified before integration into the CPS.

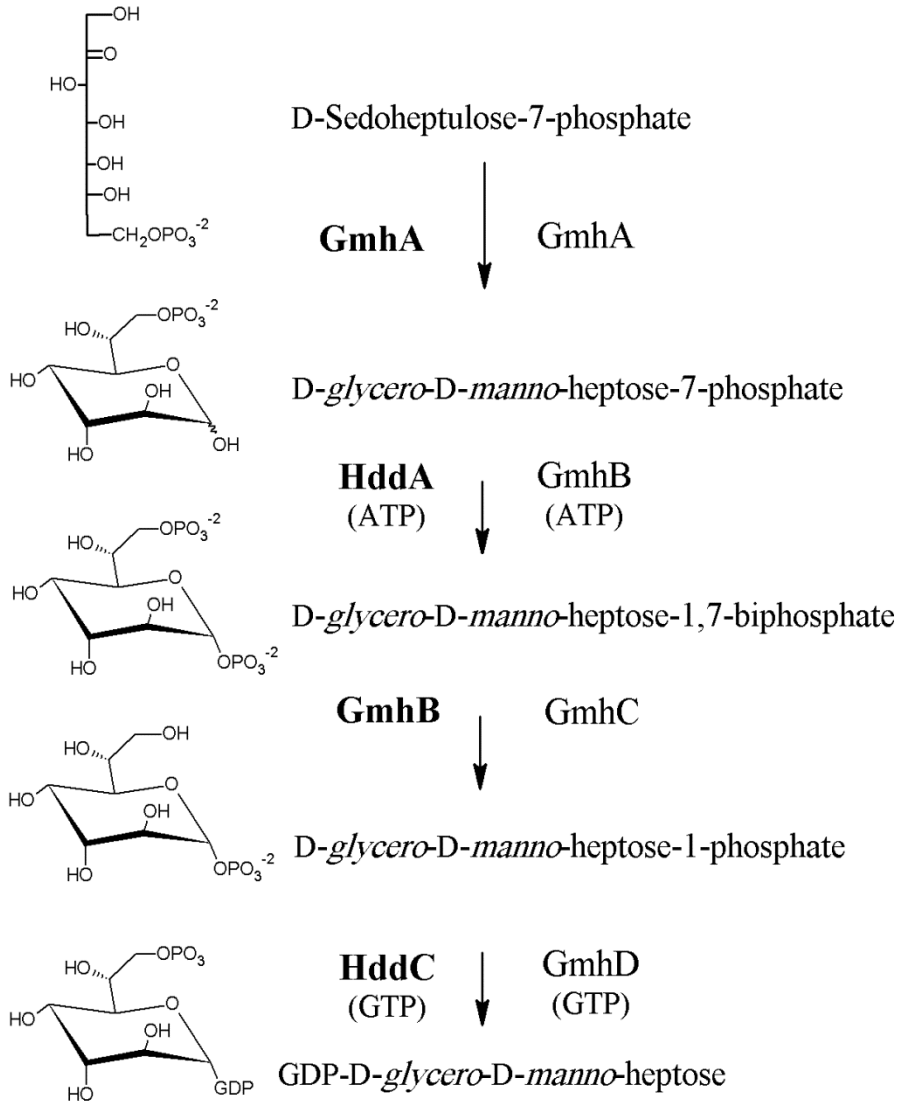

Figure 4: Synthesis of GDP-D-*glycero*-D-*manno*-heptose. The biosynthesis enzymes of GDP-D-*glycero*-D-*manno*-heptose in *C. jejuni* are in bold to the left of the reaction arrows, and the synthesis enzymes in *Aneurinibacillus thermoaerophilus* are to the right side of the arrows.

1.6. *C. jejuni* GDP-*manno*-heptose modification:

Unique configurations of heptose are expressed in the CPS of different pathogenic bacteria, in *C. coli,* and in *Burkholderia pseudomallei* (9, 10, 144, 160). They are also found in molecules other than the CPS such as in the exopolysaccharide of *C. lari* and the lipopolysaccharide of *Yersinia pseudotuberculosis* (13, 151). These modified heptoses are important for bacterial virulence and could be involved in bacteria-host interaction.

In *C. jejuni* 81-176 and NCTC 11168 strains, two modified heptoses were identified, 6-deoxy-D-*altro*-heptose and 3,6-OMe-L-*gluco*-heptose, respectively (9, 160). The genes involved in the synthesis of the modified heptoses, as well as their synthesis pathways, have been characterized (110-112).

1.6.1. The modified heptose role in virulence:

Complex carbohydrates are usually found on the bacterial cell surface and they are involved in virulence or immune evasion. They are essential components of the CPS and LOS in pathogenic bacteria. Enzymes involved in the biosynthesis and modification of these sugars have gained much attention as antibacterial targets due to their involvement in virulence. For example, a well-studied C3/C5 epimerase (RmlC) and other homologous enzymes, in *E. coli*, *Pseudomonas aeruginosa*, *Streptococcus mutants*, and *Mycobacterium tuberculosis,* are involved in the dTDP-L-rhamnose synthesis pathway (143, 163). Deletion of one of the genes involved in this pathway resulted in a significant decrease in virulence (143, 173). Likewise, a C3/C5 Epimerase/C4 reductase (GFS) is involved in the GDP-L-fucose synthesis pathway. L-fucose is essential for

virulence and host mimicry of some pathogenic bacteria, such as *E. coli* and *H. pylori* (124, 157).

All these examples are for hexose derivatives made by hexose-modifying enzymes. The enzymes that are involved in the synthesis of heptose derivatives are also found to play a key role in the virulence of many pathogens, such as *Yersinia pseudotuberculosis*, *E. coli*, and *C. jejuni* (70, 175, 184). In *Y. pseudotuberculosis,* disrupting the synthesis of these modified heptoses has been shown to decrease virulence. Mutants lacking the 6-deoxyheptose in the LPS are less motile and more sensitive to antimicrobial peptides (70). Recently, the involvement of the modified heptoses in the virulence of *C. jejuni* NCTC 11168 has been elucidated *in vitro* by testing four heptose biosynthesis mutants, *wcaG::cat, mlghB::cat, mlghC::cat,* and *wcaGΔ::cat* (Figure 5) (184). In the serum and bile salt killing assay, all mutants were more susceptible to killing than the wild type, with different survival ratio for each. In the epithelial cells adhesion and invasion assay, *mlghB::cat* and *mlghC::cat* were not invasive to epithelial cells (130, 184). In addition, all mutants showed less colonization in the chicken intestine compared to the wild-type with variation between the mutants (184). All these data indicate the role that the modified heptoses have with respect to bacterial colonization, invasion of host cells, and response to host defense.

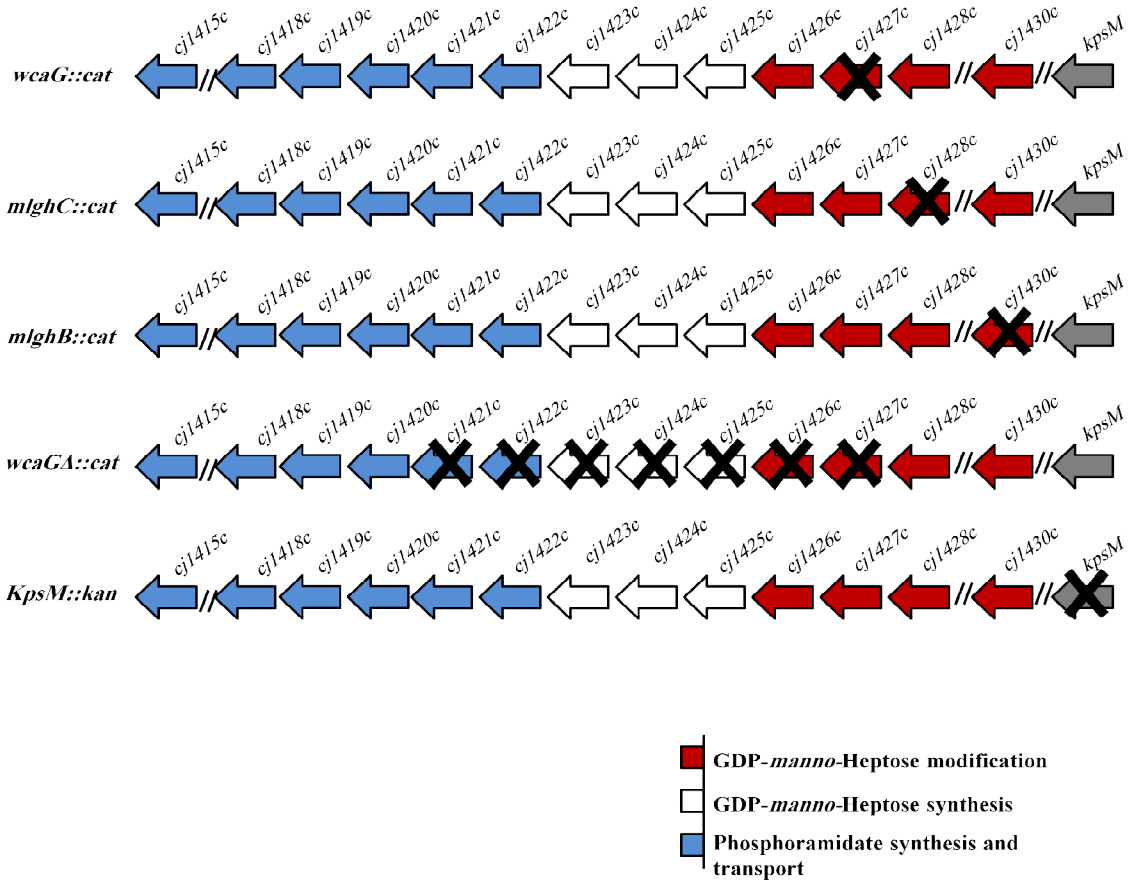

Figure 5: Schematic representation of region 2 of *C. jejuni* NCTC 11168 heptose biosynthesis mutants and the capsule-less mutant. From top to bottom, showing the deletion positions in each of *wcaG::cat, mlghC::cat, mlghB::cat, wcaGΔ::cat,* and *kpsM::kan* strains **(184)**.

1.6.2. The modified heptose synthesis enzymes:

Several nucleotides modifying enzymes are encoded in region 2 of *C. jejuni* 81-176 and NCTC 11168 CPS cluster. The 6-deoxy-D-*altro*-heptose synthesis enzymes in *C. jejuni* 81-176 are DdahA, DdahB, and DdahC, a C4/C6-dehydratase, C3-epimerase, and a C4 reductase, respectively. A post-transcriptional regulatory enzyme, WcaG, is a C4 reductase. On the other hand, the enzymes involved in the 3,6-OMe-L-*gluco*-heptose synthesis in *C. jejuni* NCTC 11168 strain are MlghB and MlghC, encode a C3/C5 epimerase and C4 reductase, respectively. A homologue to WcaG has also been identified (110-112). In addition, two methyltransferases were identified. The O6 methyltransferase is Cj1426, and it was renamed MlghD following the alphabetical order of the synthesis enzymes in the pathway. Preliminary data from Creuzenet lab showed the O3 methyltransferase could be Cj1419, renamed as MlghE (unpublished).

1.6.3. The modified heptose synthesis pathways:

The homologous epimerases, DdahB and MlghB, are 81% identical and 98% similar in their protein sequence. While the homologous reductases, DdahC and MlghC, are 57% identical and 90% similar. Despite this similarity, these enzymes perform a strain-specific activity to generate strain-specific modified heptoses.

The synthesis pathway for GDP-6-deoxy-D-*altro*-heptose in *C. jejuni* 81-176 was first established in our laboratory by the characterization of the first enzyme in the pathway, DdahA, and the regulatory enzyme WcaG (110, 112). DdahA performs sequential dehydration activity on C6 and C4 of the substrate GDP-*manno*-heptose to

generate GDP-6-deoxy-4-keto-D-*lyxo*-heptose (P1). This product can be either reduced at C4 by WcaG, with the co-factor NADPH, in a side-branch pathway to down-regulate the end product formation, or epimerized in a linear pathway to produce the final product. In the linear pathway, DdahB epimerizes P1 on C3 to produce GDP-6-deoxy-4-keto-D-*arabino*-heptose. This product is then reduced at C4 by DdahC, with the co-factor NADPH, to yield the final product GDP-6-deoxy-D-*altro*-heptose (Figure 6-A).

In NCTC 11168 strain, the 4-keto derivative of the GDP-*manno*-heptose is predicted to be generated by C4 oxidation activity. This oxidation is necessary to generate the substrate for the epimerase MlghB. However, no gene coding C4-oxidases was identified in the heptose modifying genes area or anywhere in the genome. *In vivo*, MlghB generates GDP-4-keto-L-*xylo*-heptose from the oxidized substrate. This product is reduced at C4 by MlghC to give the final modified heptose GDP-L-*gluco*-heptose that is O-methylated at O6 and O3 by MlghD and MlghE, respectively (Figure 6-B). However, the location of the methylation events in the pathway is still under investigation.

Because the potential GDP-*manno*-heptose oxidase has not been identified, MlghB's substrate is not available for biochemical studies. The GDP-6-deoxy-4-keto-D-*lyxo*-heptose (P1) generated by DdahA was used as a surrogate substrate for MlghB in an experimental pathway (Figure 7). MlghB performs C3, C5, or both epimerizing activity on P1 to generate three products in equilibrium, GDP-6-deoxy-4-keto-L-*arabino*-heptose (P4α), GDP-6-deoxy-4-keto-L-*ribo*-heptose (P4β), and GDP-6-deoxy-4-keto-L-*xylo*-heptose (P4γ). An interconversion between P1 and the three epimerized products was observed. Finally, P4γ is reduced by MlghC at C4 to produce the final modified heptose

GDP-6-deoxy- L-*gluco*-heptose (P5γ). The C3 epimerized product (P4α) generated by MlghB from the surrogate substrate was identical to the DdahB product. This observation was supported by the fact that the DdahC can also use P4α obtained by MlghB to generate GDP-6-deoxy-D-*altro*-heptose (P5α).

The existence of strain-specific features of these enzymes suggests the importance of understanding the molecular structure and the mechanism of performing such specific activity. No structure for these enzymes or for homologous GDP-*manno*-heptose modifying enzymes was available at the onset of our studies.

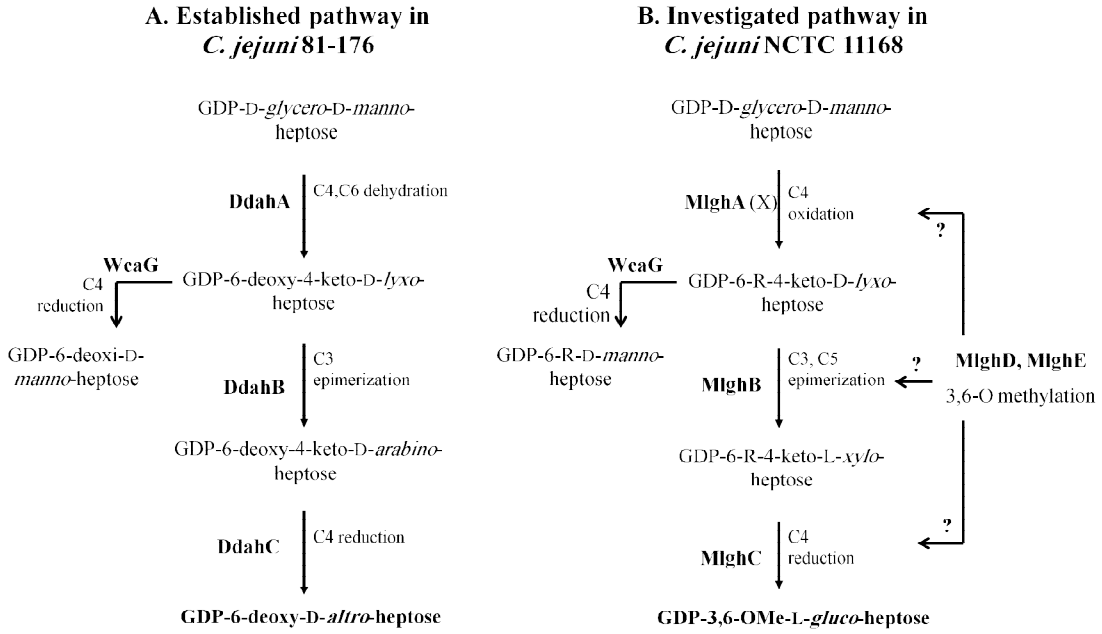

Figure 6: Comparative GDP-6-deoxy-D-*altro*-heptose and GDP-3,6-O-Me-L-*gluco*-heptose in vivo synthesis pathways of *C. jejuni*. A. The established synthesis pathway of GDP-6-deoxy-D-*altro*-heptose in 81-176 strain. B. The investigated synthesis pathway of GDP-3,6-O-Me-L-*gluco*-heptose in NCTC 11168 strain. MlghA is an oxidase (unknown). MlghD and MlghE are the methyl transferase that introduces methyl group to O6 and O3, respectively in yet unidentified locations along the pathway. Possible methylation sites are denoted by a question mark. Reproduced figure from (McCallum, 2013) **(111)**.

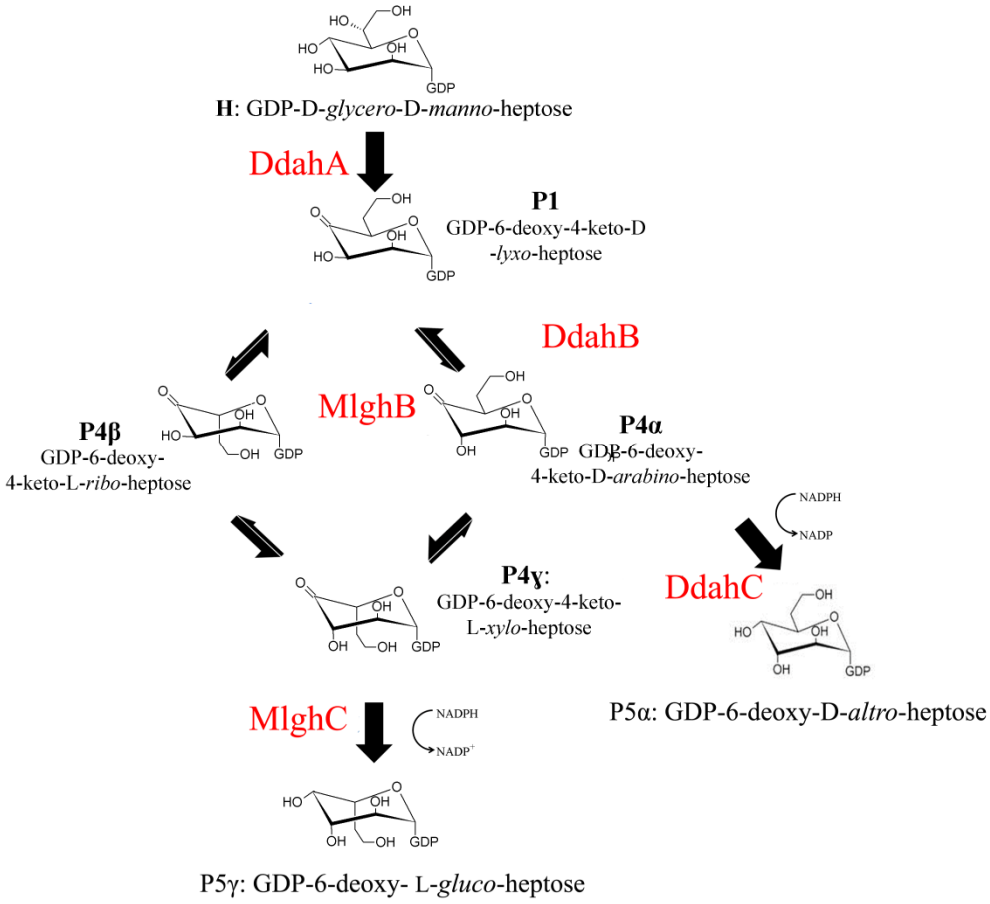

Figure 7: Experimental pathway for GDP-6-deoxy-D-*altro*-heptose and GDP-6-deoxy- L-*gluco*-heptose synthesis in vitro. MlghB generates P4α, P4β and P4γ from the surrogate substrate P1 that is formed by dehydration of GDP-*manno*-heptose by DdahA. MlghC reduces P4γ to form the final product GDP-6-deoxy- L-*gluco*-heptose. While DdahC reduces P4α to give for GDP-6-deoxy-D-*altro*-heptose. Reproduced figure from (McCallum, 2013) (111).

1.7. Enzymes structure:

To study the configuration of an enzyme binding site, it is crucial to solve the three-dimensional structure. The 3D structure will provide essential biological and biochemical data that cannot be provided by a linear amino acid sequence. The tertiary structure can be obtained by a well-established experimental methods such as X-ray crystallography and nuclear magnetic resonance (NMR) (97). There are also computational methods dedicated to determine the structure *in silico*, known as protein structure modeling.

1.7.1. Homology modeling:

Homology modeling, also known as template-based modeling (TBM), refers to the prediction of the 3D structure of a protein based on its homology with a protein of experimentally determined structure (186). Four decades have been spent on establishing and developing ways to solve proteins structures by computational scientists (108). Homology modeling is an important and feasible method to solve the structure of proteins that cannot be solved experimentally due to the limitations and the difficulties of the experimental approaches (1, 108, 186).

There are four main steps for homology modeling (96, 186). The primary sequence of the protein is needed first to identify homologous proteins through the protein data bank (PDB). Second, the sequence is aligned to the template sequence using one of the different reliable alignment softwares. Sequence alignment is the most important step in homology modeling, and any error in this step is irreversible (186).

Based on the alignment between the protein and the template, the model building can be achieved by the generation of the backbone and modeling the structural loops and side-chains (96). Then comes to the last step, which is the model refinement and optimization. In this step, the side-chains are tuned by predicting the side-chain rotamers with high accuracy based on different parameters (96, 186)

There are many software that are widely used for model building available for public, such as NEST, COMPOSER, SWISS-MODEL, and MODELLER (186). SWISS-MODEL is a web-based workspace that uses a structure template database derived from the Protein Data Bank (7). The closest homology of the template to the target is identified using BLAST query. The templates with the highest quality are selected for model building (7). Model quality estimation is done using the Qualitative Model Energy Analysis (QMEAN) scoring system. It is a scoring system that describes the major geometrical conditions of protein structures (20).

1.7.2. X-ray crystallography:

X-ray crystallography is one of the most advanced techniques to investigate the molecular structure of a protein. X-rays are high-energy electromagnetic waves with a very short wavelength. Crystallographers use x-rays that range from 0.5 to 1.5 angstrom as rulers to measure the distance between atoms in a crystal (156). In crystalline solids, the interatomic spacing is used as a diffraction gradient for x-rays with a wavelength of approximately one angstrom.

There are three main steps for protein crystallography analysis (117). Taking into account the fact that each step has its limitation, the whole technique can be time consuming and may not be successful with all proteins (1, 42). The first step is protein crystallization. The principle of crystallization is to obtain the protein in a solid form out of the solution in a fixed biological conformation. The protein crystals are grown by precipitation and condensation (156). The second step is firing a beam of x-rays at the tiny crystal of the studied protein. The crystal scatters the x-ray into specific diffraction patterns that are photographed by an electronic detector. Different orientations of the crystal are needed to capture in three dimensions different diffraction patterns of the x-ray. These patterns are used to mathematically solve the precise position and arrangement of atoms in the crystal using Bragg's law (75). The last step is data processing and analysis (159). Although it is a mathematically complex procedure, there are well-established softwares to process the data (136, 159, 174). After several stages of analysis and troubleshooting, comes the refinement to produce a three-dimensional digital image of the protein.

1.8. Enzymes active site:

Enzymes are one of the most studied biological molecules because they catalyze numerous reactions in nature. The functional portion contains a combination of residues side chains that form the catalytic unit (191). This unit is also known as the catalytic toolkit. In this catalytic toolkit, the polar and charged amino acids are generally involved directly in catalysis (63). Hydrophobic residues are also observed in the active site of the

enzymes. Although the hydrophobic residues are not involved directly utilizing reactions, they do have an important roles in some enzymes, such as providing a proper medium environment in the active site (63). Catalytic residues are defined by Zvelebil. et. al as the amino acids that are directly involved in the catalysis by acting as general acid-base, electrophiles, or nucleophiles (191). They also can be involved in polarizing or stabilizing transition state intermediates. Bartlett. et. al added that residues that have an effect on other residues or water molecules that are directly involved in catalysis should also be classified as catalytic (19). Other group proposed that catalytic residues cloud have a secondary interaction with other residues, which were classified as non-catalytic, to aid the catalysis (63). This means that catalytic residues do not function independently. The microenvironment provided by other residues in the active site is important for the catalytic residues to function.

One of the catalytic residues that are most often found in enzymes active sites is histidine. Histidine has a p*K*α close to neutral, which allows it to function as an acid-base catalyst. It can also donate or accept hydrogen atom, stabilizes charged transition states, and function as a nucleophile. Glutamate, aspartate, arginine and lysine are also commonly found in active sites. These residues can provide charges that exert an effect on other residues or on the substrate. Serine, threonine, tyrosine, glutamine and asparagine are found less often. These residues need to be activated by interacting with other residues to function.

1.9. Rational and hypothesis:

The existence of modified bacterial surface carbohydrates and their involvement in bacterial virulence urge to further investigate their contribution to the pathogenesis in details. The identification of these modified carbohydrate synthesis genes shed light on important sugar-nucleotide modifying enzymes including dehydratases, epimerases and reductases. Several studies showed that deletion of one of the sugar-nucleotide modifying enzymes encoding genes results in interruption of the pathway and consequently reduces the virulence of the organism (70, 143, 173, 175, 184) . These findings suggest that theses enzymes could be potential antimicrobial targets. In fact, successful attempts were made to design inhibitors for different enzymes, such as RmlC in *M. tuberculosis,* and the first two enzymes in the GDP-*manno*-heptose synthesis pathway (16, 47).

In *C. jejuni*, heptose epimerases and reductases were identified in two strains, 81-167 and NCTC 11168. These enzymes are highly similar yet perform strain-specific activities to generate different modified heptoses. They possess an interesting substrate and products specificity, which warrants an investigation of their binding sites. However, no structure of these enzymes or of homologous GDP-*manno*-heptose modifying enzymes is available. Therefore, **we hypothesized that the heptose modifying enzymes in *C. jejuni* have specific catalytic residues that allow for substrate and product specificity toward heptose-based substrate rather than hexose-based substrate. These catalytic residues allow the enzymes to function differently on heptose despite the high sequence and structure similarity.**

The role of the modified heptoses has been investigated with regards to bacterial resistance to serum and bile salt, adhesion and invasion to host cells, as well as colonization of the chicken reservoir of *C. jejuni*. However, their role in biofilm formation, which is one of the virulence factors that allows bacterial persistence in nature, still needs to be investigated. For this, **we hypothesized that synthesis of the modified heptoses is important for biofilm formation.**

1.10. Objectives:

First, to investigate the structure and the active site of the epimerases (DdahB and MlghB) and the reductases (DdahC and MlghC), enzymatic and structural approaches were employed. All enzymes were structurally modeled on well-studied hexose-modifying enzymes homologues. The molecular structures of the enzymes were solved by X-ray crystallography, done by a collaborator (Laura Woodward, under supervision of Dr. James Naismith, St, Andrews University, UK). The starting substrate, GDP-*manno*-heptose, was synthesized in the lab for structural and enzymatic analysis. We also applied site-directed mutagenesis to test specifically targeted residues for their involvement in catalysis or substrate specificity. The enzymatic activity, product formation, and kinetics were analyzed by capillary electrophoresis.

Second, to study biofilm formation, an *in vitro* biofilm formation experiment was performed on the wild type *C. jejuni* NCTC11168 and on five capsular and heptose biosynthesis mutants, *kpsM, mlghB::cat, mlghC::cat, wcaG::cat,* and *wcaGΔ::cat*.

CHAPTER 2 – MATERIAL AND METHODS

2.1. Bacterial growth and culture conditions:

Escherichia coli strains, DH5α, ER2566, and BL21(DE3)pLysS were routinely grown from -80°C freezer stocks at 37°C on Luria Broth (LB) media (Bioshop, Canada). They were grown either on agar plates or in broth shaking at 200 rpm. Antibiotic supplements were added based on specific selection used at final concentration of 100 µg/ml ampicillin (Biobasic, Markham, Canada), 100 µg/ml carbenicillin, 30 µg/ml kanamycin (Biobasic, Markham, Canada), and 34 µg/ml chloramphenicol (Fisher Scientific, Canada). *C. jejuni* ATCC 700819 (NCTC 11168), wild type and mutant strains, were grown initially from -80°C freezer stocks overnight on Tryptic Soy Agar (TSA; BD, Canada). The media was supplemented with 10 µg/ml vancomycin (Biobasic, Markham, Canada), 5 µg/ml trimethoprim (Sigma-Aldrich, Canada), and 5% sheep blood (Cedarlane, Burlington, Canada). Either 15 µg/ml chloramphenicol or 90 µg/ml kanamycin was added for selection of the mutants. *C. jejuni* cells were grown in a microaerobic incubator (Nuaire) at 37°C in 5% oxygen, 10% carbon dioxide, 85% nitrogen, and 90% humidity. Cells were then transferred onto another TSA plate and grown for 24 hours. To grow *C. jejuni* in liquid media, Tryptic Soy Broth (TSA; BD, Canada) was used. Media was supplemented with vancomycin, trimethoprim, 0.05% pyruvate (Alfa Aesar, USA), and 5% horse serum (Invitrogen, Canada) and grown shaking at 90 rpm.

2.2. Calcium chloride competent *E. coli* preparations:

To prepare competent *E. coli* DH5α, ER2566, and BL21 (DE3) pLysS, 3 ml overnight culture was used to inoculate 100 ml of LB and incubated to reach an OD_{600} of 0.6. The cells were centrifuged at 5000 ×g (Eppendorf 5415D) for 10 minutes at 4°C. The pellet was resuspended in 20 ml of cold 50 mM calcium chloride solution and incubated on ice for 30 minutes then centrifuged as above. The pellet was resuspended in 5 ml of 50 mM calcium chloride and 5 ml of 50% glycerol, aliquoted to 200 µl and stored at -80°C.

2.3. Transformation into competent *E. coli:*

A volume of 100 µl of the competent cells was incubated on ice after adding 10 µl of the transforming DNA for 30 min. Cells were then incubated at 42°C for two min for heat shock then immediately placed on ice for 10 min. After that, 600 µl of LB was added to the cells, and they were incubated shaking at 37°C for 90 min. Cells were then plated on LB plates with antibiotic as specified for selection and incubated overnight. Transformed colonies were patched the next day on a new plate and re-incubated for 6 hours. Every cell patch was used to inoculate 3 ml LB to grow overnight. Next day, aliquots with 25% glycerol were made and stored at -80°C.

2.4. Plasmid extraction and agarose gel electrophoresis:

Plasmids were extracted from 3 ml LB overnight cultures of the transformed DH5α. Cells were centrifuged at 5000 ×g. The pellet was resuspended in 100 µl of

solution I (50 mM glucose, 25 mM Tris-HCl pH 8, 10 mM ethylenediaminetetraacetate (EDTA, pH 8). Then 200 µL of Solution II (1% SDS, 0.2 M NaOH), and 350 µL of Solution III (3M sodium acetate) were added with gentle mixing of the sample. After 10 minutes centrifugation at 4000 ×g, the supernatant was treated with the same volume of cold isopropanol and mixed by ten times inversion and incubated at room temperature for 10 minutes. Samples were centrifuged as above, the pellet washed with 1 ml of cold 70% and 100% ethanol. The pellet was left to dry at 37°C and finally resuspended in 50 µl of sterile water. DNA samples were analyzed by agarose gel electrophoresis using TAE buffer (40 mM Tris-acetate pH 8.3, 1 mM EDTA), 0.7% of agarose gel with 0.01% ethidium bromide. Samples in 2× DNA loading buffer (Invitrogen) as well as 1 Kb DNA ladder standard (Genedirex) were loaded on the gel and separated at 100 V. UV light was used to visualize DNA bands.

2.5. GDP-*manno*-heptose synthesis:

GDP-*manno*-heptose synthesis from sedoheptulose 7-phosphate (Carbosynth) was performed using GmhA/B/C/D enzymes following previously established conditions (31). Gmh enzymes were cloned previously from *Aneurinibacillus thermoaerophilus* into pDEST-17 with a histidine tag, for GmhA, GmhB, and GmhC, and into pDEST-15 with a GST tag for GmhD (31). After expression and purification (see section 2.12 for details) small scale reactions were prepared to test sequential conversion of sedoheptulose 7-phosphate by each enzyme. A master mix of 120 µl containing 0.5 mM sedoheptulose 7-phosphate, 200 mM ammonium bicarbonate buffer pH 9.0, 0.52 mM ATP (Sigma) and

2.5 mM $MgCl_2$ was equally divided into five reaction tubes. The first reaction has no enzyme added as a negative control. The other reactions had 0.2 µmol of either GmhA only, GmhA and GmhB, GmhA, B, and C, or all enzymes, also contained GTP (Roche) in a total volume of 50 µl. All reactions were incubated at 37°C for 12 hours, centrifuged at 5000 ×g for 30 minutes. The supernatant was passed through a 10 kDa cut-off centricon and lyophilized. The lyophilized pellet was finally resuspended in 25 µl MilliQ water for further analysis.

A large scale reaction of 15 ml was prepared in two steps. In the first step, the reaction contained 2.6 mM sedoheptulose 7-phosphate, 400 mM ammonium bicarbonate buffer pH 9.0, 10 mM $MgCl_2$, 2.7 mM ATP, 1.0 µmol of GmhA, GmhB, and GmhC. The reaction was incubated at 37°C for 12 hours. After incubation, it was centrifuged and passed through a 10 kDa cut-off centricon. The flow through was used for the second step of the reaction to generate GDP-*manno*-heptose by the addition of 1.0 µmol of GmhD and 1.9 mM GTP. After 12 hours incubation at 37°C, the reaction was centrifuged and passed through the centricon. The final conversion into GDP-*manno*-heptose was monitored by the capillary electrophoresis.

2.6. High-performance liquid chromatography analysis (HPLC):

To analyze various sugar products, anionic exchange HPLC with pulsed amperometric detection (PAD) was used on a Dionex ICS 3000 instrument. CarboPac PA1 column (4 ×250 mm; Dionex) was used after it had equilibrated with 100 mM NaOH for 10 minutes. The samples from the small scale synthesis of GDP-*manno*-

heptose were lyophilized and resuspended in deionized water (MilliQ-water) and 10 µl was injected to the column. A linear gradient from 100- 500 mM of 1M NaOAc in 100 mM NaOH was applied for 40 minutes at 1 ml/min as reported previously (31).

2.7. GDP-*manno*-heptose purification:

GDP-*manno*-heptose was purified using anion-exchange chromatography using a High Q Econopac 5 ml column (Bio-Rad) as reported previously (31). A linear gradient from 50 mM -1 M triethylammonium bicarbonate (TEAB) pH 8.5, was applied for 20 column volumes at 1 ml/min. Detection of sugar nucleotide was by UV light (260 and 214 nm). Desired fractions containing the suspected GDP-*manno*-heptose were pooled and lyophilized twice with resuspension in water between both lyophilization steps. Finally, they were resuspended in water and analyzed by CE along with previously characterized GDP-*manno*-heptose for product identification and purity assessment. Quantitation of GDP-*manno*-heptose was performed using a Nanodrop spectrophotometer using εGTP = 12000 mol-1 L cm-1.

2.8. Comparative functional analysis:

A comparative functional analysis between the heptose modifying enzymes and well-studied homologous enzymes with known structure was done. The function of residues in the binding site was predicted based on structural sequence alignment to residues of known function in the homologues. The epimerases were compared to a dTDP-hexoluse C3/C5 epimerase (RmlC) from *Salmonella enterica* and *Streptococcus*

suis (45, 55). The reductases were compared to the GDP-fucose synthetase (GFS), a GDP-4-keto-6-deoxy-D-mannose C3/C5 epimerase and C4 reductase from *E. coli* (55).

2.9. Structural modeling:

Homology modeling approach was used to model the structure of the epimerases, DdahB and MlghB, and the reductases, DdahC and MlghC. SWISS-MODEL workspace (http://swissmodel.expasy.org/) was used to build the structure model for the wild type and mutant enzymes (7). In the main page of SWISS-MODEL workspace, the protein sequence of the wild type or the mutant was entered in the target sequence field. The protein name was written in the project title field then the option of searching for a template was chosen. The software then showed a list of templates ordered from the highest identity to the target sequence to the lowest identity. On the top of the list, several tabs allow the user to check the selected templates before model building. The sequence similarity tab shows how similar the selected template is to the target protein. The alignment tab shows the protein sequence of the target aligned with the template sequence. The user can select more than one template for model building. After template selection, model building was started by clicking on build models button. In a new window, all build models are shown. The best model was chosen based on the QMEAN score and exported from SWISS-MODEL as protein data bank files (PDB) (20). The 3D structures were then visualized and analyzed using PyMol software (https://www.pymol.org/).

2.10. Subcloning and crystallography:

The epimerase genes *ddahB* and *mlghB* were subcloned into a pEHISTEV vector for crystallography purposes. The pEHISTEV plasmid was received from Dr. Naismith (St Andrews, UK) and transformed into DH5α with kanamycin selection (103). After plasmid extraction and purification, cohesive ends were generated by restriction digest using 1.0 U of BamHI and NcoI restriction enzymes (BioLabs) and 1×REact® 3 buffer (Invitrogen). Both *ddahB* and *mlghB* genes were PCR amplified from pET-*ddahB* and pET-*mlghB* plasmids by iMax DNA polymerase (iNtRON) and the primers listed in Appendix 1 (112). PCR products were then analyzed by agarose gel electrophoresis and purified using PCR purification kit following manufacturer's instructions (Geneaid). PCR products were then subjected to restriction cut using AflIII (Invitrogen) and BamHI for *ddahB,* NcoI and BamHI for *MlghB* in 1×REact® 3 buffer. To insert the cut PCR product into the pEHISTEV vector, reactions containing each insert, the vector, 26 U ligase (BioLabs), and 1× ligation buffer were incubated at room temperature overnight. After analyzing the products by gel electrophoresis, they were transformed into DH5α. Extracted plasmids from recovered clones were sequenced for confirmation using T7 promoter primer (Roberts Research Institute sequencing facility, London, Ontario).

The crystallography was done by collaborators, Dr. James Naismith and a PhD. candidate, Laura Woodward in St. Andrews' University, UK. The molecular structure of both epimerases DdahB and MlghB were solved by molecular replacement on the crystal

structure of RmlC. The structure of MlghB/GDP-mannose was solved by co-crystallization with GDP-mannose as an analog substrate.

2.11. Site-directed mutagenesis:

Site-directed mutagenesis was performed following the QuikChange® mutagenesis procedure using iMax DNA polymerase. To generate the mutants, reactions containing 10 pmol of either the forward or the reverse primer (Appendix 2), 20 ng of the template plasmid, and 0.05 U of iMax polymerase in 1× iMax buffer were set up. The PCR was programmed to 30 cycles of denaturation at 98°C for 30 seconds followed by annealing at each primer annealing temperature, and extension at 72° based on the iMax polymerases speed, 1kb/min. After ten PCR cycles, individual reactions containing either the forward or the reverse primer were combined, 0.05 U of iMax enzyme was added, and PCR was resumed for 20 more cycles and final extension at 72°C for 7 minutes. The PCR product was then treated with DpnI (Stratagene) for one hour and transformed into *E. coli* DH5α as explained above. Purified plasmids were sequenced with T7 promoter primer for confirmation (Roberts Research Institute sequencing facility, London, Ontario).

2.12. Protein expression and purification:

The modified heptose synthesis genes, *mlghB* and *mlghC*, from *C. jejuni* NCTC11168, and *ddahA*, *ddahB*, *ddahC* from *C. jejuni* 81-176, were previously cloned into pET vector with N-terminus 6× histidine tags (110, 112). The GDP-mannose

dehydratase, *hp0044* gene, was previously cloned from *Helicobacter pylori* into pGEX-2T with N-terminus GST-tag (31). Genes for GDP-*manno*-heptose synthesis were cloned from *Aneurinibacillus thermoaerophilus* (87). The *gmhA*, *gmhB,* and *gmhC* genes were previously cloned into pDEST17 with N-terminus 6× histidine tag, while *gmhD* was cloned into pDEST15 with N-terminus GST tag (31). Expression of all proteins was carried using *E. coli* ER2566, BL21 (DE3) pLysS, or DH5α expression strains (see Table 1 for specifics). Cells were grown in LB with shaking at 37°C to OD_{600} of 0.6. To induce expression 0.1 mM isopropyl β-D-1-thiogalactopyranoside (IPTG) was added. For the modified heptose synthesis enzymes, 300 ml cultures were induced for three hours at 37°C for MlghB, MlghC, DdahA, DdahC, and at 25°C for DdahB. The GDP-mannose dehydratase, HP0044, was induced from DH5α at 37°C for three hours. For GDP-*manno*-heptose synthesis enzymes, 1 L cultures were induced at 25°C for three hours for GmhA, GmhB, GmhC, and 16 hours for GmhD.

Purification of all proteins was done using affinity chromatography purification using FPLC. For N-terminally histidine-tagged proteins, the expressed cell pellets were resuspended in binding buffer (0.1 M NaCl, 20 mM imidazole, 20 mM Tris-HCl) with a pH away from the protein isoelectric point (Table 1). After cell disruption under 25 psi and ultracentrifugation, the proteins were purified by nickel chelation using a 1.6 ml of Poros MC 20 column (4.6 ×100 mm; Applied Biosystems). After washing the non-specific binding proteins, His-tagged proteins were eluted using a gradient of imidazole concentrations. The GST-tagged GmhD and HP0044 were resuspended in PBS binding buffer (140 mM NaCl, 2.7 mM KCl, 10 mM Na_2HPO_4, and 1.8 mM KH_2PO_4. pH 8.0).

They were purified using 1 ml GSTrap FF column (GE Healthcare). Unbound proteins were washed with binding buffer. Bound proteins were eluted using 0.01 M reduced glutathione (Sigma). Pure protein fractions were preserved in 25% glycerol at -20 °C.

Table 1: Expression and purification conditions:

Strain	Gene	Vector	Tag	Mass (kDa)*	Purification pH	*E. coli* expression strain
C. jejuni NCTC 11168	*mlghB*	pET	His	22.2	8.0	BL21 (DE3) pLysS
	mlghC	pET	His	41.7	7.0	ER2566
C. jejuni 81-176	*ddahA*	pET	His	40.5	8.0	BL21 (DE3) pLysS
	ddahB	pET	His	22.1	7.0	BL21 (DE3) pLysS
	ddahC	pET	His	40.7	7.0	ER2566
H. pylori	*hp0044*	pGEX-2T	GST	73.9	8.0	DH5α
A. thermoaerophilus	*gmha*	pDEST17	His	25.0	7.5	BL21 (DE3) pLysS
	gmhb	pDEST17	His	39.1	7.5	
	gmhc	pDEST17	His	24.7	7.5	
	gmhD	pDEST15	GST	52.6	8.0	

* Protein mass with the tag

2.13. SDS-polyacrylamide gel electrophoresis of proteins:

SDS-PAGE analysis for proteins was performed using stacking gel (4 % polyacrylamide (Bio-Rad, mini-gel system), 125 mM Tris pH 6.8, 0.1 % SDS, 0.5% ammonium persulfate (APS), and 0.1 % tetramethylethylenediamine (TEMED)), and separating gel (12% polyacrylamide, 375 mM Tris pH 8.8, 0.1 % SDS, 0.1 % APS, and 0.1 % TEMED). Before loading on the gel, protein samples were incubated for 10 min at 100°C in SDS loading buffer (0.625 M Tris pH 6.8, 2% SDS, 2% β-mercaptoethanol, 10% glycerol, and 0.002% bromophenol blue). Gels were run in Tris-glycine running buffer (25 mM Tris, 190 mM glycine, 1% w/v SDS. pH 8.3) at 10 mA through stacking gel and 20 mA through the separating gel. Proteins were visualized by Coomassie blue staining (10% acetic acid, 25% ethanol, 0.001% (w/v) Coomassie blue).

2.14. Western blotting:

Western blotting was performed after SDS-PAGE. Proteins were transferred from the gel to a nitrocellulose membrane (Bio-Rad). The transfer was performed for 45 minutes in Tris-Glycine Transfer buffer (192 mM glycine, 25 mM Tris pH 8.3, 20% methanol, 0.01% SDS) with a constant current of 180mA (Bio-Rad transblot system). After transfer, the membrane was washed with water and stained with 0.1% Ponceau S Red to visualize the transferred proteins. After scanning the membrane, the Ponceau stain was washed by 1× PBS buffer (137 mM NaCl, 2.7 mM KC1, 8 mM Na_2HPO_4, and 1.46 mM KH_2PO_4, pH 7.2). The membrane was blocked with 5% skim milk in 1× PBS buffer

overnight at 4°C, or 2.5% for 30 minutes at room temperature. After blocking, the membrane was washed twice in PBS-Tween-20 (PBS and 0.1% Tween-20) and once in PBS buffer for 5 minutes each. Primary antibody (Sigma) was added to the membrane and incubated for one hour. After washing twice in PBS-Tween-20 and once with PBS, the secondary antibody (Sigma) was added and incubated 40 minutes in the dark. See Appendix 3 for the list of antibodies used. Finally, the membrane was washed again as above and the protein was visualized using Licor Infrared Imaging system at wavelengths of 700nm or 800nm.

2.15. Bradford assay:

Total protein concentration was measured from pure protein fractions before adding the 25% glycerol. The assay standard curve was made using serial dilutions of bovine serum albumin (BSA). The procedure was performed according to the manufacturer's instructions (Bio-Rad). Absorbance was taken at 595 nm. All samples were measured in triplicate.

2.16. The epimerases reactions and kinetics:

2.16.1. GDP-*manno*-heptose reactions:

To test the activity for the epimerases, a master mix of 80 µl containing 0.17 mM GDP-*manno*-heptose, 1.5 µmol DdahA, 200 mM Tris pH 7.5, and 0.13 mM $NADP^+$ that was used as an internal standard to facilitate peak alignment on the capillary electrophoresis (CE) electeropherograms. The master mix was incubated at 37°C for 30

minutes then frozen at -20°C before further usage. The total conversion of GDP-*manno*-heptose into the desired substrate for the epimerases (P1) was confirmed by testing an aliquot from the master mix using CE. The master mix was then divided into nine tubes, 8 µl each. To each tube, 1.0 pmol of either MlghB or DdahB, wild type or mutants were added. All reaction tubes were incubated at 37°C for 30 minutes. At the end of the incubation, they were frozen at -20°C.

The kinetics were performed with the same substrate and enzymes concentrations in master mixes as mentioned above. The reactions were incubated for 5, 10, 15, 20, 30, and 45 minutes. At each time point, the reactions were snap frozen in dry ice/ ethanol mixture and individually analyzed by CE.

2.16.2. GDP-mannose reactions:

For the epimerases, a master mix of 80 µl containing 0.77mM GDP-mannose, 2.0 pmol HP0044, 200 mM Tris pH 7.5, and 0.1 mM $NADP^+$ was incubated at 37°C for 90 minutes. After the total conversion of GDP-mannose into P1' was confirmed by CE, the mix was frozen at -20°C then divided into nine tubes, 8 µl each. For each tube 5 pmol/ul of DdahB or 1 pmol/ul of MlghB, wild type or mutants was added. Reaction tubes were incubated one hour for MlghB and 5 hours for DdahB at 37°C.

The kinetics were performed only for MlghB with the same substrate and enzymes concentrations in master mixes as mentioned above. The reactions were incubated for 20, 30, 60, 150, 240, and 300 minutes. At each time point, the reactions were snap frozen in dry ice/ ethanol mixture and individually analyzed by CE

2.17. The reductases reactions and kinetics:

2.17.1. GDP-*manno*-heptose reactions:

To test the activity of the reductases, a master mix of 56 µl containing 0.17 mM GDP-*manno*-heptose, 1.5 µmol DdahA, 2 pmol MlghB, 200 mM Tris pH 7.5, and 0.5 mM NADPH as a co-factor for the reductases. The master mix was incubated at 37°C for 30 minutes then frozen at -20°C. An aliquot tested by CE for the generation of the epimerized sugar nucleotide by MlghB, P4α, P4β, and P4γ. The master mix was then divided into six tubes, 8.0 µl each, and 1.0 pmol of either MlghC or DdahC, wild type or mutants was added. Reactions were incubated at 37°C for 30 minutes then frozen -20°C.

To test the substrate specificity of the reductases, wild type and mutants, a base reaction containing 0.17 mM GDP-*manno*-heptose, 1.5 µmol DdahA, 2 pmol MlghB, 200 mM Tris pH 7.5, and 0.5 mM NADPH as a co-factor for the reductases. The master mix was incubated at 37°C for 30 minutes then frozen at -20°C. An aliquot tested by CE for the generation of the epimerized sugar nucleotide by MlghB, P4α, P4β, and P4γ. The master mix was then ultrafiltered to remove MlghB from the reaction using a 10 kDa cutoff centricone. The filtrate was eluquted and 1.0 pmol of either MlghC or DdahC, wild type or mutants was added. Reactions were incubated at 37°C for 30 minutes then frozen -20°C then analyzed by CE. The same method was used to perform the kinetics of the reductases. The same concentrations of the substrate and the enzymes were used to incubate the reductases, wild type and mutants for 7 time points, 5, 10, 15, 20, 30, 45, and

60 minutes at 37°C. All reactions were snap frozen in dry ice/ ethanol mixture at each time point and individually analyzed by the CE.

2.17.2. GDP-mannose reactions:

The activity of the reductases was tested on different GDP-mannose substrates in two different reaction sets. The activity of the wild type DdahC and MlghC were tested on both P4' and P1', as well as on P1' by itself. For the first set, a master mix of 30 µl containing 1.25 mM GDP-mannose, 2.0 pmol HP0044, 2.0 pmol MlghB, 200 mM Tris pH 7.5, and 0.5 mM $NADP^+$ was incubated at 37°C for 90 minutes. After the total conversion of GDP-mannose into P1', and formation of P4' was confirmed by CE, the reaction was divided where 1.0 pmol of DdahC or MlghC were added and incubated for 60 minutes at 37°C then frozen -20°C then analyzed by CE.

The second set was to test the activity on P1' only. A base reaction containing 0.77 mM GDP-mannose, 2.0 pmol HP0044, 200 mM Tris pH 7.5, and 0.1 mM $NADP^+$ was incubated at 37°C for 90 minutes. After the total conversion of GDP-mannose into P1' was confirmed by CE, the mix was ultrafiltered to remove HP0044 from the reaction. The filterate was divided and 1.0 pmol of eather DdahC or MlghC was added and incubated for 60 minuts at 37°C then frozen -20°C then analyzed by CE.

To test the differences between the wild and the mutants of DdahC and MlghC, a reaction containing 0.77 mM GDP-mannose, 2.0 pmol HP0044, 200 mM Tris pH 7.5, and 0.5 mM $NADP^+$ was incubated at 37°C for 90 minutes and ultrafiltered after total conversion of GDP-mannose into P1'.

The kinetics were performed in a similar reaction to the first set mentioned above. The reactions were incubated for 10, 20, 35, 50, 70, and 95 minutes at 37°C. All reactions were snap frozen in dry ice/ ethanol mixture at each time point and individually analyzed by the CE.

2.18. Capillary electrophoresis analysis:

Capillary electrophoresis for sugar nucleotides analysis was performed on a Beckman MDQ/ Gold instrument using the 32 Karat software and 57 cm bare silica capillary. The sample running method includes initial washing of the capillary with 200 mM Borax buffer pH 9.0 for two minutes at 20 psi, followed by four seconds of sample injection. The separation of the sample was done under 26 kV and detection was at 254 nm. After each sample, the capillary was washed for two minutes with water, two minutes with 0.1M NaOH, and two minutes with water again. Using the 32Karat software, product formation was estimated by integration of surface areas under the substrate and product peaks.

2.19. Biofilm assay:

The wild-type strain, *C. jejuni* NCTC11168, was tested for biofilm formation along with four heptose biosynthesis mutants and a capsule-less mutant that were generated previously in our lab, *wcaG::cat, mlghC::cat, mlghB::cat, and wcaGΔ::cat* (184). *KpsM::kan that* is known to be a capsule-less strain was used as a negative control. All strains were grown as explained in section 2.1. In a 100mm diameter glass tube, one ml of a cell suspension adjusted to OD_{600} of 0.7 was incubated under aerobic or

microaerobic static conditions at 37°C for 3 days. Three replicates were prepared for each strain. After the three days incubation, a set of tubes was taken out of the incubator every day for four days, washed three times with water to remove planktonic cells, and left to dry for 30 minutes. To stain biofilm, 1 ml of 1% crystal violet was added to each tube and incubated at room temperature for one hour. Excess stain was washed with water three times, and the tubes were left to dry for 30 minutes. Finally, the stained biofilms were detached from the glass wall by adding 1 ml of 30 % acetic acid and incubating for an hour. Two hundred µl of each sample were transferred to a 96-well microtiter plate to measure the absorbance at 950 nm (146). Statistics were done using one-way ANOVA test for two independent experiments.

2.20. Hitchcock and Brown method for CPS and LOS extraction:

The cell pellets from 1 ml of the same cell suspensions that were used for the biofilm assay were washed and resuspended in lysis buffer (2% SDS, 4% 2-mercaptoethanol, 10% glycerol, 1 M Tris pH 6.8), and bromophenol blue). After heating the sample at 100°C for 30 min, it was treated with 2.5 µg of proteinase K (Roche) at 60°C for an hour (69). Finally, 15 µl of the sample were loaded on SDS gels with Tris-Glycine buffer as explained bellow.

2.21. SDS-polyacrylamide gel electrophoresis for CPS:

SDS-PAGE analysis for CPS samples was performed using stacking gel (4 % polyacrylamide, 125 mM Tris pH 6.8, 0.1 % SDS, 0.5% APS, and 0.1 % TEMED), and

separating gel (14% polyacrylamide, 3 M Tris, 1 M HCl, and 0.3% SDS buffer, pH 8.4, 0.1% APS, and 0.1 % TEMED). CPS cell suspensions were treated according to Hitchcock and Brown method or saline extraction as explained above then loaded. The gel was run in Tris-glycine buffer at 20 mA. The CPS was finally visualized by silver staining as explained below.

2.22. Silver staining:

Silver staining of the carbohydrate samples that were separated by SDS-PAGE was done according to Fomsgaard et al protocol (51). The gels were incubated shaking in oxidizing solution (0.7% periodic acid, 40% ethanol and 5% acetic acid in MilliQ water) at room temperature for 20 minutes. They were then washed four times over 15 minutes with MilliQ water. After washing, the gels were stained with staining solution (0.19% (v/v) 10 N NaOH, 1.3% (v/v) ammonium hydroxide, 0.7% (w/v) silver nitrate) for 10 minutes, followed by five washes with MilliQ water. The gel was developed in 0.005% (w/v) citric acid and 0.05% (v/v) formaldehyde (37%) until bands became visible. Finally, they were washed with MilliQ water and scanned.

CHAPTER 3 - RESULTS

3.1. GDP-*manno*-heptose synthesis:

The synthesis of GDP-*manno*-heptose from sedoheptulose-7-phosphate was done following previously optimized conditions using GmhA, GmhB, GmhC, and GmhD enzymes (31). GmhA, GmhB, and GmhC are histidine-tagged proteins and were purified using nickel affinity chromatography. GmhD is GST-tagged and was purified by GST affinity chromatography (Figure 8-A).

The synthesis of GDP-*manno*-heptose was initially carried on a small scale to monitor the activity of the purified biosynthesis enzymes, GmhA, GmhB, and GmhC. Because the last enzyme in the pathway, GmhD, has a very short lifespan, it was not tested in the small scale analysis. Based on the HPLC analysis, the conversions of 0.5 mM sedoheptulose-7-phosphate into heptose-7-phosphate by GmhA was successful, but not complete (Figure 8-B). The reaction where both GmhA and GmhB along with ATP were used showed complete conversion of the sedoheptulose-7-phosphate into heptose-1,7-biphosphate. Adding all the three enzymes, GmhA, GmhB, and GmhC resulted in the formation of the heptose-1-phosphate (Figure 8-B). In a large scale, 5.4 mM of the sedoheptulose-7-phosphate was used to generate the heptose-1-phosphate using 5 μmol of GmhA, GmhB and GmhC. The products formation was analyzed by HPLC using sedoheptulose-7-phosphate as a standard. The products migration time was assessed based on the previously established methods where the products were identified by mass spectrometry analysis (31).

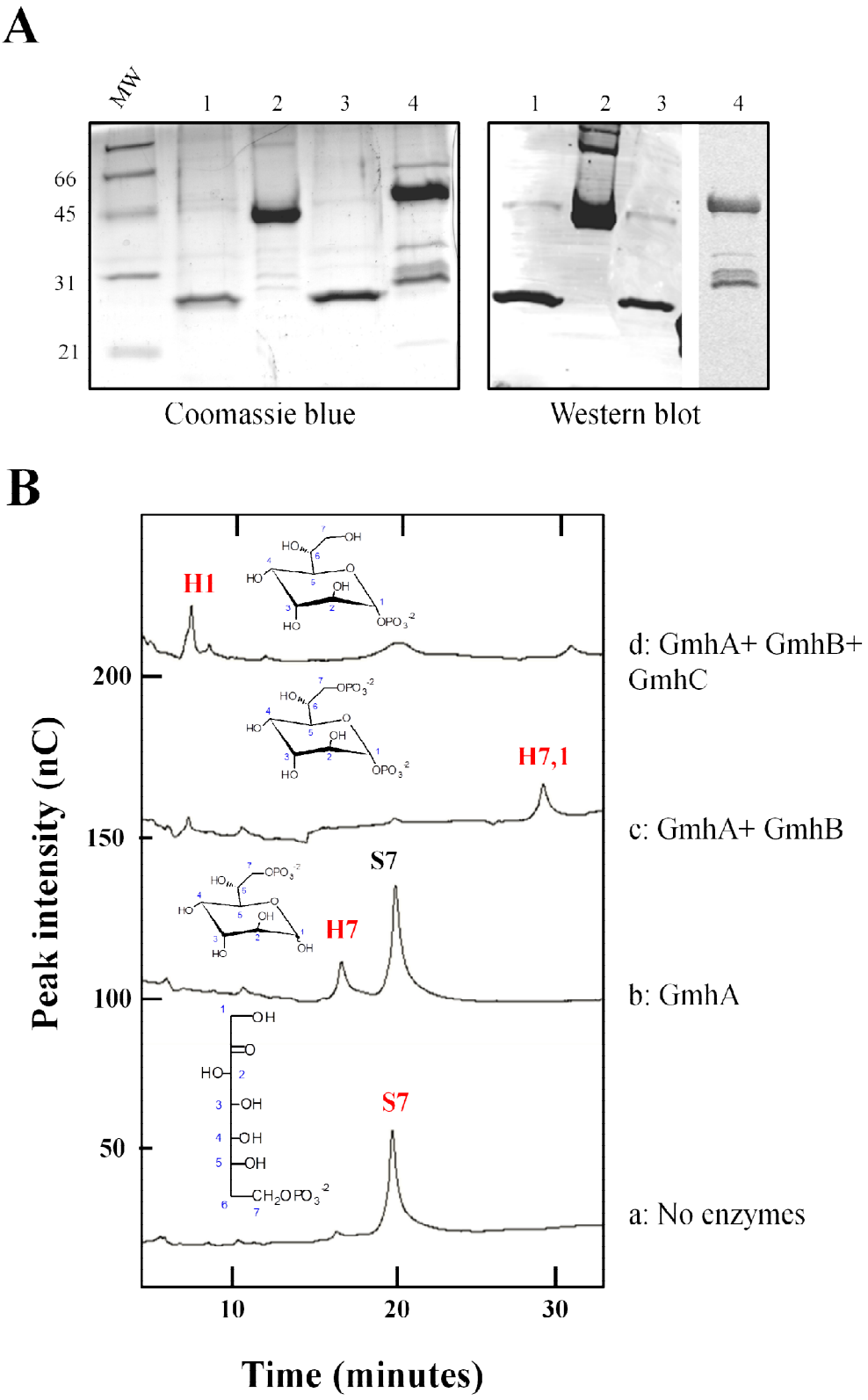
A
MW
1
2
3
4
66
45
31
21
Coomassie blue
Western blot
B
H1
H7,1
S7
H7
S7
d: GmhA+ GmhB+ GmhC
c: GmhA+ GmhB
b: GmhA
a: No enzymes
Peak intensity (nC)
200
150
100
50
10
20
30
Time (minutes)

Figure 8: Synthesis of GDP-*manno*-heptose in small scale. A. SDS-PAGE analysis of the purified GDP-*manno*-heptose synthesis enzymes. From 1 to 4, showing GmhA (25 kDa), GmhB (38 kDa), GmhC (25 kDa), and GmhD (52 kDa). The left panel shows the Coomassie blue stain, while the right panel shows the anti-histidine western blot, for GmhA, GmhB, and GmhC, as well as the anti-GST tag western blot for GmhD. **B.** HPLC chromatograms of small scale sequential conversion of sedoheptulose-7-phosphate into heptose-1-phosphate. GmhA converts sedoheptulose-7-phosphate (S7) into heptose-7-phosphate (H7) (trace b). GmhB converts H7 into heptose-1,7-biphosphate (H1,7) by adding phosphate group from ATP molecule that was provided in the reaction (trace c). GmhC removes one phosphate from H1,7 to generate heptose-1-phosphate (H1) (trace d). The sugar peaks are labeled in red, and their chemical structures are represented.

3.2. Epimerases comparative functional analysis and structure:

3.2.1. Comparative functional analysis:

The analysis of the active site of DdahB, a C3 epimerase, and MlghB, a C3/C5 epimerase, was based on the knowledge obtained from studied RmlC enzymes (45, 46, 55). RmlC, a dTDP-6-deoxy-D-*xylo*-4-hexulose C3/C5 epimerase, is the third enzyme in the dTDP-L-rhamnose synthesis pathway. RmlC substrate has a 4-keto group that is important to initialize the epimerization. In *St. suis's* RmlC, Asn127 recognize the O4-keto group and binds it through the amide group, which lowers the pKa of the protons attached to C3 and C5 (4, 45). The epimerization at C3 and C5 is obtained in two chemical steps, deprotonation from one face of the sugar ring followed by reprotonation at the opposite face at C3 and C5 position (45, 46). Deuterium incorporation analysis indicates that RmlC could perform sequential C5, C3 epimerization where C5 epimerization is faster than C3 epimerization (46). The C3/C5 epimerized product that is generated by RmlC could not be detected in a chemical reaction or directly quantified by biochemical assays (60, 118, 163). The activity of RmlC was rather confirmed by coupled assay with the downstream reductase, RmlD, by measuring the conversion rate of NADPH upon formation of dTDP-L-rhamnose (46, 60). The explanation of why the RmlC product has never been isolated is that it can exist only as an enzyme-bound intermediate that can only disassociate after reduction by RmlD, which could form a complex with RmlC (118).

The residues that are involved in RmlC activity, His63-Asp170 dyad, Tyr133, and Lys73, were identified in *S. enterica's* RmlC by structural and biochemical

assays (46). These residues are highly conserved among studied RmlC enzymes in other bacteria. The His63-Asp170 dyad is important for both C3 and C5 epimerization of the substrate. Based on deuterium incorporation and mutagenesis coupled with enzymes assays, His63Ala is catalytically inactive. This, together with its location in the binding site suggests that His63 acts as a base to deprotonate the sugar from the lower face of the ring at C3 and C5 positions, as it has a flexible side chain conformation (45). The proton abstraction results in the formation of an enolate anion that could be stabilized by Lys73 (45, 46). At the opposite face of the sugar ring, Tyr133 donates a proton at C5 position. Tyr133Phe had 1000 fold reduction in activity and some deuterium incorporation only at C3 but not at C5. This indicates that the hydroxyl group of the Tyr133 side chain is essential for C5 but not for C3 epimerization. A conserved water molecule found close to C3 could be compensating for Tyr133 function in the Tyr133Phe mutant by donating a proton (46). On the other hand, Lys73Ala had 100 fold reduction in activity and a small amount of deuterium incorporation at C5 but not at C3, suggesting that Lys73 is essential for epimerization at C3 (46).

Based on co-crystallography of *S. enterica's* RmlC with dTDP-phenol, the residues that are involved in the ribose nucleotide binding are Phe27, Tyr139, Asn50 and Phe20 (55). The thymidine ring is stacked between the aromatic residues Phe27 and Tyr139. Asn50 is also interacting with the thymidine ring, while Phe20 from B monomer stacks against the ribose ring of the nucleotide. The residues that interact with the sugar ring, Asn127, Phe129, and Tyr138, were identified in *St. suis's* RmlC

(45). The Asn127 residue is important for the 4-keto substrate recognition by binding to O4, which predicted to lower the transition state energy of C3 and C5 protons, while both Phe129 and Tyr138 make Van der Waals interactions with C6 and O6. The last two residues, Phe129 and Tyr138, are conserved among RmlC enzymes as aromatic residues and most commonly found as Phe/Phe pair, which means that they could be involved in stacking interactions with the sugar (54).

Similar to RmlC, *C. jejuni* NCTC 11168 epimerase, MlghB, is able to perform C3/C5 epimerization on a different substrate, GDP-6-deoxy-4-keto-D-*lyxo*-heptose. However, MlghB can release the three epimerized products that were detected by capillary electrophoresis and identified by mass spectrometry (111). On the other hand, the epimerase in *C. jejuni* 81-176, DdahB, can only epimerize the GDP-6-deoxy-4-keto-D-*lyxo*-heptose at C3 generating one product under same conditions as MlghB (111, 112). Based on sequence alignment with *St. suis's* and *S. enterica's* RmlC with, both DdahB and MlghB have the conserved catalytic His67-Asp173 dyad, Tyr134, and Lys74 residues (the numbers are for DdahB and MlghB protein sequences) (Figure 9) (Table 2). Therefore, His67 is predicted to be catalytic for epimerization at C3 and C5 of the heptose substrate. On the other hand, Tyr134 and Lys74 could be essential for epimerization at C5 and/or C3. Similar to RmlC's nucleotide binding residues, Phe27, Tyr139, Asn50 and Phe20 both DdahB and MlghB have the residues that could be important for the nucleotide binding, Ile31, Tyr142, Lys54, and Phe24. Aligned with the residue Asn127 that bind the 4-keto group of the sugar ring in RmlC, DdahB and MlghB have Asn121. Therefore, it could

be involved in the recognition of the 4-keto group of the substrate. Replacing the Phe129 and Tyr138 in *S. enterica's* RmlC, which are usually found as Phe/Phe pair in other RmlC enzymes, DdahB and MlghB have His123 and Tyr132. Both residues could function for catalysis or for stacking reaction with the substrate (32, 54, 55). In *S. enterica's* RmlC, there is a second His120-Asp84 dyad with unknown function that is not conserved among other RmlC (46, 55). Conversely, in DdahB and MlghB the aspartic acid is substituted by Gln85 that is positioned in close location to interact with Asn121 through the amide group by a hydrogen bond (21, 63). This interaction could be important for catalysis (45, 46, 55). The residues Asn121, His67, Tyr134, Tyr132, and Lys74 have been targeted for mutagenesis to test their predicted function in catalysis.

3.2.2. Site-directed mutagenesis:

Five and six mutants were successfully generated for DdahB and MlghB respectively using a pET construct that was cloned previously in the lab, some of which were generated by other lab members as indicated in Table 3 (112). The table shows the rational of each mutant and the substituted amino acid. Asn121 that was predicted to recognize the substrate by binding to O4 was mutated into serine, which has a shorter side chain, lacks the amide group but has conserved polarity. For the His67, two mutants were generated. It was mutated into alanine, which has a non-functional side chain, or into asparagine to conserve the polarity (46). The Tyr134, as well as Tyr132, were mutated into phenylalanine to conserve the aromatic structure

and eliminate the hydroxyl function (46). Finally, Lys74 was mutated into alanine to eliminate the function of the side chain (46).

Table 2: Comparative functional analysis of the conserved residues in the epimerases binding site:

RmlC *St. suis*	Function (45)	RmlC *S. enterica*	Function (46, 55)	DdahB MlghB *C. jejuni*	Predicted function
H76	Catalytic. Acts like a base for epimerization at C3 and C5	**H63**	Catalytic. Acts like a base for epimerization at C3 and C5	**H67**	Catalytic for epimerization at C3 and C5
D180	His76-Asp dyad. Increases basicity of H76	**D170**	His63-Asp dyad. Increases basicity of H63	**D173**	Catalytic His67-Asp dyad.
Y140	Catalytic. The OH group is 3.7Å from C3 and 3.5Å from C5.	**Y133**	Catalytic. Proton donor for epimerization at C5 and not essential at C3	**Y134**	Catalytic for epimerization at C3 and C5
K82	Catalytic. Stabilizes the negative charge after deprotonation	**K73**	Catalytic. For epimerization at C3	**K74**	Catalytic for epimerization at C3
F36	Interact with thymidine ring.	**F27**	Interact with thymidine ring.	**I31**	Interact with thymidine ring.
Y145		**Y139**		**Y142**	
N63		**N50**		**K57**	
H29	Stacks against the ribose ring.	**F20**	Stacks against the ribose ring.	**F24**	Stacks against the ribose ring.
N127	Binds O4 (substrate recognition)	**H120**	Unknown. Could interact with O4	**N121**	Binds O4 (substrate recognition)
F129	Makes VDW interactions with C6 and O6. not conserved in all RmlC	**F122**	Unknown	**H123**	Interact with the sugar ring
Y138		**F131**	Unknown	**Y132**	Catalytic
G94	Unknown	**D84**	His120-Asp dyad. Unknown function	**Q85**	Catalytic. Possible interaction with N121 (63).

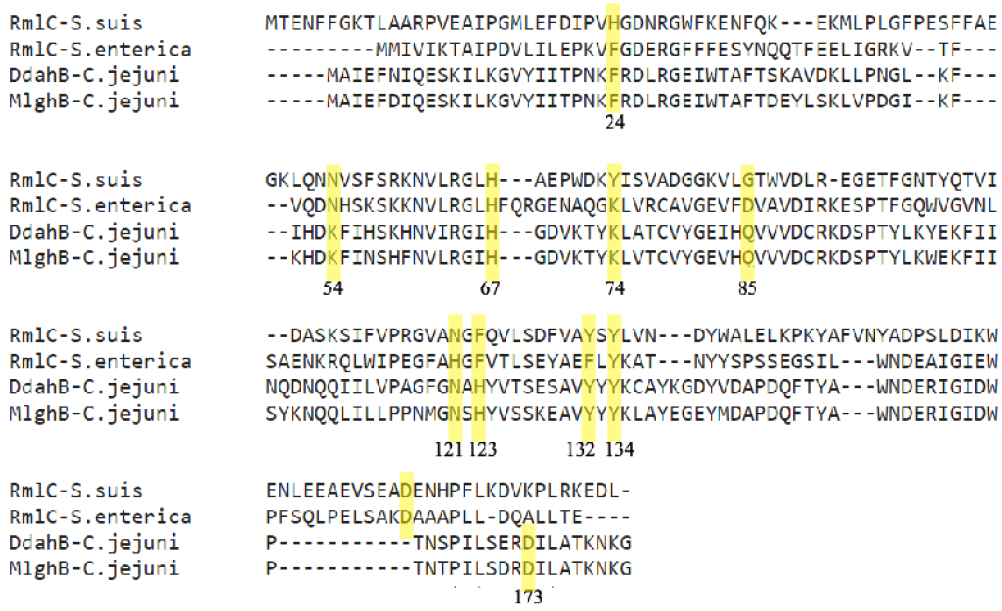

Figure 9: Protein sequence alignment of the epimerases. Alignment of both RmlC enzymes from *S. suis* and *S. enterica* with *C. jejuni* epimerases DdahB and MlghB sequences. The residues of interest are highlighted, and the numbering is for *C. jejuni* epimerases.

3.2.3. Structure modeling:

Since the experimental approaches could be unsuccessful and time consuming to solve the structure of some proteins, the structural modeling was used because it is a feasible approach to solve the molecular structure of DdhaB and MlghB.

The best template for DdahB and MlghB used for modeling from SWISS-MODEL workspace was within the highest QMEAN scoring templates (20). They were modeled on dTDP-6-deoxy-D-xylo-4-hexulose C3/C5 epimerase (RmlC) from *S. enterica* (PDB code 1DZR) (55). The resolution of the template is 2.17 Å. The overall structure of both DdahB and MlghB showed that they are dimeric and highly similar (Figure 10-A). Based on the structural alignment with RmlC, the sugar-nucleotide binding site is located in the accessible cavity between the β-sheets within each monomer (Figure 10-B). The residues in the binding site that are predicted to have a role in substrate binding or catalysis based on the comparative functional analysis have been represented in the model (45, 55).

The fact that DdahB can only epimerize at C3 in the same conditions as MlghB whereas MlghB can do either or both epimerization at C3/C5 suggests two hypotheses. The first is that DdahB could be lacking the catalytic residues that function for C5 epimerization. No significant difference between the conserved catalytic residues in DdahB and MlghB active site based on structural alignment. Furthermore, most of the non-conserved residues had small hydrophobic side chains. In fact, it has been shown previously in our lab that under prolonged incubation conditions and high concentration of DdahB, DdahB can perform limited C5

epimerization generating small amounts of the C5 and C3/C5 epimers. This means that it has the functional residues to perform C5 epimerization. The second hypothesis is that DdahB could have less flexible conformation of the active site than MlghB. Several studies have shown that homologous enzymes with conserved active site sequences can perform different catalysis (17, 53, 138). This feature was referred to as active site flexibility, which allows specific enzymes to perform specific functions based on the conformational changes that occur upon substrate binding or during the catalysis (89, 180).

To look for possibility of side chain conformational changes and compensation upon mutation, the mutants were also modeled. The mutants' models were obtained by modeling the mutated protein sequence in SWISS-MODEL rather than replacing the side chain in the modeled wild type enzyme. The wild type model was superimposed with each mutant model. Based on the superimposed structure, all mutants' models showed no differences in the highlighted residues' conformation compared to the wild type, except for two mutants of MlghB, Y134F and N121S. Both mutants showed changes in the orientation of Tyr132 (Figure 12). This indicates that Tyr132 could have a flexible orientation of its side chain.

Table 3: SDM list for the epimerases:

Epimerases	Mutation	Rational	Rational of the substitution choice
DdahB	N121S*	Substrate recognition (binds O4)	Shorter with no amide group and conserved polarity.
	H67A	Catalytic, inactivate.	No functionality.
	H67N	Catalytic, inactivate.	Conserved polarity
	Y134F **	Catalytic, inactivate.	Conserved structure with no functionality.
	K74A	Catalytic, inactivate.	No functionality.
MlghB	N121S*	Substrate recognition (binds O4)	Shorter with no amide group and conserved polarity.
	H67A*	Catalytic, inactivate.	No functionality.
	H67N	Catalytic, inactivate.	Conserved polarity with no charge.
	Y134F*	Catalytic, inactivate.	Conserved structure with no functionality.
	Y132F*	Catalytic, inactivate.	Conserved structure with no functionality
	K74A	Catalytic, inactivate.	No functionality.

*SDM done by Michael Roubakha, 2013

** SDM done by Chelsea Kubinec, 2015

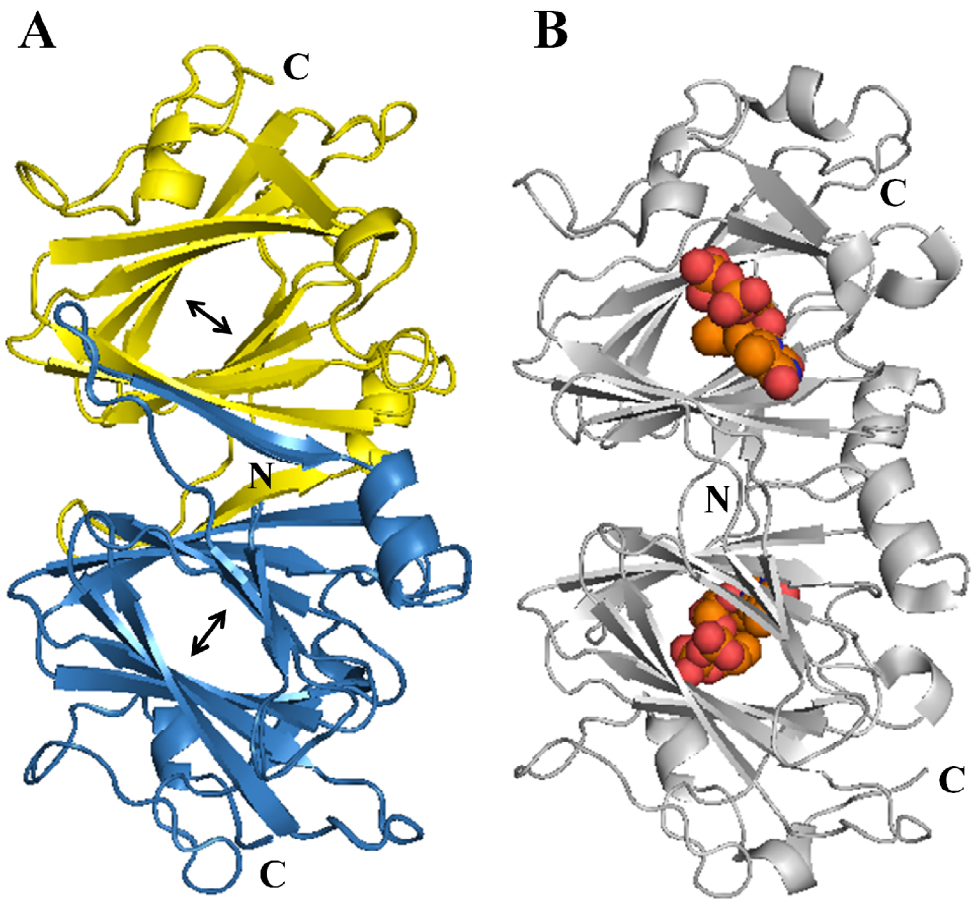

Figure 10: The tertiary and quaternary structure model for the epimerases compared to the crystallography structure of RmlC. A. Ribbon representation of the superimposed structure model for both DdahB and MlghB shown as a dimer where (A) monomer is in yellow and (B) monomer is in blue. N and C annotate the N and C termini respectively. The sugar-nucleotide binding site in both monomers is indicated by a double arrow. **B.** Ribbon representation of RmlC crystallography structure from *S. enterica* in gray ribbon with dTDP-phenol, a substrate analog, in orange spheres (PDB code 1DZR).

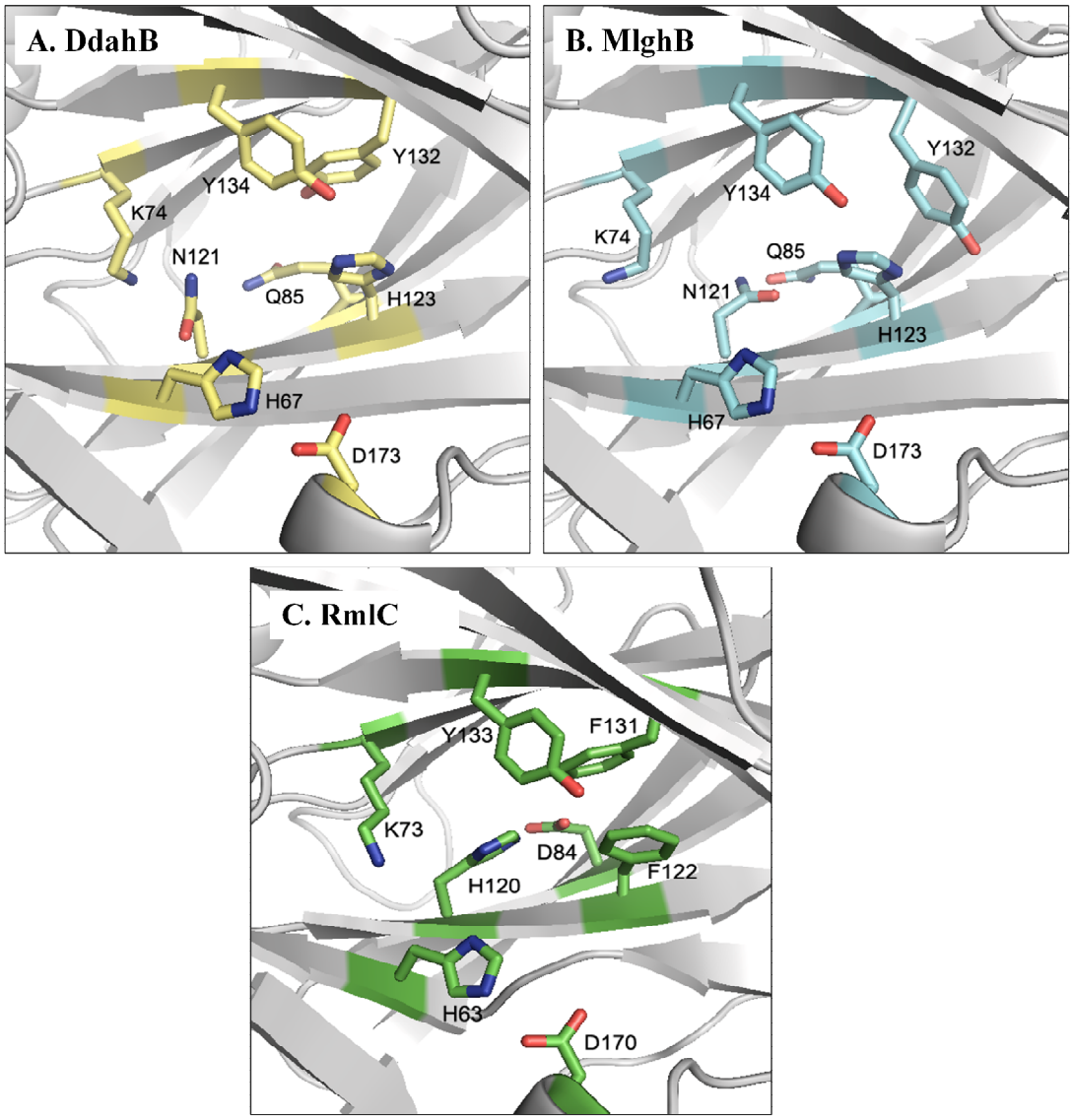

Figure 11: The epimerases binding site structure model compared to the binding site of RmlC. Ribbon and stick representation of the residues that are predicted to be involved in catalysis or substrate binding **A.** DdahB model **B.** MlghB model. No obvious differences were noted between the conserved residues in the binding site of both DdahB and MlghB. **C.** The binding site structure of RmlC from *S. enterica* (PDB code 1DZR).

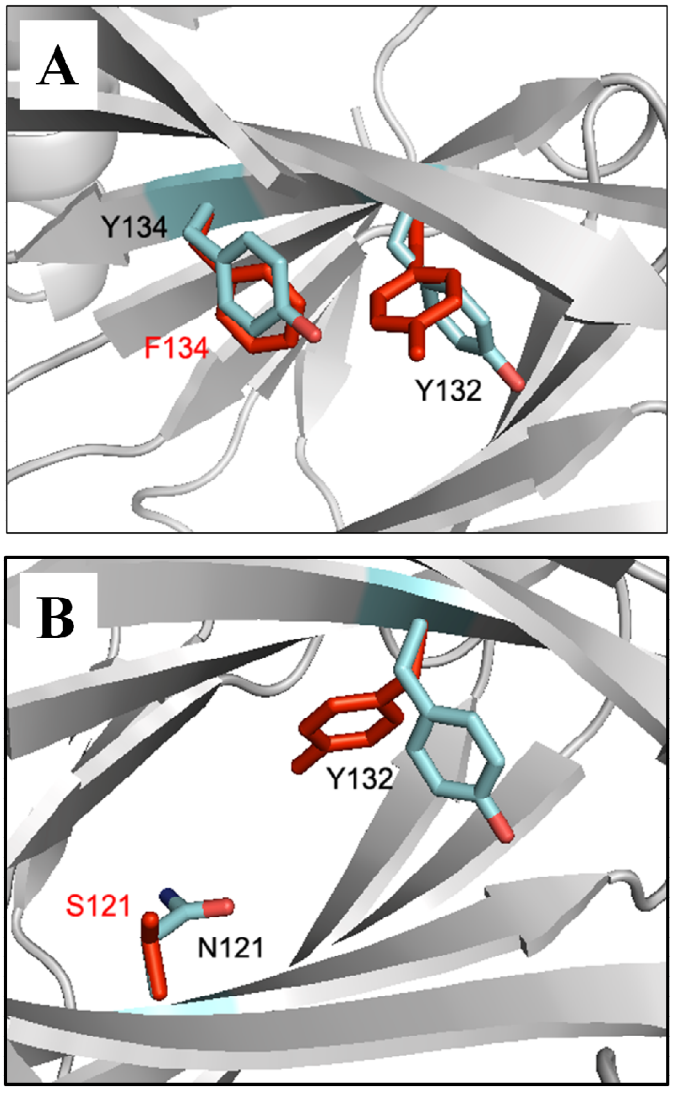

Figure 12: MlghB mutants structure model. Ribbon and stick representation of the superimposed structure of MlghB WT in cyan, and mutants in red. **A.** Change of Tyr132 orientation in Y134F mutant. **B.** Change of Tyr132 orientation in N121S mutant.

3.2.4. Crystallography:

The crystallography data was obtained from Laura Woodward (Dr. James Naismith, St. Andrews University, UK). Both DdahB and MlghB crystal structures are solved by molecular replacement using *S. enterica's* RmlC crystallography data. The resolution of DdahB and MlghB structures is 1.9 Å and 2.3 Å, respectively. There was no difference in the location and orientation of the conserved residues between DdahB and MlghB binding sites except for the Asp173, which could form a chemical dyad with His67 (Figure 13). In DdahB, Asp173 is conserved in the protein sequence but its location is not conserved. If this His67/Asp173 dyad is important for C5 epimerization, this may explain why DdahB cannot perform it like MlghB. By overlying the crystallography structure with the modeling by superimposing both structures , it can be concluded that the homology modeling approach is feasible to identify the overall structure of the enzymes active sites. However, the limitation is the slight inaccuracy of some side chains orientation, such as Tyr132, Tyr134, and Asn121. MlghB was co-crystallized with GDP-mannose as an analog substrate to identify the possible substrate binding residues (Figure 13-C) (Figure 15). The electron density map of the mannose ring was not included in the final structure because it can occupy a wide range of positions in the binding site resulting in a very low electron density map, but the GDP portion could be detected. MlghB/GDP-mannose co-crystal structure revealed the possible interaction of the residues highlighted in Table 2 with the substrate. In addition, it sheds light on residues that bind the GDP, Ile32, Tyr142, Lys54, and Phe24. Additional residues were identified including Asp144 and the N-terminus of the B monomer Met1 (Figure 15).

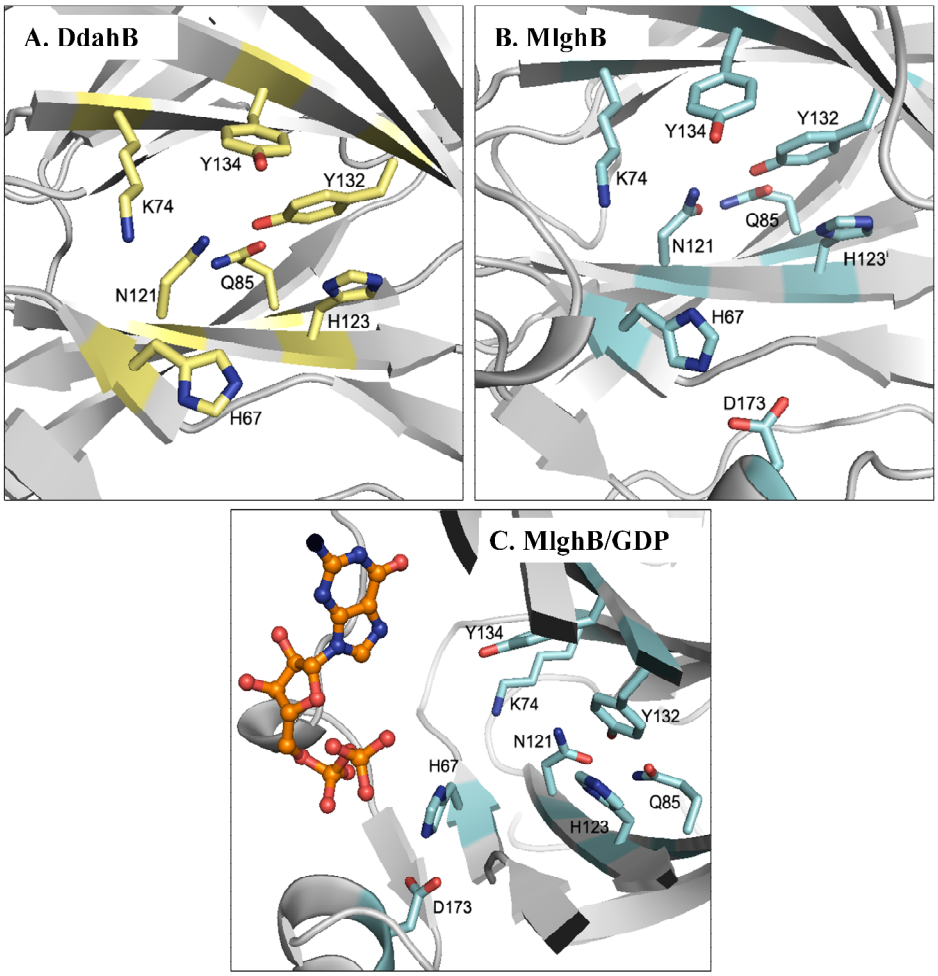

Figure 13: The epimerases binding site crystallography structure (Laura Woodward and Dr. James Naismith). Ribbon and stick representation of the residues in the sugar-nucleotide binding site. **A.** DdahB binding site. **B.** MlghB binding site. C. Side view of MlghB binding site with the GDP molecule in orange, showing the residues that could be involved in the catalysis and substrate binding.

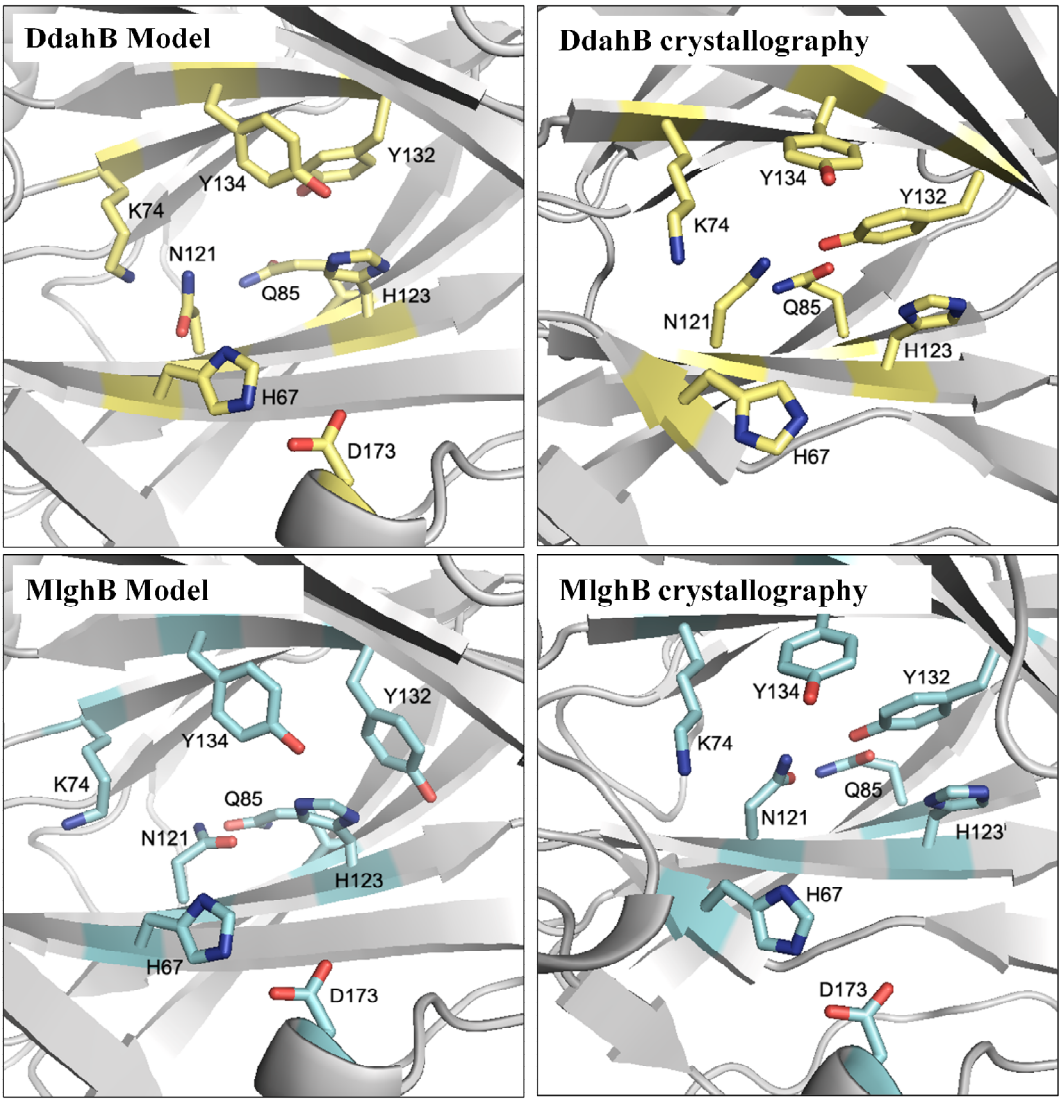

Figure 14: Comparison between the modeling and the crystallography structures of the binding site of the epimerases. The right panel shows the modeling while the left panel shows the crystallography structures (Laura Woodward and Dr. James Naismith) of DdahB and MlghB binding site. One of the differences observed is the DdahB Asp173 that is not conserved in location as shown in crystallography. The other difference is the orientation of the side chains of some residues.

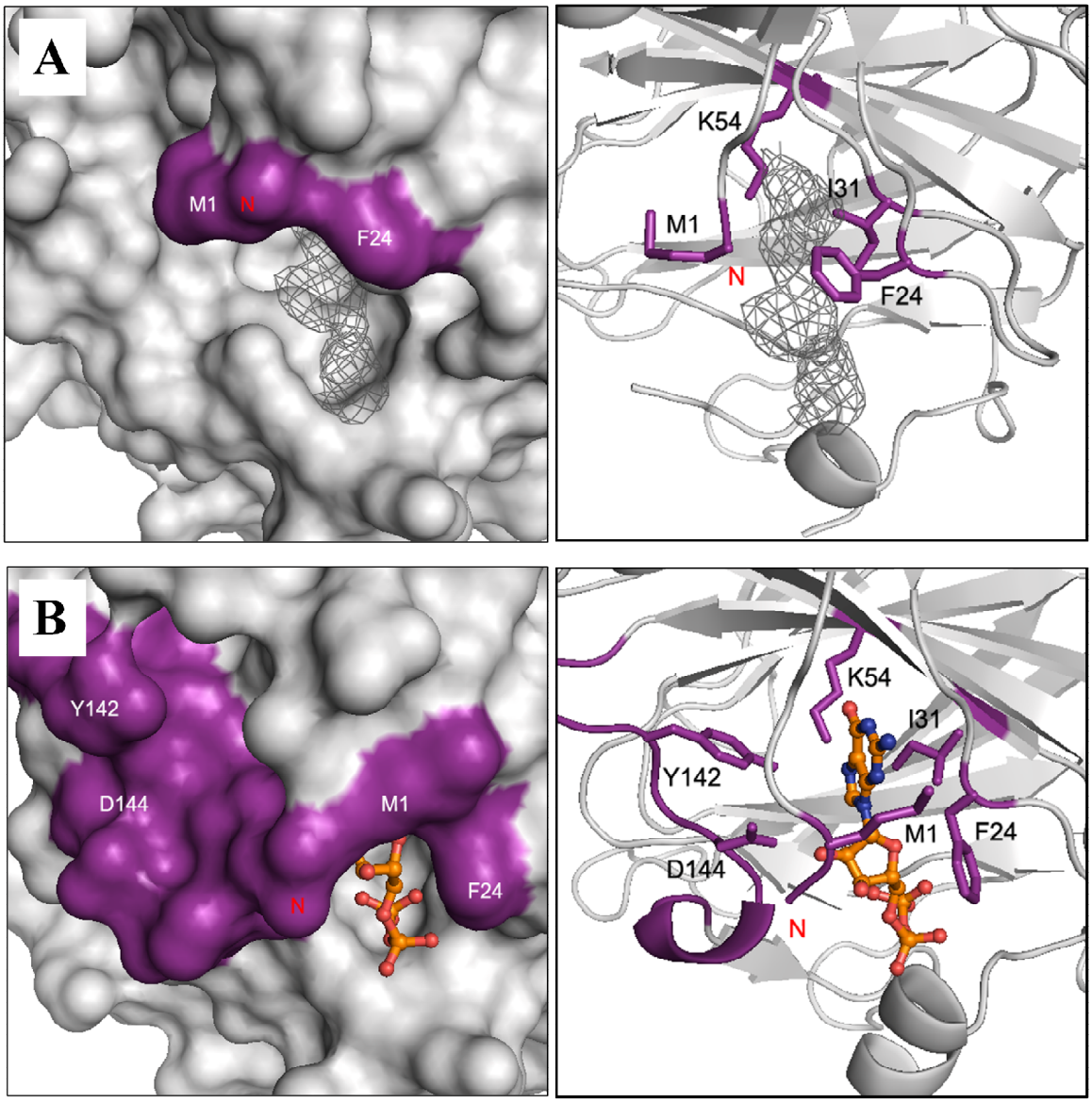

Figure 15: GDP binding in MlghB. The structure of MlghB and MlghB/GDP-mannose (Laura Woodward and Dr. James Naismith). **A.** MlghB structure docked with GDP-mannose electron density map in gray net. **B.** MlghB/GDP-mannose co-crystal structure. GDP molecule is in orange. The loop and the residues that are involved in GDP binding are in purple. N annotates the N-terminal end of MlghB.

3.3. Reductases comparative functional analysis and structure:

3.3.1. Comparative functional analysis:

The analysis of the active site of the C4 reductases, DdahC and MlghC, was based on the knowledge obtained from GFS, GDP-4-keto-6-deoxy-D-mannose C3/C5 epimerase, C4 reductase, from *E. coli* (99, 157, 158). The remarkable feature of GFS enzyme is its ability to catalyze three distinct reactions within a single active site to generate GDP-L-fucose. These include epimerizations at C3 and C5, as well as an NADPH-dependant reduction at C4 of the 4-keto substrate (99). The initial step is deprotonation at C3 from one face followed by reprotonation on the other face of the sugar ring to generate the first product. This product is then epimerized at C5 by deprotonation from one face and reprotonation from the other. Finally, an NADPH-dependant reduction converts the C3/C5 epimer into GDP-L-fucose by converting the C4 carbonyl into a hydroxyl group (99). Based on crystallography, GFS is a member of the short-chain dehydrogenase reductase (SDR) family (79). The substrate binding domain include a pocket forming hydrophobic residues to bind the GDP, Leu184, Val201, and Val180, as well as Trp202 that moves after the substrate binding to cover this pocket (99, 157). GFS possesses the catalytic triad, Ser107, Tyr136, and Lys140 (SYK), which is characteristic of SDR enzymes (79). Tyr136 protonates the C4 carbonyl during the reduction step (99). The Ser107 and Lys140 are important to lower the pKa of the catalytic Tyr136, which allows it to function as a general acid or base during catalysis (157). In addition, two catalytic residues that are not conserved among SDR members were identified by modeling coupled with mutagenesis, Cys109 and His179. Both

residues are implicated in the epimerization reaction (99). Other residues were predicted to interact with the sugar ring based on structural modeling, Ser108 and Asn165. However, their role in catalysis is unknown.

DdahC and MlghC are predicted to be C3/C5 epimerases and C4 reductases. However, based on biochemical studies conducted in our lab, it has been shown that they only perform the C4 reduction on the already epimerized 4-keto form of GDP-*manno*-heptose (111). Based on sequence alignment of *E. coli* GFS with *C. jejuni* reductases, DdahC and MlghC substrate binding domain contain the hydrophobic residue that make the GDP binding pocket, Ile185, Ile231, and Val181, as well as Trp232 that could be involved in covering the substrate after binding as observed in GFS (DdahC numbering). The substrate binding domain of DdahC possesses the same SYK catalytic triad that found in GFS, Ser108, Tyr137, and Lys141 (DdahC numbering). However, MlghB has both Lys140 and Ser107, but not the tyrosine residue of the triad (MlghC numbering). Instead, a phenylalanine was found based on the sequence alignment (Figure 16) (Table 4). Aligned with the His179 and Cys109 in GFS, which are predicted to be catalytic residues for the epimerization, DdahC has His180 and Thr110 while MlghC has Arg181 and Tyr109. The residues that are predicted to interact with the sugar ring are Asn166 and Thr109 in DdahC, Asn165 and Gly108 in MlghC. The hydrophobic guanidine pocket forming residues are found in both DdahC and MlghC. The sequence alignment also showed that there is an extra sequence of 29 amino acids in DdahC and MlghC not found in GFS, which could correspond to a specific structural motif (Figure 16).

It has been shown that DdahC and MlghC are highly specific in their choice of substrate, and both generate different products (111). The fact that the catalytic residues are not conserved between DdahC and MlghC suggests that they could be involved in the substrate and products specificity. Therefore, the catalytic residues in DdahC His180 and Thr110 have been targeted for mutagenesis to test their role in specificity. Although these residues are predicted to catalyze epimerization reactions, DdahC and MlghC do not perform epimerization reaction on their substrates (111). Thus, His180 and Thr110 could be only involved in substrate binding and specificity.

Table 4: Comparative functional analysis of the conserved residues in the reductases binding site:

GFS ***E. coli***	**Function (99)**	**DdahC** ***C. jejuni***	**MlghC** ***C. jejuni***	**Predicted function**
S107	Catalytic triad for reduction at C4	**S108**	**S107**	Catalytic triad in DdahC. **M110** instead of F136 in MlghB based on the structure.
Y136		**Y137**	**F136**	
K140		**K141**	**K140**	
C109	In suitable position as a general acid or base for the epimerization at C3 and C5.	**T110**	**Y109**	Catalytic
H179		**H180**	**R181**	
S108	Predicted to interact with the sugar ring	**T109**	**G108**	Interact with the sugar ring
N165		**N166**	**N165**	
L184	Hydrophobic pocket for the guanidine ring of the nucleotide	**I185**	**L184**	Hydrophobic pocket for the guanidine ring of the nucleotide
V201		**I1231**	**I230**	
V180		**V181**	**V180**	
W202		**W232**	**W233**	
G67	Unknown	**G68**	**C68**	Located close to the co-factor. Could be important for binding.

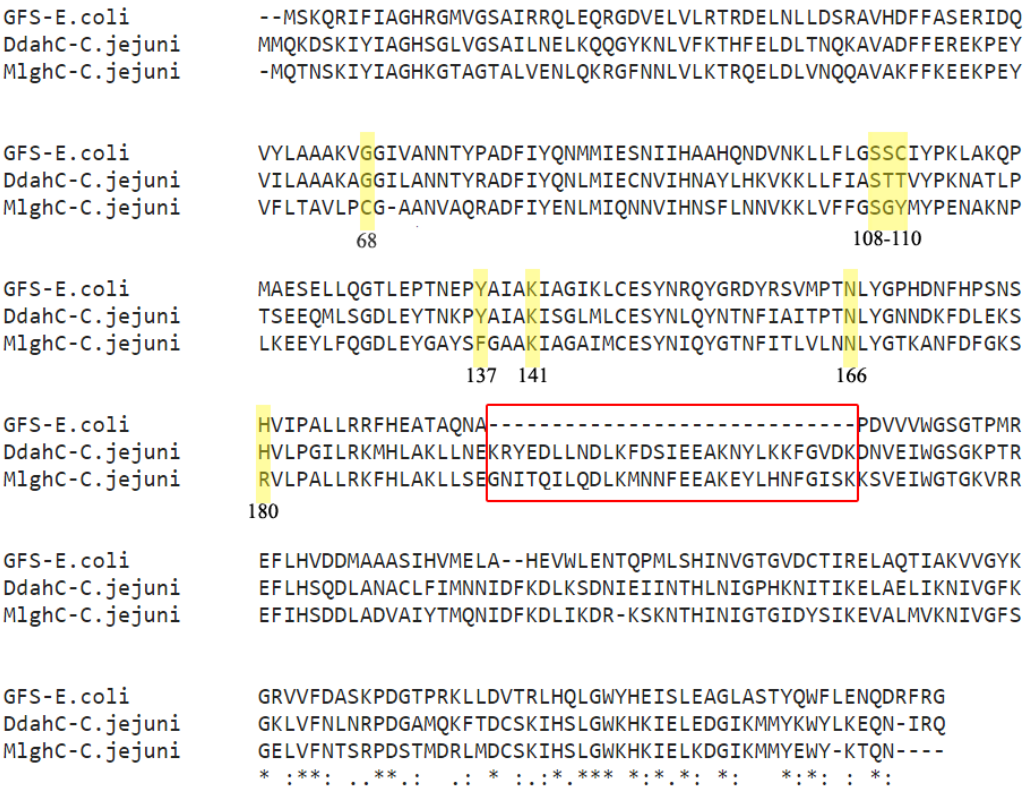

Figure 16: Protein sequence alignment of the reductases. Alignment of GFS from *E. coli* with *C. jejuni* reductases DdahC and MlghC protein sequence. The residues of interest are highlighted, and the numbering is for DdahC. In red box is the 29 amino acid sequence that is found in *C. jejuni* reductases but not in GFS.

3.3.2. Reductases structure modeling:

Within the highest QMEAN scoring templates for DdahC and MlghC, the GDP-4-keto-6 deoxy-mannose C3/C5 epimerase, C4 reductase GFS from *E. coli* was used as a template (PDB code 1BSV) (157). The resolution of GFS structure is 2.20 Å. Both reductases structures were similar to each other and existed as dimers (Figure 17). Nevertheless, there were unstructured loops that are not found in the GFS structure corresponding to the extra 29 amino acids sequence in both DdahC and MlghC. Based on the structural alignment with GFS, both DdahC and MlghC have two domains, the co-factor binding domain and the substrate binding domain. The co-factor binding domain was located by superimposing the structure with GFS/$NADP^+$ co-crystal structure (Figure 17-B). The residues that are predicted to catalyze or to bind the sugar ring in the binding site based on the functional analysis were highlighted (Figure 18).

Based on structural modeling, the catalytic triad is conserved in location in DdahC compared to GFS, while in MlghC the tyrosine is substituted by phenylalanine (Figure 18) (Table 4). There is no adjacent tyrosine in the active site that could function as an alternative. However, Met110 was found close enough to form Ser106, Met110, and Lys139 (SMK) catalytic triad that has been previously identified in a UDP-GlcNAc C6-dehydratase, C4-reductase, WpbM (Figure 18-B) (40). In WpbM, the methionine residue of the catalytic triad was shown to be essential for catalysis (40). In addition, a cysteine residue, C68 that could be important for catalysis was found hanging on a loop in close location to the active site in MlghC (Figure 18-B).

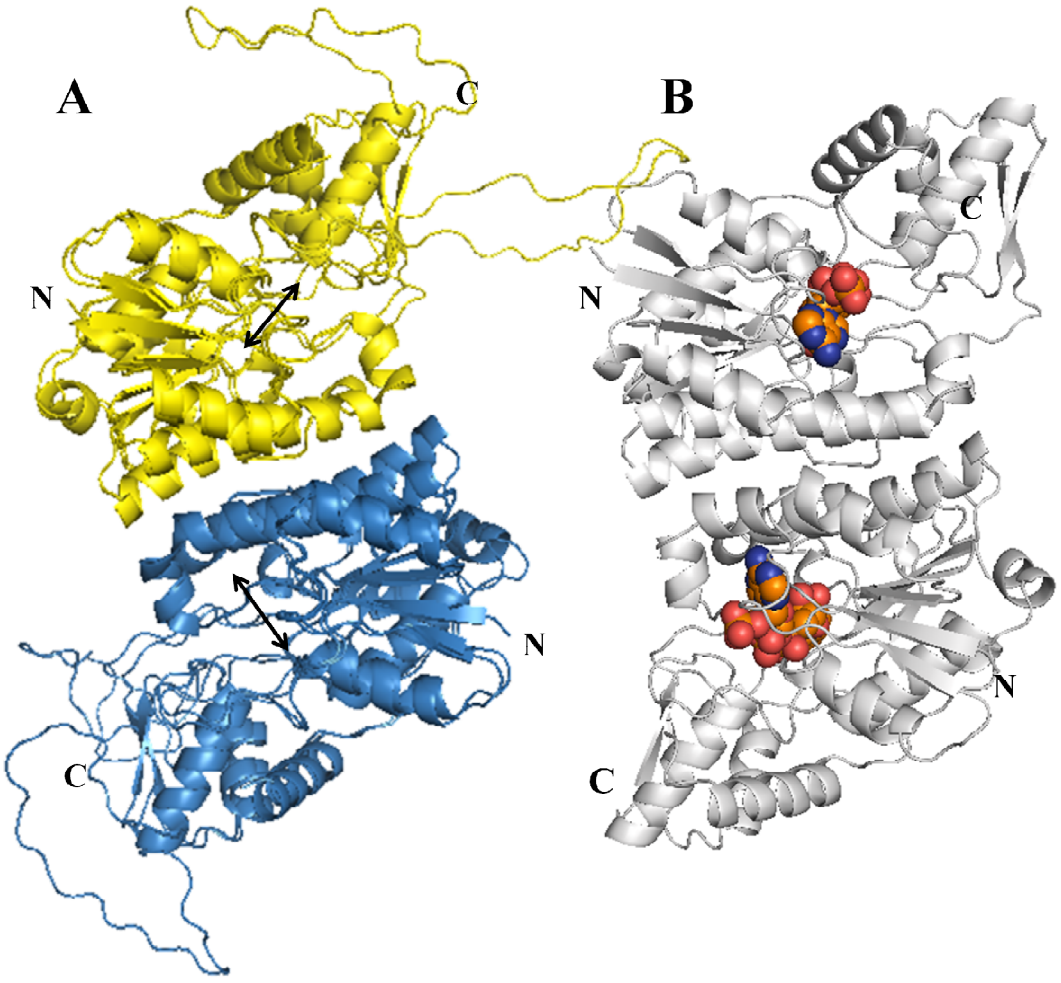

Figure 17: The tertiary and quaternary structure model for the reductases. A. Ribbon representation of the superimposed structure model for DdahC and MlghC. Showed as a dimer where (A) monomer in yellow and (B) monomer is in blue. N and C annotate the N and C termini respectively. The co-factor binding site in both monomers is indicated by a double arrow. **B.** Ribbon representation of GFS from *E. coli* in gray ribbon with the co-factor NADPH in orange spheres (PDB code 1BSV). DdahC and MlghC overall structure resemble GFS structure except the unstructured loops.

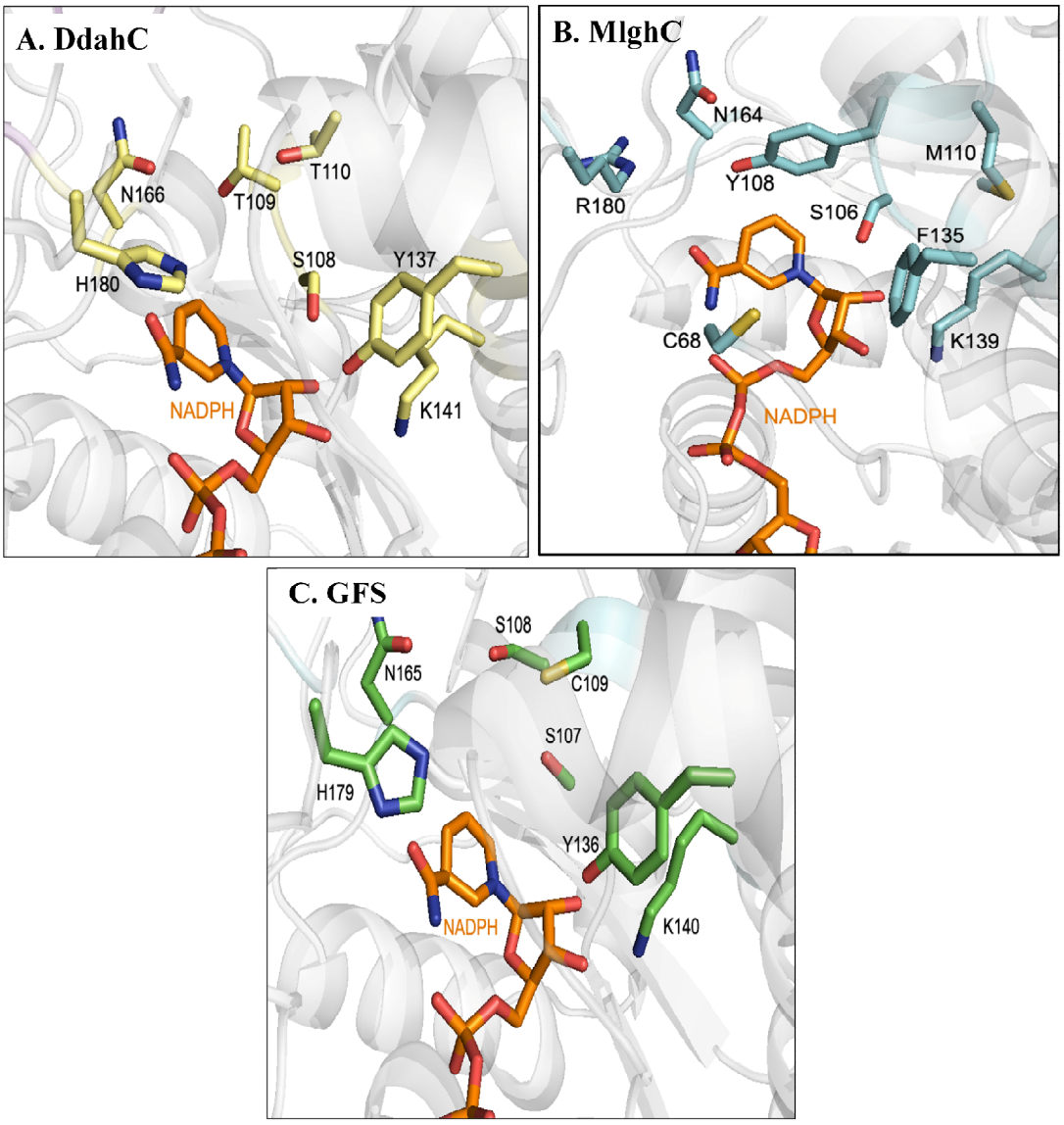

Figure 18: The reductases binding site structure model compared to the binding site of GFS. Ribbon and stick representation of the residues that are predicted to be involved in catalysis or substrate binding **A.** DdahC model superimposed with NADPH molecule of GFS structure. **B.** MlghC model superimposed with NADPH molecule of GFS structure. **C.** GFS/NADPH co-crystal structure from *E. coli* (PDB code 1BSV). DdahC resembles GFS binding site more than MlghC.

3.3.3. Site-directed mutagenesis:

For DdahC, four mutants were planned, three of which were generated by a previous lab member. T110C mutant was generated to mimic GFS activity. H180R and the double mutant H180R/T110Y mutants were generated to mimic MlghC activity. Several attempts made to generate the single T110Y mutant failed. However, it will be generated using reverse mutagenesis on the H180R/T110Y template to revert the mutated His180. For MlghC, only one mutant was planned and generated, C68A, to test the function of the cysteine in catalysis (Table 5).

Table 5: SDM list for the reductases:

Reductases	Mutation	Rational	Rational of the substitution choice
DdahC	T110C	Catalytic, testing specificity	Mimic GFS catalysis
	H180R	Catalytic, testing specificity	Mimic MlghC catalysis
	H180R/T110Y		
	T110Y*		
MlghC	C68A	Unknown function	No functionality

All mutations in this table were made by Michael Roubakha, 2013

* Is to be generated.

3.4. Protein expression and purification:

The GDP-*manno*-heptose modifying enzymes, wild type and mutants, were successfully purified using affinity chromatography purification (Figure 19). The concentrations of the enzymes obtained by Bradford assay were optimized to have equal concentration of the wild type and mutants as shown in Figure 19-D.

3.5. Epimerases enzymatic assays and kinetics:

The enzymatic activity was tested for the wild-type and mutants of DdahB (N121S, H67A, and H67N) and MlghB (N121S, H67A, H67N, and Y134F) at the same enzymes concentrations following previously established conditions. The activity was tested on GDP-*manno*-heptose (kindly provided by Dr. Creuzenet) to see if the mutants fulfill their purpose of inactivating the enzyme if they are indeed catalytic residues. In addition, they were tested on GDP-mannose substrate, which is a hexose-based sugar nucleotide. Since our prediction for the residues' function is based on the structural modeling and the comparison to enzymes that use hexose-based substrate, it is important to test the activity on such substrate. This analysis allows us to identify the residues that are specific to GDP-*manno*-heptose modification.

3.5.1. Epimerases reactions on GDP-*manno*-heptose:

The activity of DdahB and MlghB wild type and the mutants was tested in three independent experiments using two different purified enzymes stocks. For the mean data of the three experiments' integrations for DdahB and MlghB activity on GDP-*manno*-heptose see Appendix 4.

Based on the *in vitro* pathway of GDP-*manno*-heptose modification, DdahB epimerizes P1 at C3 to generate one product, which is P4α (Figure 20-A1). The DdahB N121S mutant that was generated to investigate the function of the Asn in the substrate recognition and thus in the catalysis showed no significant difference compared to the wild type (Figure 21-A2). However, H67A and H67N mutants, which were predicted to be catalytically inactive had produced P4α, but significantly less than the wild-type ($p < 0.001$) (Figure 21-A2).

On the other hand, MlghB is known to generate P4α, P4β, and P4γ by C3, C5, and C3/C5 epimerization respectively as observed for the MlghB wild type (Figure 21-B1). There is an inter conversion between the substrate P1 and MlghB products toward P1 and P4γ. MlghB N121S mutant generated the same products with no significant difference to the wild type (Figure 21-B2). The histidine mutants of MlghB, H67A and H67N were unable to epimerize at C5 (no P4β or P4γ), but they could generate the C3-epimer (P4α), although significantly less than the wild type ($p < 0.001$). The MlghB Y134F mutant that was predicted to be catalytically inactive produced all the three products, although significantly less P4α and P4β ($p < 0.001$ and $p < 0.01$), respectively.

The kinetics of DdahB and MlghB were measured for the wild type and the mutants for four time points. Due to the high efficiency of the enzymes, most of the products were at their maximum production yield in 5 minutes with no further changes at later time points (Figure 22). This experiment is to be repeated using lower enzymes concentration to highlight the differences between the wild type and the mutants' kinetics. Nevertheless, the results were interpreted from the currently available data set

represented in Figure 22 with regards to differences in maximum product formation. For DdahB C3-epimerization (P4α), N121S mutant seemed to have no significant difference compared with the wild type (Figure 22-A). Both His67 mutants were significantly less active. For MlghB C3-epimerization (P4α production), N121S mutant was 10% less active than the wild type during the 20 min (Figure 22-B). Bothe MlghB His67 mutants, as well as Y134F were significantly less active than the wild type. For MlghB C5 and C3/C5-epimerization (P4β and P4γ production), N121S mutant was comparable to the wild type. The Y134F mutant was almost inactive and was very slow. No P4β or P4γ were detected for the His67 mutants.

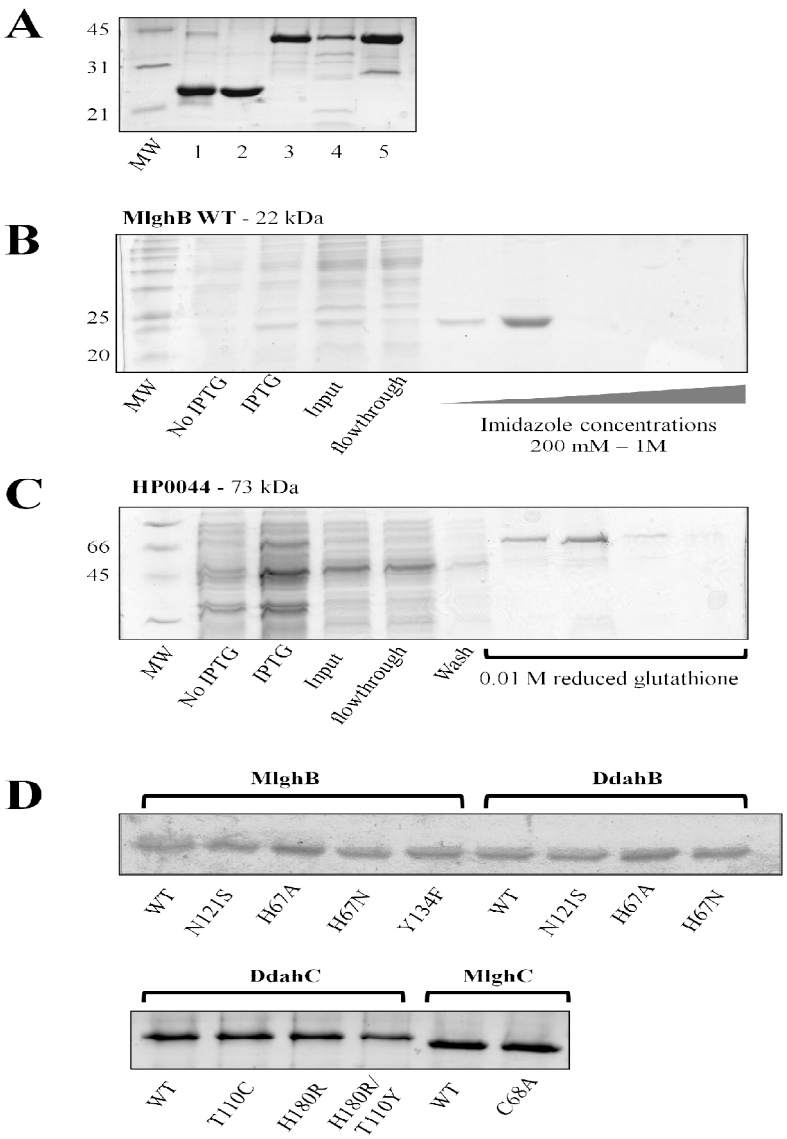

Figure 19: SDS-PAGE analysis of the purified GDP-*manno*-heptose modifying enzymes. A. Purified GDP-*manno*-heptose modifying enzymes. From 1 to 5 showing, DdahB (22 kDa), MlghB (22 kDa), DdahC (40 kDa), MlghC (41 kDa), and DdahA (40 kDa) respectively. **B.** An example of the affinity chromatography purification of the His-tagged proteins. **C.** Purification of the GST-tagged HP0044 (73 kDa) by GSTrap FF column. **D.** Optimized concentrations for the epimerases and reductases. All gels were stained with Coomassie blue.

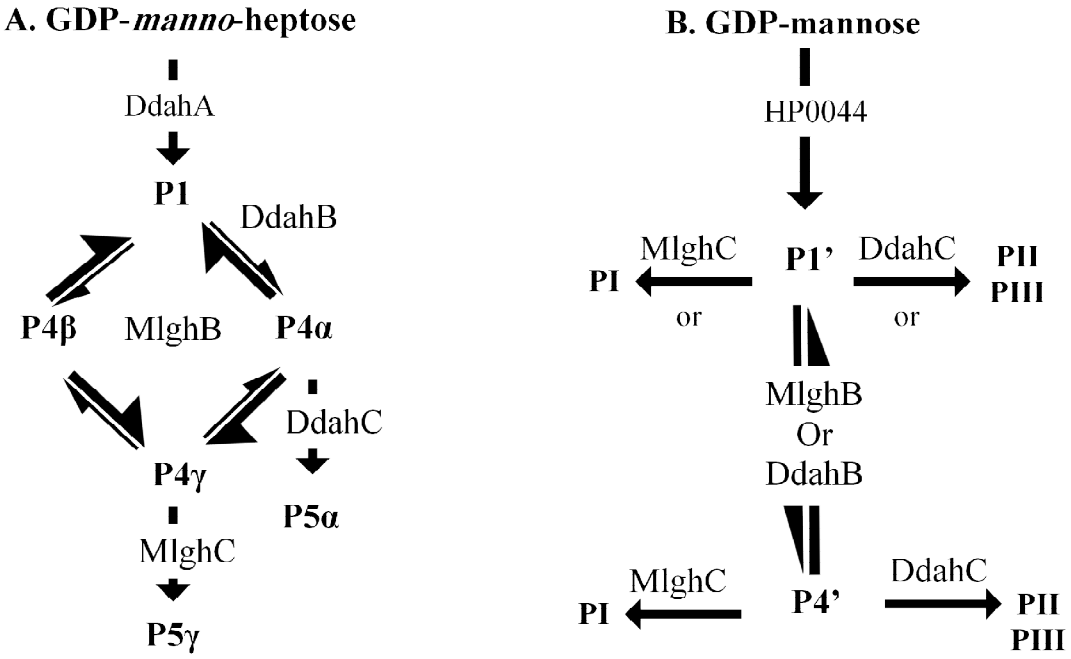

Figure 20: *In vitro* experimental pathways for GDP-*manno*-heptose and GDP-mannose modification. A. GDP-*manno*-heptose is dehydrated by DdahA generating P1. DdahB epimerizes P1 at C3 to generate P4α in equilibrium. MlghB epimerizes P1 at C3 giving P4α, at C5 giving P4β, and at both C3 and C5 giving P4γ. The two directions arrows indicate interconversion in MlghB reaction preferably towered P1 and P4γ. DdahC reduces P4α at C4 to generate P5α. MlghC reduces P4γ at C4 to generate P5γ. **B.** GDP-mannose is dehydrated by HP0044 to generate P1'. MlghB generates P4' in equilibrium by epimerization at unknown location. DdahC produces two products, PII and PIII, from P1' or P4'. MlghC produces only PI from either P1' or P4'.

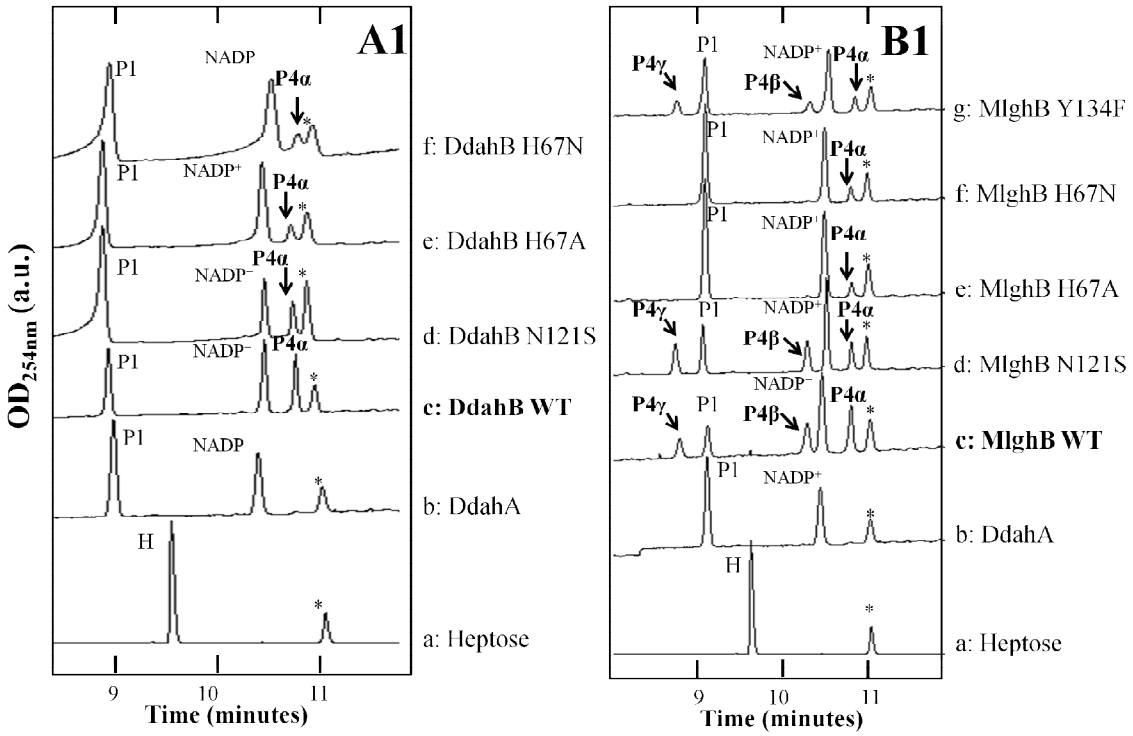
A1
B1
NADP
NADP+
NADP−
P1
P4α
P4β
P4γ
H
f: DdahB H67N
e: DdahB H67A
d: DdahB N121S
c: DdahB WT
b: DdahA
a: Heptose
g: MlghB Y134F
f: MlghB H67N
e: MlghB H67A
d: MlghB N121S
c: MlghB WT
b: DdahA
a: Heptose
OD254nm (a.u.)
Time (minutes)
9
10
11

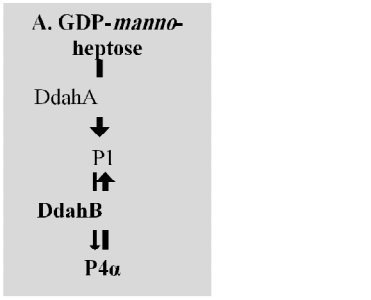
A. GDP-manno-heptose
DdahA
P1
DdahB
P4α

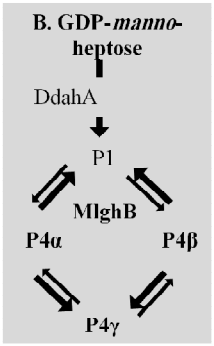
B. GDP-manno-heptose
DdahA
P1
MlghB
P4α
P4β
P4γ

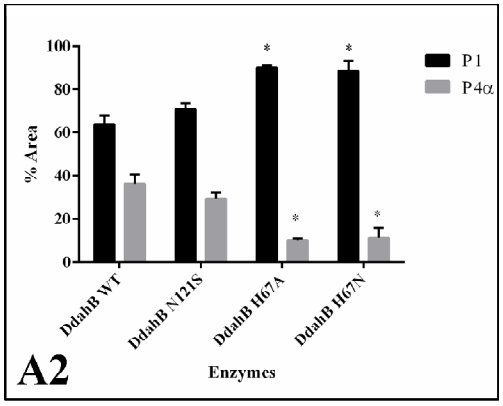
A2
% Area
P1
P4α
DdahB WT
DdahB N121S
DdahB H67A
DdahB H67N
Enzymes

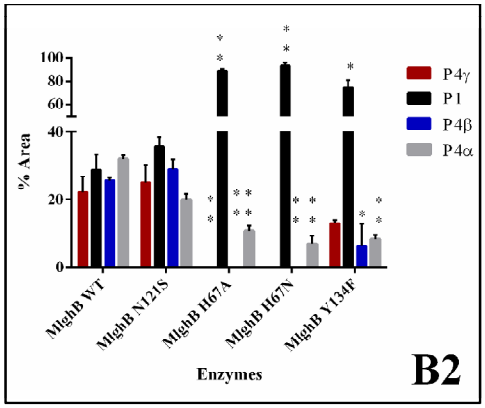
B2
% Area
P4γ
P1
P4β
P4α
MlghB WT
MlghB N121S
MlghB H67A
MlghB H67N
MlghB Y134F
Enzymes

Figure 21: CE electropherograms and peaks percentage areas highlighting the activity of the epimerases, wild type and mutants, on GDP-*manno*-heptose. The electeropherograms are example of one of the experimental repeats. For both panels (A1 and B1), a base reaction (trace b) containing 0.17 mM P1 was prepared by incubating the GDP-*manno*-heptose (trace a) with 1.5 µmol DdahA and 0.13 mM $NADP^+$ as an internal standard. **A1.** The activity of 1.0 pmol DdahB wild-type and mutants on P1 for 30 minutes. **B1.** The activity of 1.0 pmol MlghB wild-type and mutants on P1 for 30 minutes. The specific products are highlighted in bold. * denotes a small impurity present in the heptose preparation. Illustrative cartoon for the experimental pathway in the grey box. Panels (**A2** and **B2**) shows the peaks percentage areas of DdahB and MlghB products for three independent experiments. * indicates ($p < 0.01$) and ** indicates ($p < 0.001$). Statistics were done using T-test.

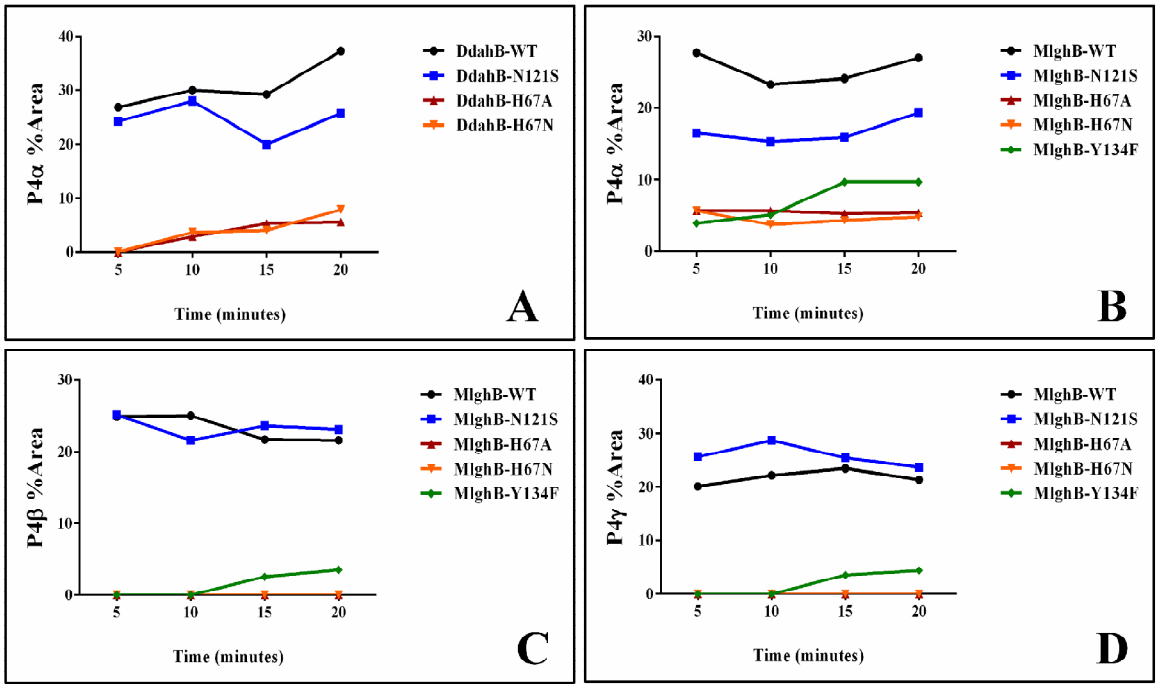

Figure 22: Kinetics of the wild type epimerases and mutants' activity on GDP-*manno*-heptose. The graphs represent the percentage area of the product to the total area per reaction (Y-axis) for four time points over 20 minutes (X-axis) **A.** DdahB C3-epimerization (P4α). **B.** MlghB C3-epimerization (P4α). **C.** MlghB C5-epimerization (P4β). **D.** MlghB C3/C5-epimerization (P4γ). Each reaction contains 0.17mM substrate and 1.0 pmol enzyme. After Incubation, the samples were snap frozen in dry ice/ethanol at each time point and analyzed by CE. (Preliminary experiment). To be repeated with lower enzymes concentration to avoid the equilibrium at the first time point.

3.5.2. Epimerases reactions on GDP-mannose:

It was established previously in our lab that the GDP-*manno*-heptose modifying enzymes act less efficiently on GDP-mannose substrate than on GDP-*manno*-heptose (111). DdahA that was used as the dehydratase to generate the 4-keto substrate for the epimerases from GDP-*manno*-heptose has a very poor activity on GDP-mannose, as longer incubation and higher enzyme concentration is needed to generate the 4-keto product (110). Therefore, HP0044, a GDP-mannose dehydratase from *Helicobacter pylori*, was used due to its high efficiency in the formation of P1' (31). Based on the preliminary pathway for GDP-mannose, MlghB and DdahB can generate one single and identical product (P4') but with different efficiencies (Figure 20-B). MlghB formation of P4' is in equilibrium with P1'. P4' could be an epimerized product, but the epimerization status and location onto P4' are unknown. Two hypotheses can be proposed. The first hypothesis is that P4' is a C3 epimer, because both MlghB and DdahB can perform C3-epimerization, thus generating the same product. However, the single C3-epimerization is only proven for the heptose substrate, and MlghB and DdahB could function differently on a hexose-based substrate. The second hypothesis is that P4' could be a double epimer, similar to RmlC, which releases a single product, a C3/C5 epimer from a hexose-based substrate. However, this requires both DdahB and MlghB to perform C3/C5 epimerization. Unfortunately, P4' cannot be identified by mass spectrometry because of its unstable nature as a 4-keto sugar.

In this analysis, the activity of the DdahB and MlghB wild type and mutant are tested on P1' that is the dehydrated form of GDP-mannose in two independent experiments using two different purified enzymes stocks. For the mean data of the two experiments' integrations for DdahB and MlghB activity on GDP-mannose see (Appendix 5). GDP-mannose was incubated with HP0044 to generate P1' as well as either DdahB or MlghB wild type or mutants. MlghB reactions are incubated for one hour. The results showed that MlghB N121S mutant generated the same product as the wild type with no significant difference (Figure 23-B1,B2). However, H67A and H67N were catalytically inactive. Y134F mutant was significantly less active than the wild-type, but generated the same P4'($p < 0.01$) (Figure 23-B2).

The kinetics showed that at later time points, the N121S mutant produced slightly more P4' than the wild-type, and the Y134F mutant produced almost the same amount of P4' as the wild type but in a slower manner (Figure 24-A). The product degradation was measured during the kinetics and showed equal degradation in the wild type and the mutants' reactions (Figure 24-B). This indicates that the differences in P4' formation between the wild type and the mutants was due to the mutation rather than the degradation of the substrate. After 5 hours, 50% of the substrate was degraded. The activity of the wild type MlghB on GDP-mannose substrate was slower and less efficient than its activity on GDP-*manno*-heptose, which suggests that MlghB possesses specificity toward GDP-*manno*-heptose.

The activity of DdahB was tested with five times the enzyme concentration and five times longer incubation time (5 hours) compared to MlghB. The wild-type had very little activity, and activity was almost undetectable for the DdahB mutants (Figure 23-A). No kinetics was performed for DdahB on GDP-mannose due to the insufficient product formation and the high substrate degradation observed over time. In contrast to the efficient activity of DdahB on GDP-*manno*-heptose substrate, DdahB had undetectable activity on GDP-mannose even at higher enzyme concentration. This difference indicates that DdahB has specificity to GDP-*manno*-heptose rather than GDP-mannose.

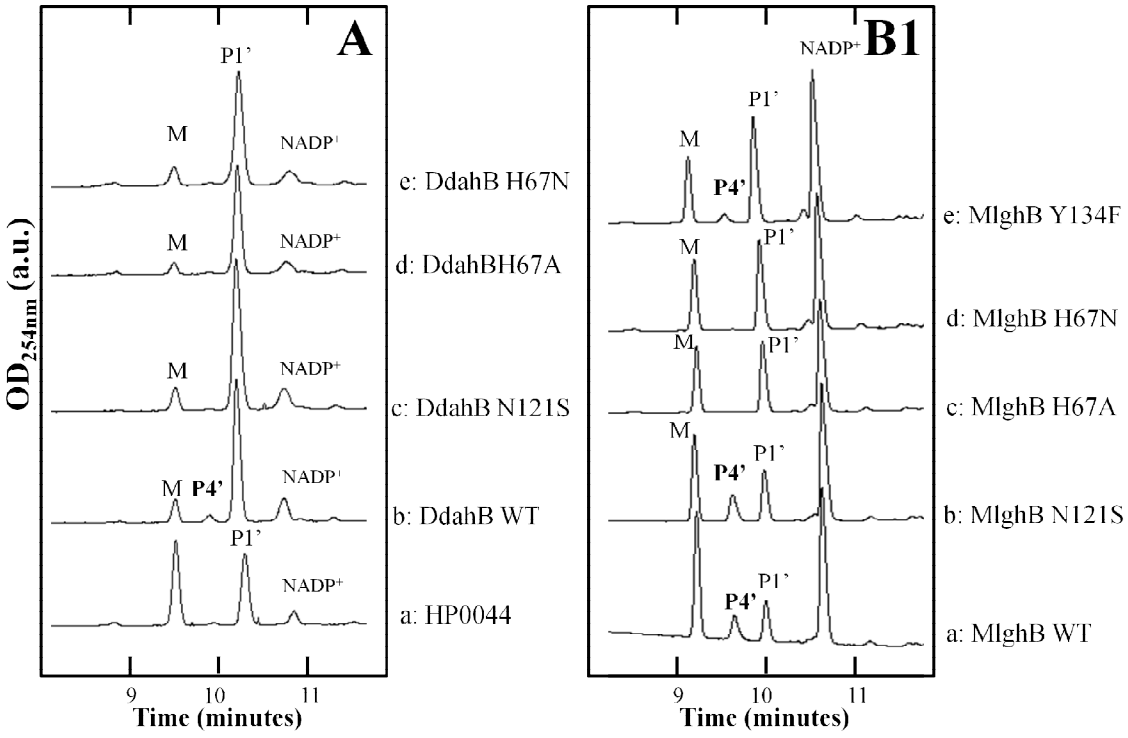

A. GDP-mannose
↓
HP0044
↓
P1'
5X DdahB
↓
P4'

B. GDP-mannose
↓
HP0044
↓
P1'
MlghB
↓
P4'

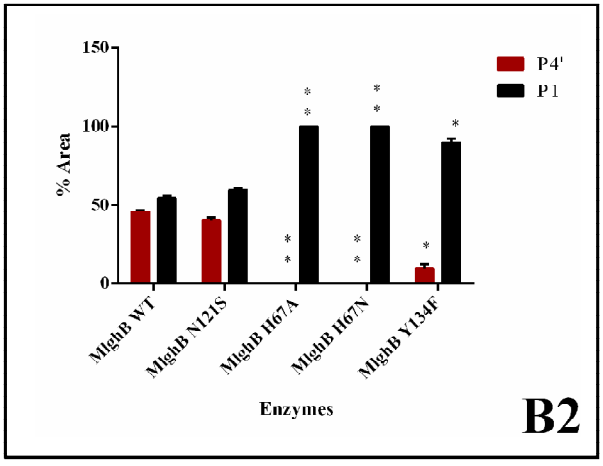

Figure 23: CE electropherograms and peaks percentage areas highlighting the activity of the epimerases, wild type and mutants, on GDP-mannose. The condition of the reactions and incubation times are different between DdahB and MlghB. **A.** The activity of 5.0 pmol of the wild type DdahB and the mutants on P1' after 5 hours incubation at 37°C. To generate P1', a base reaction containing 0.77mM GDP-mannose, 2.0 pmol HP0044, and 0.1 mM $NADP^+$ was incubated at 37°C for 90 minutes (trace a). **B1.** The activity of 1.0 pmol of the wild type MlghB and the mutants on P1' after one hour incubation at 37°C. To generate P1', a base reaction containing 0.77mM GDP-mannose, 2.0 pmol HP0044, and 0.5 mM $NADP^+$ was incubated at 37°C for 90 minutes. $NADP^+$ was used as an internal standard. Illustrative cartoon for the experimental pathway in the grey box. **B2.** Shows the peaks percentage areas of MlghB products for two independent experiments. * indicates ($p < 0.01$) and ** indicates ($p \leq 0.001$). Statistics were done using T-test.

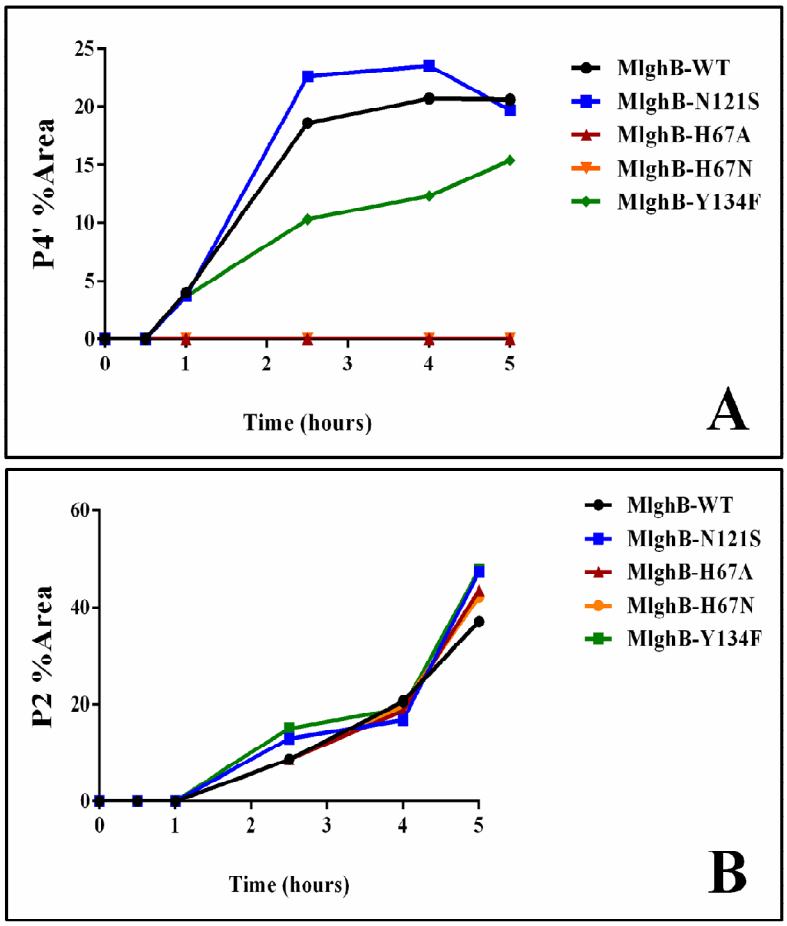

Figure 24: Kinetics of MlghB wild type and mutants' activity on GDP-mannose. The graph represents the percentage area of the product to the total area per reaction (Y-axis) for four time points over 20 minutes (X-axis). Each reaction contains 0.4mM substrate and 1.0 pmol enzyme. After Incubation, the samples were snap frozen in dry ice/ethanol at each time point and analyzed by CE. **A.** The kinetics of P4' formation by the wild type MlghB and the mutants. **B.** The degradation of the substrate over time (P2). The substrate was equally degraded in the wild type and the mutants' reaction to 50% at the end of the kinetics. (Preliminary experiment). To be repeated to confirm the kinetics differences detected between the wild type and the mutants.

3.6. Reductases enzymatic assays and kinetics:

The activity and the substrate specificity of the reductases were tested for DdahC (T110C, H180R, and H180R/T110Y) and MlghC (C68A) compared to the wild type on heptose or mannose-based substrates. The epimerized products of the dehydrated GDP-manno-heptose, P4α, P4β, and P4γ, were used as substrates to test the specificity of the mutated reductases. On the other hand, both the dehydrated (P1') and the epimerized (P4') forms of GDP-mannose were used as substrates to test the activity and product formation of the wild type. This analysis was performed to test the involvement of the mutated residues in either the activity or the substrate specificity of the reductases. It was also done to determine if the reductases would function differently on a mannose-based substrate rather than their heptose substrate.

3.6.1. Reductases reactions on GDP-*manno*-heptose:

The epimerized products of the GDP-6-deoxy-D-*altro*-heptose, P4α, P4β, and P4γ, were generated using MlghB, which can generate them in equilibrium, to test the activity and the substrate specificity of the reductases mutants. The activity and the substrate specificity of DdahC and MlghC have been established previously (111). Although they were predicted as C3/C5-epimerases, C4 reductases, they only perform NADPH-dependent reduction of their epimerized substrates at C4 generating different products. DdahC reduces the C3-epimer (P4α) into P5α, which is the end product of GDP-*manno*-heptose modification pathway in *C. jejuni* 81-176. MlghC reduces the C3/C5-epimer (P4γ) to generate P5γ.

The general activity of DdahC and MlghC mutants was tested in two independent experments. For data integration see Appendix 6. No statistics were done for the reductases activity on GDP-*manno*-heptose because no repeats were done for each of the two experiments because the experimental conditions were different. The first experment was done using a reaction where MlghB was still available in the mix to continuously generate the three epimerized substrates throughout the reaction. The activity was interpreted from the formation of the reduced product, and the conversion of NADPH into $NADP^+$. DdahC mutants, T110C generated 50% more P5α than the wild type with total conversion of NADPH. H180R mutant had the same production of P5α as the wild type (Figure 25-A). However, the double mutant H180R/T110Y was catalytically inactive. On the other hand, MlghC C68A had 10% lower activity than the wild type in the formation of P5γ with total conversion of NADPH into $NADP^+$ (Figure 25-A). Despite the differences in the activity, the active mutants were able to generate the specific product just like the wild type, indicating that there is no change in the specificity of the products formed. However, the substrate specificity cannot be interpreted from this experiment set because all the substrates are being resupplied from P1 by MlghB that was still in the reaction.

The second experiment was done using a reaction where MlghB was ultrafiltered after the generation of the three epimerized substrates, P4α, P4β, and P4γ to test the reductases mutants' substrate specificity. The T110C mutant of DdahC showed more P5α formation than the wild type with an increase in $NADP^+$ (Figure 25-B). H180R showed slightly less activity than the wild type. H180R/T110Y was catalytically inactive.

Changes in P4α were undetectable compared to the MlghB control reaction (Figure 25-B, trace a). Unfortunately, the MlghB control trace was obtained from an aliquot withdrawn before the ultrafiltration, which results in further interconversion of P4α into P1 as shown by the integration. Therefore, we could not interpret differences in the substrate utilization by the reductases by using MlghB reaction as a control. However, we used the inactive mutant H180R/T110Y reaction as a virtual control. A slight decrease in P4α was observed in the wild type DdahC and the active mutants, while a corresponding increase in P5α was observed. More decrease in P4α level was observed for T110C mutants as a result of the formation of more P5α. No change was observed in P4γ for all DdahC mutants. P4β was undetectable because it usually migrates with $NADP^+$. For MlghC, the C68A mutant was less active than the wild type and showed the same substrate specificity as the wild type. A decrease in P4γ upon formation of P5γ was observed for MlghC wild type and C68A mutant, indicating that there is no change in the substrate specificity for the mutant.

The kinetics of the wild type DdahC and MlghC were performed in the same way where MlghB was ultrafiltered from the reaction before adding the reductases. The results are interpreted as percentage of the products area to the total area of the product and substrate (Figure 26). With regards to the activity of DdahC and MlghC mutants, the results confirmed that T110C mutant was two times more active than the wild type, while H180R showed no difference. The double mutant H180R/T110Y was inactive even with longer incubations (Figure 26-A). The kinetics showed that the gradual increase in P5α formation is related to a gradual reduction in P4α, meaning that there was no change in

the substrate specificity of DdahC mutants. On the other hand, MlghC C68A mutant had comparable activity to the wild type at early time points but less activity after an hour of incubation with no change substrate specificity (Figure 26-B).

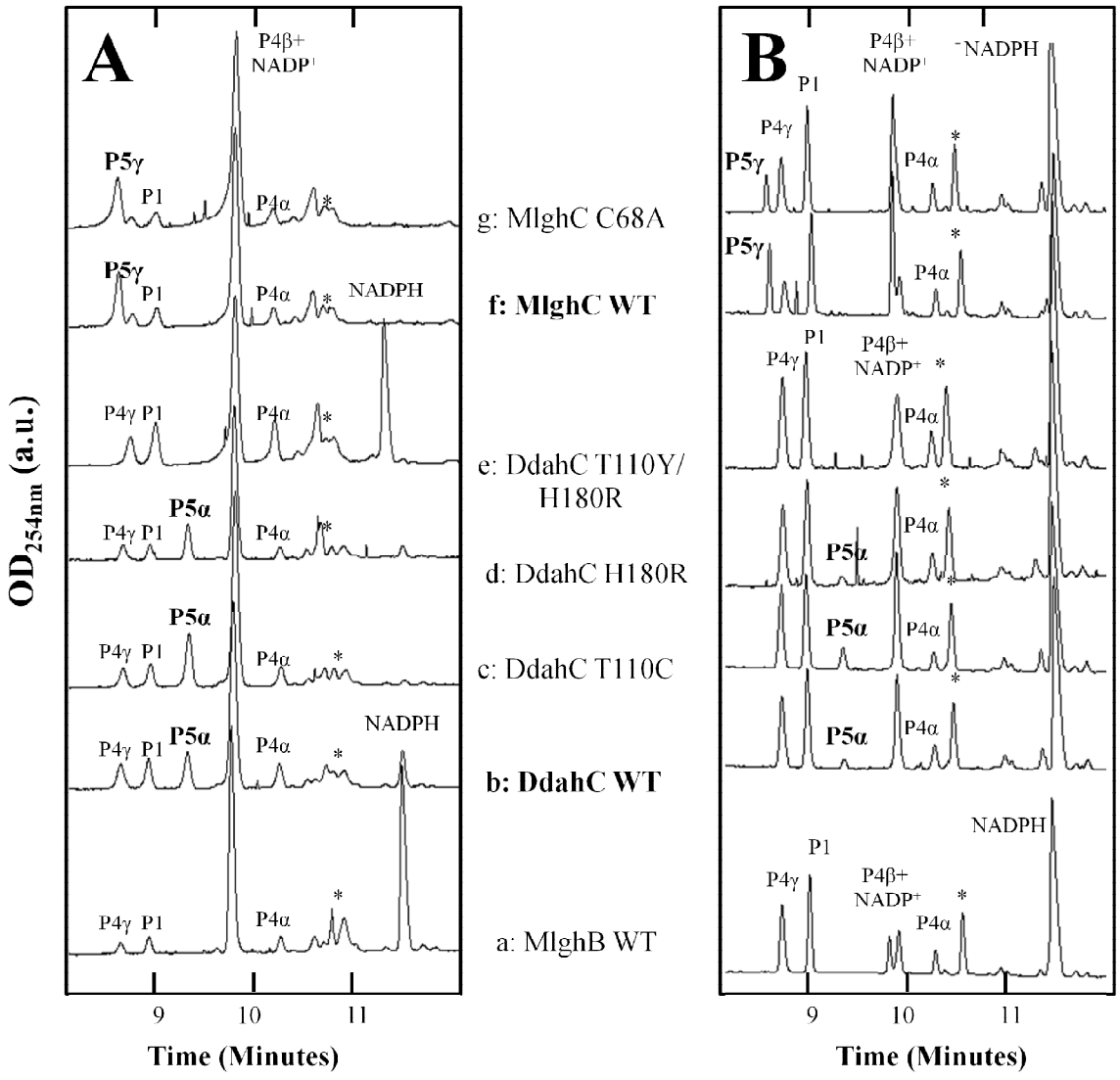
A
B
P4β+
NADP+
NADPH
P1
P4γ
P5γ
P4α
P5α
*
g: MlghC C68A
f: MlghC WT
e: DdahC T110Y/
H180R
d: DdahC H180R
c: DdahC T110C
b: DdahC WT
a: MlghB WT
OD254nm (a.u.)
9
10
11
Time (Minutes)
Time (Minutes)


A. GDP-manno-heptose
DdahA
P1
MlghB
P4α P4β P4γ
DdahC
MlghC
P5α
P5γ
B. GDP-manno-heptose
DdahA
P1
MlghB
P4α P4β P4γ
DdahC
MlghC
P5α
P5γ

Figure 25: CE electropherograms highlighting the activity of the reductases, wild type and mutants, on GDP-*manno*-heptose. A. The reductases activity in the presence of MlghB which can continuously supply P4α, P4β, and P4γ to the reductases as long as the P1 substrate is available. This allows testing the level of the activity of the wild type and the mutants. P4β was very difficult to resolve, as it often co-migrates with $NADP^+$. A base reaction containing the three epimerized substrates (P4α, P4β, and P4γ) was generated to test the activity and the specificity of the reductases by incubating MlghB with 0.17 mM of freshly synthesized P1 out of GDP-*manno*-heptose (trace a) and 0.5mM NADPH. To that, 1.0 pmol of either DdahC and MlghC wild type or mutants was added and incubated for 30 minutes. DdahC reduces P4α into P5α, while MlghC reduces P4γ into P5γ. **B.** The reductases activity on fixed amounts of the preformed P4α, P4β, and P4γ substrate. This was done to facilitate determination of the substrate specificity of the mutants. A base reaction was set up using MlghB and 0.37 mM of freshly synthesized P1 to generate the three epimerized substrates (Trace a). It also contained 0.5mM NADPH. This reaction was ultrafiltered (red dash line) to remove MlghB. Either DdahC or MlghC, wild type or mutants, was added to the filtrate and incubated for 30 minutes. The specific products are highlighted in bold. There is no change in the specificity of the mutants. * denotes a small impurity in the NADPH or the GDP-*manno*-heptose stocks. Illustrative cartoon for the experimental pathway in the grey box. See Appendix 6 for peaks integrations.

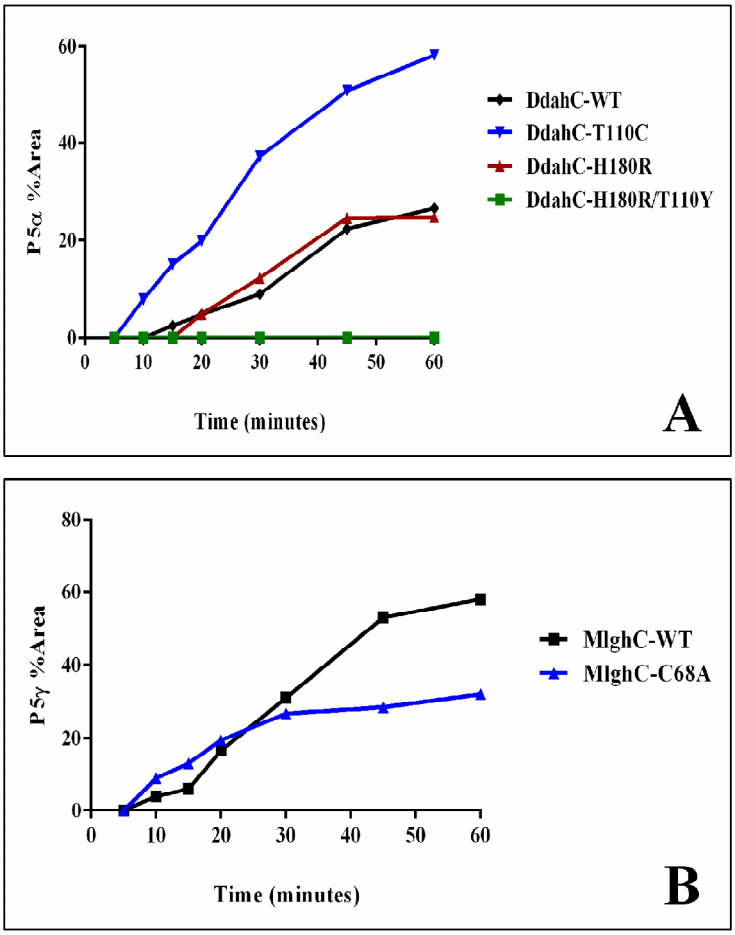

Figure 26: Kinetics of the reductases wild type and mutants on GDP-*manno*-heptose. The graphs represent the percentage area of the reduced product to the total area of the substrate and the product per reaction (Y-axis), for seven time points over an hour (X-axis). **A.** DdahC C4 reduction of P4α. **B.** MlghC C4 reduction of P4γ. A base reaction containing 0.5mM NADPH and 0.37 mM of freshly synthesized P1 was incubated with MlghB to generate the epimerized substrates. This reaction was ultrafiltered to remove MlghB. Then it was equally divided in aliquots to which 0.5 pmol of each reductase was added. After incubation, the samples were snap frozen in dry ice/ethanol at each time point and analyzed by CE. (Preliminary experiment).

3.6.2. Reductases reactions on GDP-mannose:

Preliminary data from our lab of the activity of DdahC and MlghC on GDP-mannose substrate showed that they can use P4', which is suspected to be epimerized, to generate different products. Two products were identified for DdahC, PII and PIII, while one product was observed for MlghC, PI. The nature of the theses products whether epimerized or reduced is unknown. In this analysis both the dehydrated (P1') and the epimerized (P4') forms of GDP-mannose were used as substrates to test the activity and the products formed by the wild type.

There are two major limitations of this analysis. The first is, because the heptose modifying enzymes, DdahC and MlghC, are less efficient on such substrates, longer incubation is needed to reach detectable levels of the products. However, both substrates, P1' and P4', are 4-keto sugar nucleotides, and they degrade rapidly during long incubations. Therefore, very small amounts of DdahC and MlghC products can be detected above the baseline. The second is that DdahC and MlghC products migrate closely to the substrate in the CE analysis. DdahC PIII migrates as a left shoulder peak to the substrate P1'. DdahC's PII migrate as a right shoulder peak to GDP-mannose, while MlghC's PI migrates as a left shoulder to GDP-mannose. This close migration of the products to the substrates limits the measurement of the products formed. Therefore, it is difficult to interpret the differences between the wild type and the mutants. An efficient HP0044 enzyme should be used to completely convert GDP-mannose into P1' to avoid any overlap between peaks and any confusion in peak assignments.

The first set of DdahC and MlghC wild type enzyme analysis was performed on both P1' and P4' (Figure 27). One part of this set was performed where GDP-mannose was incubated with HP0044 and MlghB, to generate P1' and P4', as well as each of DdahC or MlghC. MlghB reaction is an equilibrium reaction, meaning that it can constantly make P4' out of P1' as long as P1' is available. Upon incubation with the wild type reductases, DdahC generates PII and PIII, while MlghC generates PI (Figure 27-A1). The co-injection of DdahC and MlghC reactions confirms that these products are different (Figure 27-A2). Despite the fact that P4' is assumed to be used by the reductases, there were detectable levels of P4' substrate in DdahC and more in MlghC reactions. This could be from the activity of MlghB that continuously regenerates P4' from P1'. P1' can also be regenerated from GDP-mannose by the activity of HP0044 that was also available in the reaction, which explain the disappearance of GDP-mannose peak in both DdahC and MlghC reactions (Figure 27-A1). The second part is performed where both HP0044 and MlghB were sequentially removed from the reaction after the generation of their products. The filtrate, containing P1' and P4' without the enzymes, was used to add either DdahC or MlghC. Upon incubation with the reductases, both enzymes generate their specific products, PII and PIII for DdahC, and PI for MlghC, with total conversion of both P1' and P4'. This indicates that DdahC and MlghC can use both P1' and P4'. In addition, NADPH was totally converted into $NADP^+$ (Figure 27-B).

The second set of the analysis was to test if they can use P1' by itself (Figure 28). GDP-mannose was incubated only with HP0044 to generate P1'. Upon incubation with DdahC and MlghC, both reductases were able to generate their specific products from

P1' (Figure 28-A). For total conversion of GDP-mannose, HP0044 was incubated for two hours resulting in more degradation of P1' and formation of an unknown peak. This unknown peak migrates similarly to P4'. To make sure that this unknown product was not used by the epimerases instead of P1', a similar experiment set was performed using newly purified HP0044 to aid the total conversion of GDP-mannose in shorter incubation time. Using newly purified HP0044 was necessary as it seems that HP0044 loses some of its activity upon long storage. HP0044 was removed from the reaction after total conversion of the GDP-mannose, and DdahC or MlghC were added to the filtrate. Upon incubation, both DdahC and MlghC generate their specific products in the absence of the unknown peak (Figure 28-B). All P1' was used by DdahC to generate PII and PIII, while some is left in MlghC reaction.

The activity and product specificity of the mutants were tested on P1' using the same conditions (Figure 29). Unlike the activity on heptose substrate, T110C mutant generates both products, PII and PIII, but less than the wild type. However, H180R mutant shows similar activity to the wild type generating PII and PIII. H180R/T110Y is catalytically active and shows less activity than the wild type. On the other hand, MlghC product peak is very small and close to the baseline. However, there is no difference between the wild type and C68A mutant (Figure 29).

The kinetics of DdahC and MlghC wild type and mutants were performed where both MlghB and HP0044 were available in the reaction. The results interpreted for the percentage of the products area to the total area of all products and substrates, P1' and P4' (Figure 30). For DdahC's PII product, T110C mutant is significantly slower than the

wild type, while H180R mutant was equivalent to the wild type in the early time points. At late time points, PII was undetectable for H180R mutant (Figure 30-A). The kinetics for H180R/T110Y was not performed at the time of this experiment. DdahC's PIII kinetics was not included. PIII was undetectable at most of the time points because of the low resolution from the migration with the substrate P1'. On the other hand, MlghC's PI product was also undetectable at early time points. C68A mutant was significantly slower than the wild type and generated less PI (Figure 30-B).

3.7. Summary of the enzymatic assays and kinetics:

The enzymatic activity and the kinetics results of GDP-*manno*-heptose wild type and mutated epimerases and reductases are summarized in Table 6.

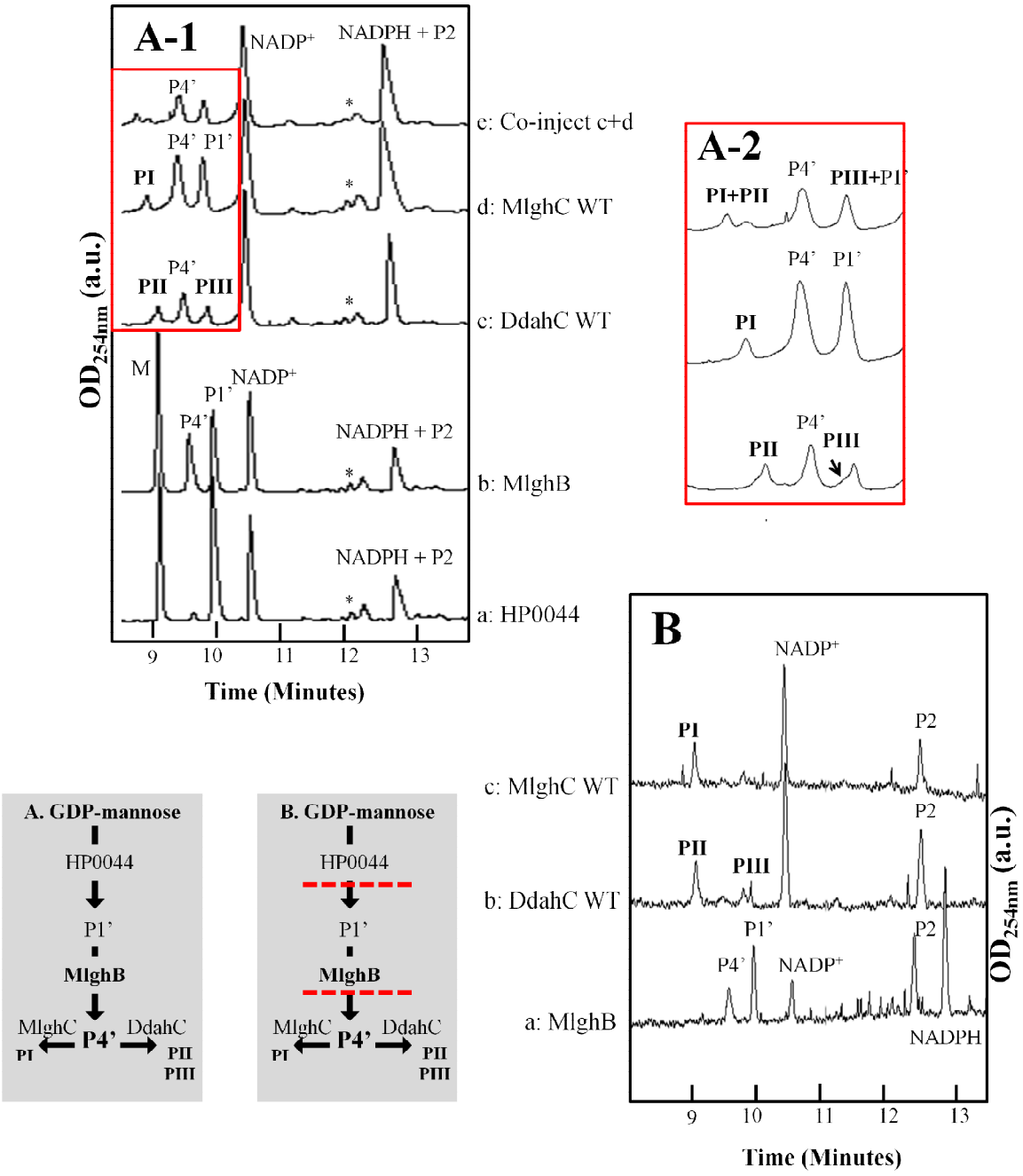
A-1
NADP+
NADPH + P2
P4'
P4' P1'
PI
PII PIII
M
P1'
e: Co-inject c+d
d: MlghC WT
c: DdahC WT
b: MlghB
a: HP0044
OD254nm (a.u.)
9 10 11 12 13
Time (Minutes)
A-2
PI+PII
PIII+P1'
B
P2
c: MlghC WT
b: DdahC WT
a: MlghB
NADPH
A. GDP-mannose
HP0044
P1'
MlghB
MlghC
DdahC
P4'
PI
PII
PIII
B. GDP-mannose

Figure 27: CE electropherograms highlighting the activity of the reductases on the dehydrated and the epimerized product of GDP-mannose (P4'). A. DdahC and MlghC can generate their products either from the dehydrated form (P1') or the epimerized form (P4') of GDP-mannose (Trace c, d). A base reaction where GDP-mannose was incubated with HP0044 and MlghB to generate both P1' and P4' in equilibrium was used to test the activity of the reductases. P1' is degraded over time into P2. Incubation with DdahC generates two products (PII and PIII) (trace c), while incubation with 1.5 pmol of MlghC generates only one (PI) (trace d). However, left over substrates were observed. Because the products migrate close to each other and to the substrate, both reactions were co-injected to show that they are different (Trace e), zoomed out in the red box. * denotes a small impurity in the NADPH stock. **B.** Confirms that the reductases are using both P1' and P4' due to the disappearance of their corresponding peaks (trace b, c). No regeneration of P1' and P4' was observed because both HP0044 and MlghB were ultrafiltered from the reaction (red dash lines) before adding the reductases. Illustrative cartoon for the experimental pathway in the grey box.

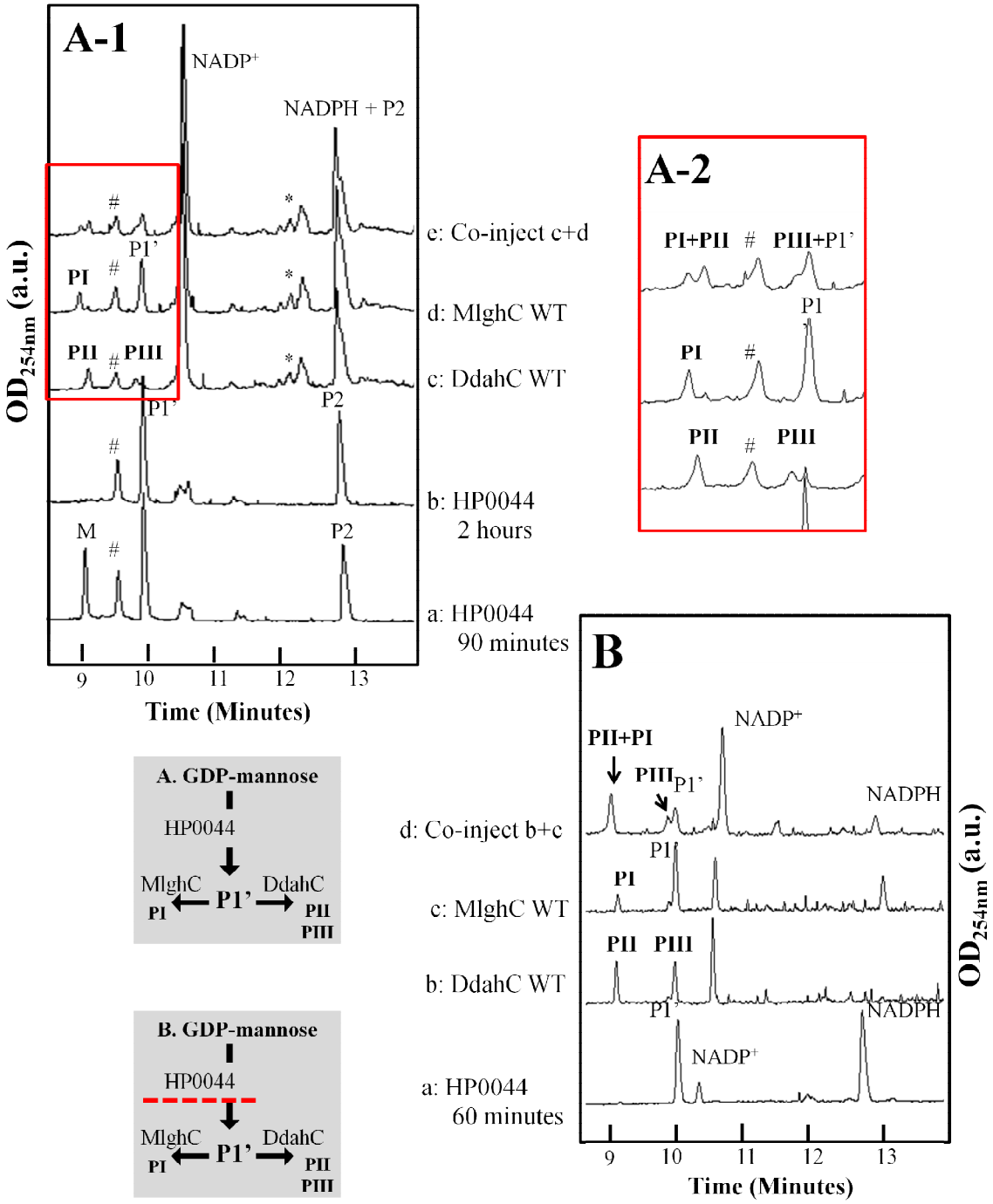
A-1
NADP+
NADPH + P2
P1'
PI
PII
PIII
P2
M
e: Co-inject c+d
d: MlghC WT
c: DdahC WT
b: HP0044
2 hours
a: HP0044
90 minutes
9
10
11
12
13
Time (Minutes)
OD254nm (a.u.)
A-2
PI+PII
PIII+P1'
P1
B
PII+PI
PIII
NADPH
d: Co-inject b+c
c: MlghC WT
b: DdahC WT
a: HP0044
60 minutes
A. GDP-mannose
HP0044
MlghC
DdahC
B. GDP-mannose
HP0044
MlghC
DdahC

Figure 28: CE electropherograms highlighting the activity of the reductases on the dehydrated product of GDP-mannose (P1'). **A.** The activity of DdahC and MlghC on P1' only. P1' was synthesized from GDP-mannose by incubation with HP0044 for 2 hours (trace b). P1' is degraded over time into P2. After total conversion of GDP-mannose into P1', the reaction was divided and each of the reductases was added separately along with NADPH. Incubation with DdahC generates two products (PII and PIII) (trace c), while incubation with MlghC generates only one (PI) (trace d). Because the products migrate close to each other and to the substrate, both reactions were co-injected to show that they are different (Trace e), zoomed out in the red box. * denotes a small impurity in the NADPH stock. # denoted an unknown product that results from long incubation of HP0044. **B.** The unknown product (#), shown in **panel A** is indeed from longer incubation of HP0044, and it is not used by the epimerases. After total conversion of GDP-mannose into P1' by newly purified HP0044 in 60 minutes (trace a), the reaction was ultrafiltered to remove HP0044. This was divided and each of the reductases was added (trace b, c). No formation of the unknown product (#) and less degradation of P1' is seen. Also, both DdahC and MlghC made their products using P1'. Illustrative cartoon for the experimental pathway in the grey box.

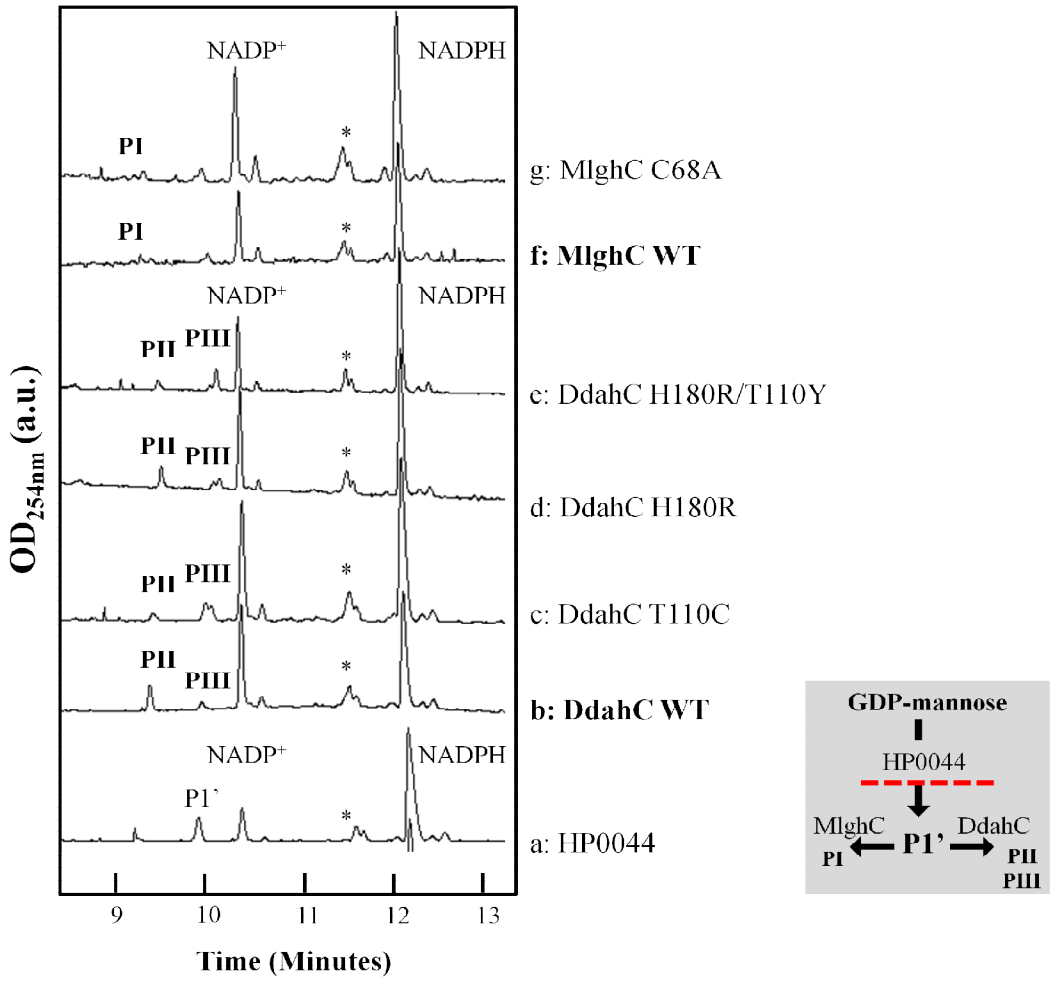

Figure 29: CE electropherograms highlighting the activity of the reductases wild type and mutants on the dehydrated product of GDP-mannose (P1'). The activity of the wild type DdahC and MlghC and the mutants on P1'. P1' was synthesized from GDP-mannose by incubation with HP0044 for 60 minutes (trace a), the reaction was ultrafiltered to remove HP0044. This was equally divided and each wild type or mutant was added separately. There was very little products formation due to an insufficient amount of the substrate. * denotes a small impurity in the NADPH stock. Illustrative cartoon for the experimental pathway in the grey box.

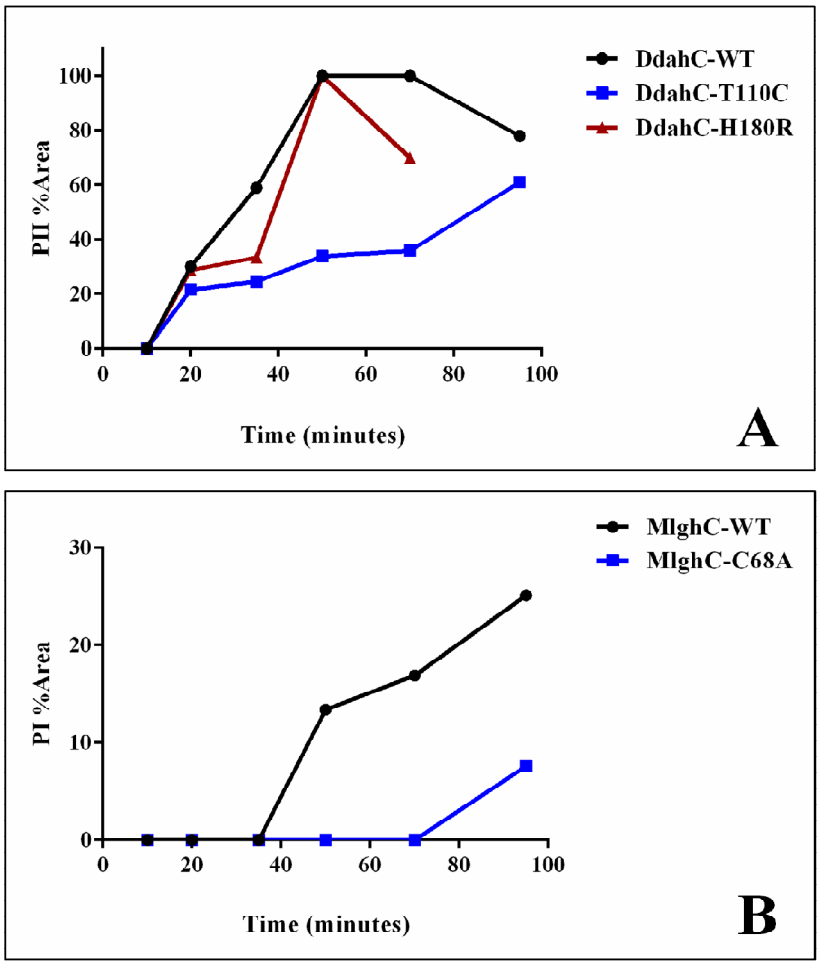

Figure 30: Kinetics of the reductases wild type and mutants' activity on GDP-mannose. P1' and P41 were the substrates for this set. Representing the percentage area of the product to the total area of sugar nucleotides per reaction (Y-axis) for six time points over 95 minutes (X-axis). **A.** The formation of PII product of DdahC. **B.** The formation of PI product of MlghC.

Table 6: Summary of the enzymatic assays and kinetics of the mutants compared to the wild type epimerases and reductases.

Epimerases	Mutation	Rational	On GDP-*manno*-heptose substrates	On GDP-mannose substrates
DdahB	N121S*	Substrate recognition (binds O4)	No significant difference in P4α formation	UD
	H67A	Catalytic, inactivate.	significantly less P4α ($p < 0.01$)	
	H67N	Catalytic, inactivate.	significantly less P4α ($p < 0.01$)	
MlghB	N121S*	Substrate recognition (binds O4)	No significant difference in P4α, P4β, or P4γ	No significant difference in P4’
	H67A	Catalytic, inactivate.	No P4β or P4γ. And significantly less P4α ($p < 0.001$)	Inactive
	H67N	Catalytic, inactivate.	No P4β or P4γ. And significantly less P4α ($p < 0.001$)	
	Y134F	Catalytic, inactivate.	Significantly less P4α and P4β ($p < 0.001$ and < 0.01), respectively	Significantly less P4’ ($p < 0.01$)

Reductases	Mutation	Rational	On GDP-*manno*-heptose substrates	On GDP-mannose substrates *
DdahC	T110C	Catalytic, testing specificity	No change in specificity. 50% more P5α (faster)	20% less PII (slower).
	H180R	Catalytic, testing specificity	No change in specificity. P5α similar to WT	PII is similar to WT.
	H180R/T 110Y		Inactive	Active
MlghC	C68A	Unknown function	No change in specificity. 10% less P5γ (slower)	70% less PI (slower)

UD: undetectable. DdahB WT is not efficient on GDP-mannose substrate.

C3, C5, C3, 5 indicate the epimerization sites.

* Results listed based on the kinetics. The percentages of the differences in the activity are for the last time points (Figure 30).

3.8. Biofilm assay:

The wild-type strain, *C. jejuni* NCTC11168, was tested for biofilm formation along with four heptose biosynthesis mutants and a capsule-less mutant that were generated previously in our lab: *wcaG::cat, mlghC::cat, mlghB::cat, wcaGΔ::cat,* and *kpsM::kan* (184). The *kpsM::kan,* a capsule-less strain, was used as a negative control as the capsule was thought to have a role in biofilm formation (178). All the other mutants have intact capsule except that it is devoid of the methylated heptose that is found in the wild type (184). The *wcaGΔ::cat* mutant has deletions of the precursor GDP-*manno*-heptose synthesis genes (*cj1423c- cj1425c*), the heptose methyl transferase gene (*cj1426c*), and other capsule MeOPN transferases genes (*cj1421c* and *cj1422c*). Therefore, *wcaGΔ::cat* mutant contains the capsule backbone with no modifications, no heptose, no methylation, and no MeOPN (184). The formation of biofilm by the wild type and the mutants was measured every day for four days after an initial incubation. The biofilm formation was tested under aerobic conditions, which are more relevant for the survival of the organism in the environment. It has been shown that *C. jejuni's* biofilm formation increases under aerobic conditions (146). Perhaps it helps to minimize the oxygen concentration for survival. The biofilm formation was also tested under microaerobic conditions, which are the favorable conditions for *C. jejuni* growth. This was done to confirm that the wild type *C. jejuni* does not need to make more biofilm under microaerobic conditions. Also to investigate whether lacking the modified heptoses would stress the bacterial cells and drive them to make more biofilm than the wild type under microaerobic conditions.

Under aerobic conditions, the wild type *C. jejuni* NCTC11168 made significantly more biofilm than the negative control, *kpsM::kan* strain, at all detection days ($p < 0.001$) (Figure 31). In addition, the amount of *C. jejuni* NCTC11168 biofilm has increased significantly at the last day compared to the first day ($p < 0.001$) (Figure 31).

Comparing the biofilms formed by the mutants to the wild type at each detection day showed that the ***wcaG::cat*** mutant had significant reduction in the biofilm amount at the first day ($p < 0.004$), as well as at the following days ($p < 0.001$). The *wcaG::cat* mutant made significantly more biofilm at the last day of detection compared to the first day ($p < 0.001$). The ***mlghC::cat*** mutant's biofilm was significantly less than the wild type at all detection days ($p < 0.001$), and comparable to the negative control *kpsM::kan* at the first three days. There was an increase in biofilm in the last day compared to the first day of detection ($p < 0.002$). The ***mlghB::cat*** mutant's biofilm was also significantly less than the wild type ($p < 0.001$), and comparable to the negative cotrol *kpsM::kan* at all detection days. No difference was observed in the biofilm between the first and the last days of detection. The ***wcaGΔ::cat*** mutant had significantly less biofilm than the wild type at all days of detection ($p < 0.001$). The biofilm of *wcaGΔ::cat* mutant was comparable to the negative control at the first two days of detection. There was a significant increase in the *wcaGΔ::cat* mutant's biofilm amount at the last day compared to the first day of detection ($p < 0.001$) (Figure 31).

In microaerobic condition, *C. jejuni* NCTC11168 wild type was able to make significantly more biofilm than the negative control, *kpsM::kan* strain ($p < 0.001$) (Figure 32). The biofilm formed at all days of detection did not change. These results suggest that

C. jejuni NCTC11168's biofilm is indeed increasing under aerobic condition, but not under microaerobic conditions.

The ***wcaG::cat*** mutant has significantly less biofilm than the wild type at the first two days of detection ($p < 0.001$). However, the amount of biofilm at the last two days of detection was comparable to the wild type. The difference between the first and the last day of detection of *wcaG::cat* mutant's biofilm was significant ($p < 0.001$), meaning that unlike the wild type, *wcaG::cat* mutant's biofilm was increasing.

There was no significant difference between the ***mlghC::cat*** mutant's biofilm amount and the wild type at all detection days, except at the second day where it was significantly higher than the wild type ($p < 0.001$). The ammount of *mlghC::cat* mutant's biofilm at the first and the last day of detection was decreased ($p = 0.004$). Compared to the increasing biofilm formed under the aerobic condition, *mlghC::cat* mutant behave differently. It decreased under microaerobic condition, but increased under aerobic condition.

There is no significant difference between ***mlghB::cat*** mutant and the wild type biofilm amount at all detection days. The *mlghB::cat* mutant has no significant difference between all days of detection. Compared to the aerobic biofilm, *mlghB::cat* mutant was better at making biofilm under microaerobic rather under aerobic conditions, yet the biofilm amount is not changing over days of incubation at both conditions.

Finally, the *wcaGΔ::cat* mutant's biofilm amount was significantly less than the wild type and comparable to the negative control at the first two days of detection. At the last day of detection, the *wcaGΔ::cat* mutant's biofilm amount had significantly increased

compared to the first day of detection ($p < 0.001$) (Figure 32). Compared to the increased biofilm formation under the aerobic condition, *wcaGΔ::cat* mutant biofilm had increased similarly under microaerobic condition.

The bacterial cell inoculums that were used in both experiments for each mutant were analyzed for the quality of the capsule by SDS-PAGE using Hitchcock and Brown method. After silver-staining, the SDS-PAGE showed that all the mutants, except the capsule-less *kpsM::kan* mutant, have the capsule patterns that are found in the wild type (Figure 33). The presence of the capsule in the heptose biosynthesis mutants indicates that the differences in biofilm formation compared to the wild could be related to the lack of the modified heptose in the capsule.

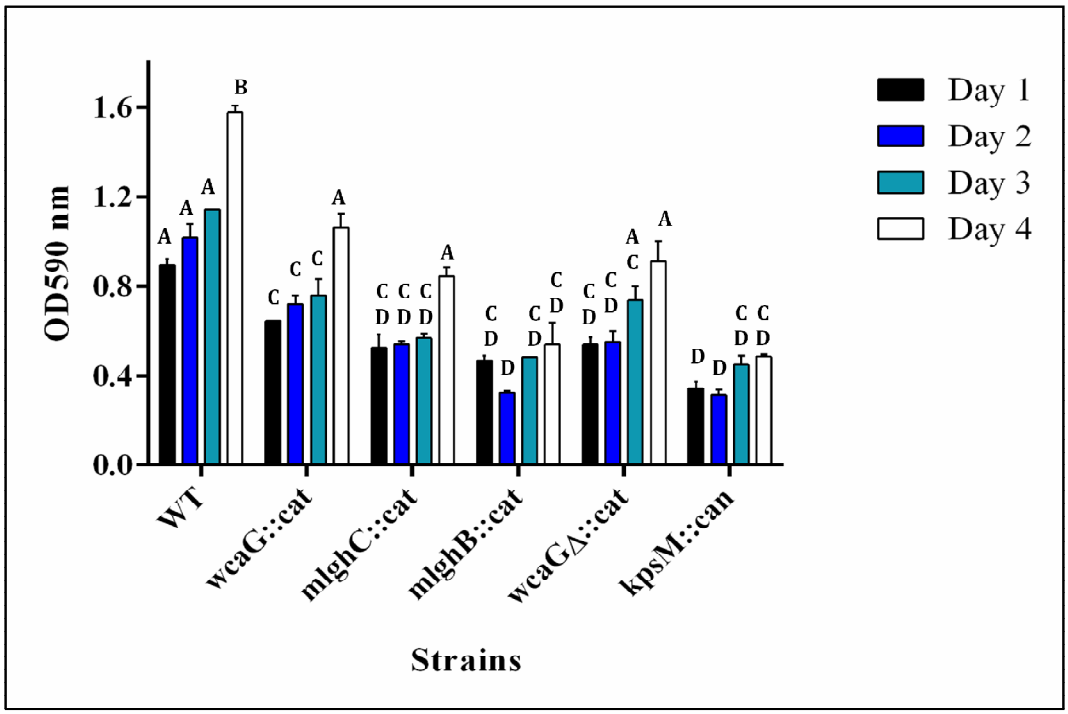

Figure 31: Biofilm formation by *C. jejuni* NCTC 11168 wild type, as well as the capsule and the heptose biosynthesis mutants under aerobic conditions. Biofilm formation was measured every day for four days after the initial incubation under aerobic conditions. Different letters indicate significant difference at ($P \leq 0.001$). Two letters indicate no significance difference with either letters. Statistics were done using one-way ANOVA test

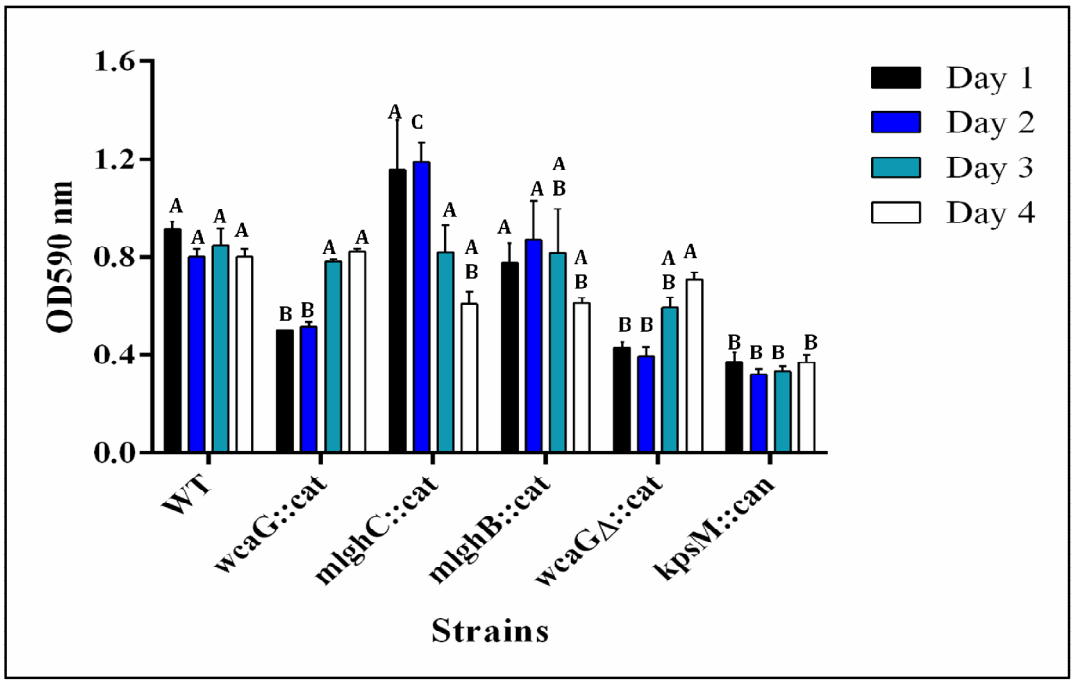

Figure 32: Biofilm formation by *C. jejuni* NCTC 11168 wild type, as well as the capsule and the heptose biosynthesis mutants under microaerobic conditions. Biofilm formation was measured every day for four days after the initial incubation under microaerobic conditions. Different letters indicate significant difference at ($P \leq 0.001$). Two letters indicate no significance difference with either letters. Statistics were done using one-way ANOVA test.

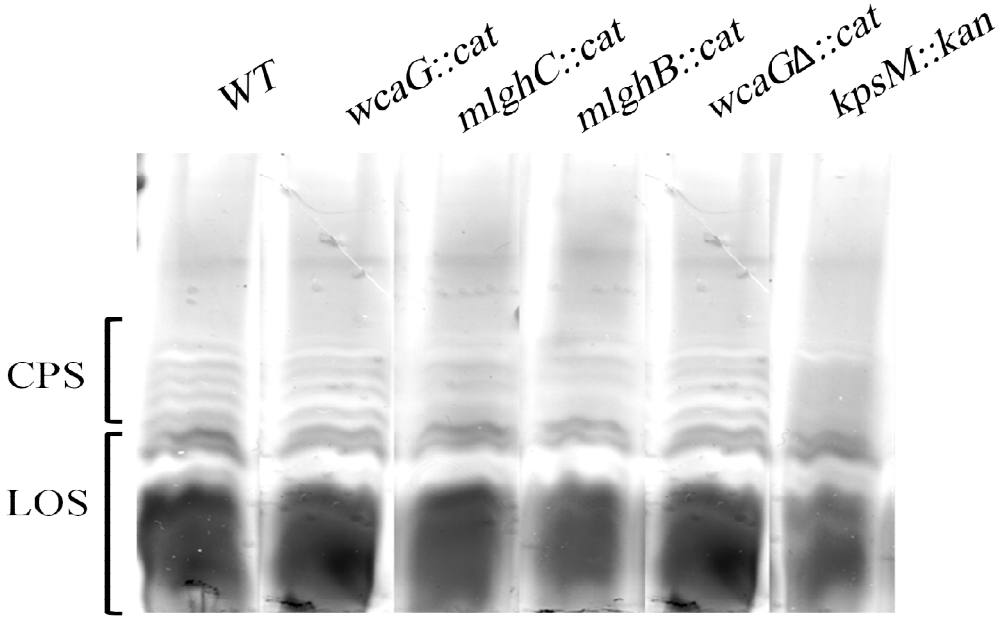

Figure 33: SDS-PAGE analysis of the capsule content of *C. jejuni* NCTC 11168 wild type, as well as the capsule and the heptose biosynthesis mutants. The capsule (CPS) and the lipooligosaccharide (LOS) fractions of cells samples prepared by Hitchcock and Brown method. The gel was visualized by silver staining.

CHAPTER 4 - DISCUSSION

4.1. The substrates and products specificity of the epimerases:

DdahB and MlghB have specificity toward GDP-*manno*-heptose rather than GDP-mannose substrate. DdahB epimerizes GDP-6-deoxy-4-keto-D-*lyxo*-heptose, P1, only at C3 generating P4α, while MlghB epimerizes P1 as a surrogate substrate at C3, C5, and both carbons generating three epimerized products, P4α, P4β, and P4γ. On the other hand, using the dehydrated GDP-mannose substrate (P1') to investigate the specificity of the active site showed that DdahB and MlghB generate a single product of unknown epimerization status (P4'), yet both are less efficiently active compared to the activity on GDP-*manno*-heptose substrate. DdahB is even less efficient than MlghB, as it failed to generate detectable products at higher enzyme concentration and longer incubation time. The epimerization status of P4' is unknown. To address what epimer P4' is, P4' should be identified using mass spectrometry combined with deuterium incorporation analysis as done previously to characterize the heptose epimers in our lab (112). However, this approach is not feasible due to the instability of P4' and the insufficient amounts that can be generated.

4.2. Substrate binding and catalytic site of the epimerases:

The binding of the enzyme to the substrate is dominated by the nucleotide portion. Therefore, the nucleotide binding determines the conformation that the ligand will adopt in the enzyme active site (46). The dTDP-phenol adopts a U shape in RmlC rather than extended conformation (34, 55). Whether there is a difference between dTDP and GDP

nucleotides in term of the conformation of binding to the enzyme cannot be derived from the data we have. However, the MlghB/GDP-mannose co-crystallography, although the mannose ring was not included in the final figure, showed that the ligand could be fitting in a U-shape in the binding site (Figure 15). The guanidine ring of the GDP moiety is found between the N-terminus Met1 of the B subunit, Ile32, and Lys54 residues. Phe24 is stacking against the ribose ring of the GDP. Other residues were identified that belong to a loop that was unstructured in the non-bound MlghB (Figure 15). Upon GDP-mannose binding, this loop, containing Tyr142 and Asp144, was shown to make a pocket for the GDP moiety. This loop could be important in regulating the substrate/product route into and out of the active site as observed in RmlC enzymes (34, 55, 60).

Based on the comparative functional analysis, the modeling and the crystallography structures, as well as the mutagenesis, some of the functional residues that are involved in the catalysis are identified in DdahB and MlghB.

The Asn121 residue is predicted to be important for binding the 4-keto group of the substrate through the amide. This binding will lower the pKa value of the protons attached to C3 and C5 to facilitate the deprotonation (4). Asn121 was mutated into serine in DdahB and MlghB to test its involvement in 4-keto group binding. Based on the enzymatic analysis, Asn121 is not essential for the catalysis of DdahB or MlghB on hexose or mannose-based substrates (Figure 21,23). However, Asn121 involvement in the substrate 4-keto binding cannot be interpreted by testing the current mutant, as the substitution into serine could be conserving the function by interacting with the 4-keto through the hydroxyl group. Another mutation where the Asn121 is mutated into a

residue with a non-polar side chain, such as alanine, can be proposed to test the Asn function.

A histidine-aspartate catalytic diad is conserved among the hexose-based epimerases (RmlC) in many gram-negative bacteria (45, 63). It is important for C3 and C5 epimerization as found in *S. enterica's* and *S. suis's* RmlC. It has been shown that in such His-Asp diad, the aspartate role is to increase the basicity of the histidine to aid the catalysis. However, the histidine still could function in the absence of the aspartate although with less activity (45, 63). The **His67-Asp173** diad was found in both DdahB and MlghB. However, based on the crystallography of DdahB, the Asp173 was away from the His67 and it was not conserved in the location compared to its location in MlghB (Figure 14). The difference in the structure could explain the inability of DdahB to function like MlghB under the same conditions to perform C5 epimerization. This can be further addressed by mutating the Asp173 in MlghB into a non-functional residue to see if MlghB will lose its C5 epimerization function.

The His67 was predicted as the catalytic residue for C3 epimerization in DdahB and it was mutated into asparagine or alanine. DdahB H67A and H67N were significantly less active than the wild type (Figure 21). The loss of activity indicates that the His67 is involved in C3 epimerization, yet there is another residue that can perform this function. In MlghB, the His67 was predicted to be catalytic for C3 and C5 epimerization. Mutating the His67 into alanine or asparagine resulted in complete loss of the epimerization function at C5. No C5-epimer (P4β) or C3/C5-epimer (P4γ) were detected even at longer incubations as shown by the kinetics. Nevertheless, both mutants, H67A and H67N were

poorly able to epimerize at C3 generating significantly less P4α than the wild type. These data indicate that His67 is the catalytic residue for MlghB's C5 epimerization. Consistent with the His67 mutant's analysis in DdahB, the slight C3 epimerization activity detected in MlghB His67 mutants indicates that His67 is involved in C3 epimerization, but there is another functional residue performing the epimerization at C3.

On GDP-mannose, the hexose-based substrate, both H67A and H67N of MlghB were catalytically inactive, even at longer incubations as shown by the kinetics (Figure 23). In RmlC, which utilizes a hexose-based substrate generating a single C3/C5-epimer, mutating the corresponding histidine resulted in inactivation of the enzyme. Therefore, it is possible that MlghB is functioning like RmlC when utilizing a hexose-based substrate by generating a single product. The loss of MlghB hexose-based product (P4') upon mutating the histidine indicates that P4' could be a C3/C5-epimer.

The Tyr134 was predicted as a catalytic residue for C3 and C5 epimerization and it was mutated into phenylalanine to test the function of the hydroxyl group in the catalysis. The data only showed the activity of MlghB Y134F but not DdahB Y134F, because the DdahB Y134F mutant was not generated at the onset of this experiment. Surprisingly, MlghB Y134F mutant was catalytically active. However it showed significantly less P4α and P4β compared to the wild type (Figure 21). The fact that P4γ production was not affected could be explained by the preferable interconversion towered P4γ. The formation of all epimerized products indicates that Tyr134 is not essential for C3 or C5 epimerization.

On GDP-mannose substrate, MlghB Y134F mutant was significantly less active than the wild type (Figure 23). The poor activity of MlghB Y134F indicate that the Tyr134 is not essential for catalysis. The structural modeling of the Y134F mutant suggested that the compensation for the mutated Tyr134 function in MlghB Y134F could be done by an adjacent Tyr132. A change in the orientation of Tyr134 was observed in Y134F model compared to the wild type (Figure 12). The same change was also observed in the N121S mutant, indicating that Y132 could have a flexible conformation of its side chain. To investigate whether Tyr132 is compensating for Tyr134 function in the catalysis of MlghB, or whether it is a catalytic residue, the single mutant Y132F, and the double mutant Y134F/Y132F were generated for DdahB and MlghB by an M.Sc candidate (Chelsea Kubinec). The activity of these mutants is under investigation.

Another function is predicted for Tyr132 based on the structure of DdahB and MlghB. Tyr132 and His123 are aligned with conserved aromatic residues in RmlC enzymes, usually Phe/Phe pairs (Figure 11). Thus, Tyr132 and His123 could function in a stacking interaction with to physically stabilize the substrate during catalysis.

The Lys74 was predicted as a catalytic residue for C3 epimerization. Based on the structure of DdahB and MlghB, Lys74 was the only residue that could function as a base on the upper face of the active site. Therefore, it could deprotonate the substrate at C3 from the upper face of the sugar ring. As shown in RmlC, the corresponding lysine was essential for C3 epimerization (45, 55). The mutation of Lys74 into alanine has been created for both DdahB and MlghB but the enzymatic activity of the mutated enzymes is under investigation.

The Gln85 was predicted to be involved in catalysis. Gln85 could not be directly involved in the epimerization because it is located at the end of the active site on the sugar-ring side (Figure 15-C). Nevertheless, it could be stabilizing an adjacent catalytic residue that is involved directly in catalysis. Gln85 may perhaps be interacting with the Asn121 through the amide group by a hydrogen bond (21, 63).

In conclusion, the role of Asn121 in the 4-keto group recognition of DdahB's and MlghB's substrates is still unknown. In order to address that, mutating the Asn121 into a residue with non- polar side chain is needed. The His67 is the catalytic residue for MlghB C5 epimerization. The Asp173 is forming a diad with His67, and it could be essential for C5 epimerization in MlghB. DdahB Asp73 is not conserved in its location in the structure. Therefore, DdahB cannot perform C5 epimerization. His67, by itself, is involved in C3 epimerization of both MlghB and DdahB, but there is another residue performing C3 epimerization. Lys74 could be the catalytic residue for C3 epimerization based on the structure. The Tyr134 is involved in C3 and C5 epimerization in MlghB, and C3 epimerization in DdahC, yet it is not essential. Tyr132 could be a catalytic residue, or it could compensate for the Tyr134 function in catalysis. Gln85 could be a secondary catalytic residue that is interacting with Asn121 to aid the catalysis. The co-crystallography of DdahB and MlghB with their GDP-*manno*-heptose substrate will increase our understanding of the residues' function in the active site.

4.3. The substrates and products specificity of the reductases:

DdahC and MlghC are highly specific in their choice of the substrate and in their products formation. The specificity of DdahC and MlghC toward their substrate was investigated previously by providing the three epimerized substrates in the reaction (111). DdahC only reduces the C3 epimer (P4α) that is generated by DdahB at C4 in an NADPH-dependent manner to generate the final product GDP-6-deoxy-D-*altro*-heptose (P5α). DdahC can also use the same P4α that is generated by MlghB C3 epimerization generating the same product P5α. DdahC does not use the P4β or P4γ generated by MlghB. *In vitro*, MlghC reduces the double epimer (P4γ) that is generated by MlghB. The reduction occurs at C4 in an NADPH-dependent manner to generate GDP-6-deoxy-L-*gluco*-heptose (P5γ) (111).

DdahC and MlghC also have specificity toward GDP-*manno*-heptose substrates rather than GDP-mannose substrates. Using dehydrated GDP-mannose substrate (P1') and/or the epimerized form (P4') to investigate the specificity of the reductases showed that both DdahC and MlghC are less efficient in utilizing these substrates compared to GDP-*manno*-heptose substrates. The analysis also showed that DdahC and MlghC can use both P4' and/or P1'. By using each of these substrates, DdahC generates two products, PII and PIII, while MlghC generates one product, PI. The nature of these products whether reduced or epimerized is unknown. Because DdahC and MlghC possess the functional residues necessary for the epimerization, they could be functioning differently when utilizing a hexose-based substrate by performing an epimerization reaction. Unlike their activity in GDP-*manno*-heptose modification, where they only

reduce an epimerized substrate, they could be epimerizing the dehydrated GDP-mannose (P1') then reducing it just like other hexose-based substrate C3/C5 epimerases, C4 reductases, such as GFS. The fact that the generated products for DdahC or MlghC from P1' and P4' are the same suggest that they could be reducing the newly epimerized P1'and the already epimerized P4' into the same products. Unfortunately, it is difficult to identify the nature of these products by mass spectrometry coupled with deuterium incorporation due to their instability and the extremely low yields.

4.4. Substrate binding and catalytic site of the reductases:

DdahC and MlghC overall structure indicates that both are members of the SDR family (79). They have two domains, the co-factor binding domain and the substrate binding domain. The residues that bind the NADPH in the co-factor binding domain are found conserved with other SDR members and they were not discussed for simplicity. Based on sequence alignment and the modeling, a set of hydrophobic residues forming the binding pocket for GDP was identified (Table 4). Based on co-crystallography of GFS and its substrate, a tryptophan residue is functioning as a gate to the substrate binding site as it moves after binding to cover the substrate (99, 157). Therefore, the corresponding tryptophan in DdahC and MlghC could be functioning in a similar fashion.

Based on the comparative functional analysis and the modeling, two residues were predicted to interact with the sugar ring, Asn166 and Thr109 in DdahC, Asn165 and Gly108 in MlghC, however, their role in catalysis is unknown. The residues that catalyze the reduction activity of DdahC and MlghC have been identified. DdahC possesses the

SYK catalytic triad that found in GFS, Ser108, Tyr137, and Lys141, while MlghC possesses SMK catalytic triad, Ser106, Met110, and Lys139, similar to what has been identified in a UDP-GlcNAc C4,6-dehydratase, WpbM (39, 40, 99). On the other hand, aligned with the residues that were predicted to catalyze epimerization activity in GFS, Cys109 and His170, DdahC had His180 and Thr110, while MlghC had Arg181 and Tyr109. In this study, the residues His180 and Thr110 in DdahC have been targeted for mutagenesis studies for two reasons. The first is that DdahC and MlghC are known to perform NADPH-dependent reduction but not epimerization reactions. The second is that theses residues are not conserved in both enzymes, which suggest their involvement in the substrate and/or the product specificity.

The Thr110 was mutated into cysteine to mimic GFS catalysis by performing an epimerization activity or by reducing a double epimer. The DdahC T110C mutant did not change its substrate and it generated the same product as the wild type, P5α, although it was faster and generated 50% more P5α than the wild type (Figure 25). This indicates that Thr110 is not involved in the substrate or the product specificity on GDP-*manno*-heptose. The cysteine in DdahC T110C could have reduction potential resulted in increasing the activity of DdahC.

Based on the available data for the activity on GDP-mannose, DdahC T110C mutant was slower than the wild type (Figure 30-A) (Figure 26-A). The differences in the catalysis rate of DdahC T110C on GDP-*manno*-heptose versus the activity on GDP-mannose indicate that Thr110 confers specificity to the substrate whether heptose-based or hexose-based substrate

The His180 was mutated into arginine in DdahC to mimic MlghC's substrate specificity by reducing the double epimer P4γ. However, the DdahC H180R mutant did not change its substrate, which is the C3-epimer P4α, and it generated the same product as the wild type in a similar amount (Figure 25). On GDP-mannose, the DdahC H180R mutant showed similar activity to the wild type. His180 perhaps is not important for the substrate specificity or the reduction activity of DdahC. However, it is possible that mutating the His180 into arginine does not affect the function simply because both the histidine and the arginine have nitrogen on their side chain.

The double mutant H180R/T110Y that was generated to mimic MlghC's reduction of P4γ was catalytically inactive (Figure 25). Because the single H180R mutant was active and comparable to the wild type, the mutation of the Thr110 into tyrosine could be the reason of inactivation. When Thr110 was mutated into cysteine, DdahC gained catalytic efficiency, while when Thr110 was mutated into tyrosine DdahC lost its function. This suggests that Thr110 is a critical amino acid for DdahC activity. The choice of a substitution to Thr110 is very important and is affecting the activity differently. The exact role of the Thr110 in DdahC cannot be identified based on these substitutions as they were chosen to mimic the catalysis of other enzymes. To address if Thr110 has a role in the reduction activity of DdahC, Thr110 needs to be substituted with a residue with a non-functional side chain.

On GDP-mannose, the double mutant DdahC H180R/T110Y was unexpectedly active, and it generated the same products as the wild type (Figure 29). This surprising

finding suggests that if Thr110 has a role in catalysis, its function is specific for utilizing GDP-*manno*-heptose substrates rather than GDP-mannose.

The Cys68 in MlghC was mutated into alanine to test its involvement in the activity of MlghC. C68A mutant generated the same product as the wild type, but 10% less. C68A mutant was slower than the wild type, and the product formation was 50% less than the wild type at longer incubation (Figure 30). This suggests that Cys68 is involved in promoting the catalysis rate, perhaps by binding to the co-factor or its reduced form. Based on the modeling Cys68 is close enough to interact with the nicotinamide ring of the co-factor.

In conclusion, testing the Thr110 and the His180 residues of DdahC showed that these residues are not involved in the specificity toward the epimerized substrates of GDP-*manno*-heptose. Nevertheless, Thr110 could be an important residue for DdahC activity. The function of Thr110 needs to be further investigated regarding its involvement in DdahC reduction activity. The choice of the substitution amino acid for Thr110 has a significant impact on the activity of DdahC. Mutating the Thr110 into cysteine resulted in an increase in the substrate utilization and catalysis rate on the heptose-based substrate. However the same mutation resulted in a decrease in the catalysis rate on a hexose-based-substrate. The type of the function performed by DdahC T110C mutant whether an epimerization, a reduction, or both still needs to be investigated. In MlghC, the Cys68 is involved in catalysis maybe by interaction with the co-factor.

To further investigate the active site specificity of DdahC and MlghC, the catalytic triad that is essential for the reduction activity needs to be targeted for mutagenesis. The difference in the catalytic triad in DdahB (SYK) versus MlghC (SMK) could be related to the substrate and/or the product specificity.

4.5. The involvement of the modified heptose of *C. jejuni* NCTC 11168 in biofilm formation.

The role of the modified heptoses with regards to bacterial resistance to serum and bile salt, adhesion and invasion to host cells, as well as chicken colonization has been investigated in *C. jejuni* NCTC 11168 (184). The wild type *C. jejuni* NCTC 11168 and the heptose biosynthesis mutants are perfect tools to test the involvement of the modified heptoses in *C. jejuni* virulence *in vitro* for two reasons.The first is that *C. jejuni* NCTC 11168 possesses the modified heptose as a side branch of the CPS backbone. The location of the modified heptose as a side branch makes it the outermost exposed structure to the extracellular environment, thus suggesting the possible interaction of the modified heptose with the host. The second is that disrupting the modified heptose synthesis is not affecting the CPS backbone structure. Therefore, the virulence phenotype of the mutant is related to the loss of the modified heptose as opposed to the loss of the capsule. Four mutants were generated containing a knockout of each of the modified heptose synthesis genes, *wcaG::cat, mlghB::cat, mlghC::cat,* and *wcaGΔ::cat.* In this study, these mutants, along with the wild type as a positive control and the capsule-less

kpsM::kan mutant as a negative control, were used to investigate the involvement of the modified heptose in *C. jejuni* NCTC 11168 biofilm formation.

It is important to address the physiological characteristics that could affect the biofilm formation of the mutants to better analyse the differences in biofilm formation compared to the wild type. All the heptose biosynthesis mutants lack the side branch modified heptose as shown previously (184). In addition, the *wcaGΔ::cat* does not have the modified heptose or any CPS modification including the MeOPN. With regards to the motility and agglutination of the mutants, all the heptose biosynthesis mutants are motile and no significance difference in the agglutination compared to the wild type(184). In contrast, the *kpsM::kan* mutant expresses non-functional flagella and has significant increases in agglutination forming cellular clumps (184). The growth rate of the mutants compared to the wild type was also analysed. The heptose biosynthesis mutants grow faster than the wild type, with the highest growth rate for *wcaGΔ::cat* mutant (184).

In this study, the biofilm formation of *C. jejuni* NCTC 11168 wild type and mutants was tested under aerobic versus microaerobic conditions. The wild type *C. jejuni* NCTC 11168 had significantly increased biofilm formation under aerobic conditions (Figure 31). In contrast, the wild type biofilm were not increasing under microaerobic conditions (Figure 32). This was consistent with other studies that showed that the same strain of *C. jejuni* is making more biofilm under aerobic condition. The increase in biofilm formation protects *C. jejuni* cells from the atmospheric oxygen and thus allowing prolonged survival.

The *wcaG::cat* mutant made significantly less biofilm at both conditions, however, at late time points the amount of the biofilm had significantly increased. This means that the loss of the modified heptose in *wcaG::cat* mutant results in defects in biofilm formation. In addition, under microaerobic conditions where *C. jejuni* wild type does not need to form more biofilm over time, the *wcaG::cat* mutant needed to, until it reached the wild type levels. The same results were observed for the *wcaGΔ::cat* mutant. The early biofilm formation in *wcaGΔ::cat* mutant was significantly less than the wild type under both conditions. However, the biofilm formation had significantly increased over time. The *mlghC::cat* mutant also had a significant reduction in biofilm formation compared to the wild type, but only under an aerobic conditions. The biofilm formation was also significantly increasing over time. However, in microaerobic conditions there was no significant difference between *mlghC::cat* mutant and the wild type. Furthermore, in contrast to the microaerobic *wcaG::cat* and *wcaGΔ::cat* mutants' biofilm, the biofilm of *mlghC::cat* mutant was significantly decreased over time. On the other hand, the *mlghB::cat* mutant made significantly less biofilm than the wild type under aerobic conditions, but comparable biofilm to the wild type under microaerobic conditions. There was no change in the amount of biofilm made by *mlghB::cat* mutant in both conditions.

In conclusion, under aerobic condition, the biofilm formation by wild type *C. jejuni* NCTC 11168 is increasing. The modified heptose is important for *C. jejuni* NCTC 11168 biofilm formation. The biofilm formation of *wcaG::cat, mlghC::cat,* and *wcaGΔ::cat* mutants were significantly increasing over time just like the wild type, yet significantly less in the amount. This indicates that the loss of the modified heptose in

theses mutants could slow down the process of making the biofilm under aerobic condition. On the other hand, *mlghB::cat* mutant's biofilm was comparable to the negative control and did not increase.

Under microaerobic conditions, the biofilm formation by wild type *C. jejuni* NCTC 11168 is not increasing over time (Figure 32). This means that under favorable conditions, *C. jejuni* does not need to increase biofilm formation. However, *wcaG::cat* and *wcaGΔ::cat* mutants had a significant increase in the late biofilm formation. This suggests that the loss of the modified heptose in these mutants is stressing the bacterial cells and drives them to increase the formation of biofilm. The opposite is found in *mlghB::cat* mutant, where the formation of biofilm had decreased over time. Because all the mutants lack the modified heptose, similar phenotypes were expected. However, in a previous phenotypic analysis the same mutants showed variation in the results. The expression profile of these mutants was previously investigated and showed that deletion of the modified heptose genes resulted in upregulation of other CPS modification genes, especially in *mlghC::cat* and *mlghB::cat* mutants. This indicated that there are transcriptional regulatory effects that could influence the functional properties of the CPS. Complemented strains were generated previously for the mutants. However, they were unfunctional due to the presence of a very strong internal promoter that resulted in significant transcriptional differences within the CPS cluster.

4.6. Future directions:

In terms of the enzymatic analysis and the kinetics, further investigations for the epimerases' and the reductases' kinetics need to be done in order to assess the catalytic

activity of the mutants on GDP-*manno*-heptose. The GDP-*manno*-heptose epimerases and reductases active sites need to be further investigated by creating additional mutations by site-directed mutagenesis. Totally inactive mutants are needed to be used as a tool for enzyme/substrate co-crystallography. Having inactive mutant will allow generating a better resolution of the enzyme/substrate complex to identify the residues that bind directly to the substrate. A pure GDP-*manno*-heptose, as well as GDP-6-deoxy-4-keto-D-*lyxo*-heptose substrates, will be used to soak the epimerase crystals for crystallography. After having the structure of the enzyme/substrate complex, the data will be used as basis to screen for inhibitors using chemical libraries and assess the inhibitory effect of the candidates if there are any.

4.7. Significance and biological implications:

In *C. jejuni*, the major cause of gastroenteritis in humans, the putative heptose epimerases and reductases of 81-167 and NCTC 11168 strains can be potential antimicrobial targets due to their involvement in *C. jejuni* virulence, such as biofilm formation. This project is the first to identify the structure and the potential role of the functional residues in the active site of theses enzymes. The identification of specific structural and functional characteristics is fundamental for designing specific inhibitors.

REFERENCES

1. **Acharya KR, Lloyd MD.** 2005. The advantages and limitations of protein crystal structures. Trends in pharmacological sciences **26:**10-14.

2. **Achen M, Morishita TY, Ley EC.** 1998. Shedding and colonization of *Campylobacter jejuni* in broilers from day-of-hatch to slaughter age. Avian diseases **42:**732-737.

3. **AL-Delaimo M.** 2008. Pathogenesis of *Campylobacter jejuni* infection with emphases on ultra structural changes. DMG **2:**17-30.

4. **Allard ST, Giraud MF, Naismith JH.** 2001. Epimerases: structure, function and mechanism. Cellular and molecular life sciences : CMLS **58:**1650-1665.

5. **Allos BM.** 2001. *Campylobacter jejuni* Infections: update on emerging issues and trends. Clinical infectious diseases : an official publication of the Infectious Diseases Society of America **32:**1201-1206.

6. **Alter M.** 1990. The epidemiology of Guillain-Barre syndrome. Annals of neurology **27 Suppl:**S7-12.

7. **Arnold K, Bordoli L, Kopp J, Schwede T.** 2006. The SWISS-MODEL workspace: a web-based environment for protein structure homology modelling. Bioinformatics (Oxford, England) **22:**195-201.

8. **Arrecubieta C, Hammarton TC, Barrett B, Chareonsudjai S, Hodson N, Rainey D, Roberts IS.** 2001. The transport of group 2 capsular polysaccharides across the periplasmic space in *Escherichia coli*. Roles for the KpsE and KpsD proteins. The Journal of biological chemistry **276:**4245-4250.

9. **Aspinall GO, McDonald AG, Pang H.** 1992. Structures of the O chains from lipopolysaccharides of *Campylobacter jejuni* serotypes O:23 and O:36. Carbohydrate research **231:**13-30.

10. **Aspinall GO, McDonald AG, Pang H, Kurjanczyk LA, Penner JL.** 1993. Lipopolysaccharide of *Campylobacter coli* serotype O:30. Fractionation and structure of liberated core oligosaccharide. The Journal of biological chemistry **268:**6263-6268.

11. **Aspinall GO, McDonald AG, Raju TS, Pang H, Kurjanczyk LA, Penner JL, Moran AP.** 1993. Chemical structure of the core region of *Campylobacter jejuni* serotype O:2 lipopolysaccharide. European journal of biochemistry / FEBS **213:**1029-1037.

12. **Aspinall GO, McDonald AG, Raju TS, Pang H, Moran AP, Penner JL.** 1993. Chemical structures of the core regions of *Campylobacter jejuni* serotypes O:1, O:4, O:23, and O:36 lipopolysaccharides. European journal of biochemistry / FEBS **213:**1017-1027.

13. **Aspinall GO, Monteiro MA, Pang H, Kurjanczyk LA, Penner JL.** 1995. Lipo-oligosaccharide of *Campylobacter lari* strain PC 637. Structure of the liberated oligosaccharide and an associated extracellular polysaccharide. Carbohydrate research **279:**227-244.

14. **Axelsson-Olsson D, Ellstrom P, Waldenstrom J, Haemig PD, Brudin L, Olsen B.** 2007. *Acanthamoeba-Campylobacter* coculture as a novel method for enrichment of *Campylobacter* species. Applied and environmental microbiology **73:**6864-6869.

15. **Axelsson-Olsson D, Olofsson J, Svensson L, Griekspoor P, Waldenstrom J, Ellstrom P, Olsen B.** 2010. *Amoebae* and algae can prolong the survival of *Campylobacter* species in co-culture. Experimental parasitology **126:**59-64.

16. **Babaoglu K, Page MA, Jones VC, McNeil MR, Dong C, Naismith JH, Lee RE.** 2003. Novel inhibitors of an emerging target in *Mycobacterium tuberculosis*; substituted thiazolidinones as inhibitors of dTDP-rhamnose synthesis. Bioorganic & medicinal chemistry letters **13:**3227-3230.

17. **Babbitt PC, Gerlt JA.** 1997. Understanding enzyme superfamilies. Chemistry As the fundamental determinant in the evolution of new catalytic activities. The Journal of biological chemistry **272:**30591-30594.

18. **Bacon DJ, Szymanski CM, Burr DH, Silver RP, Alm RA, Guerry P.** 2001. A phase-variable capsule is involved in virulence of *Campylobacter jejuni* 81-176. Molecular microbiology **40:**769-777.

19. **Bartlett GJ, Porter CT, Borkakoti N, Thornton JM.** 2002. Analysis of catalytic residues in enzyme active sites. Journal of molecular biology **324:**105-121.

20. **Benkert P, Tosatto SC, Schomburg D.** 2008. QMEAN: A comprehensive scoring function for model quality assessment. Proteins **71:**261-277.

21. **Berka K, Laskowski R, Riley KE, Hobza P, Vondrášek J.** 2009. Representative Amino Acid Side Chain Interactions in Proteins. A Comparison of Highly Accurate Correlated ab Initio Quantum Chemical and Empirical Potential Procedures. Journal of Chemical Theory and Computation **5:**982-992.

22. **Berndtson E, Tivemo M, Engvall A.** 1992. Distribution and numbers of *Campylobacter* in newly slaughtered broiler chickens and hens. International journal of food microbiology **15:**45-50.

23. **Biswas D, Itoh K, Sasakawa C.** 2003. Role of microfilaments and microtubules in the invasion of INT-407 cells by *Campylobacter jejuni*. Microbiology and immunology **47:**469-473.

24. **Black RE, Levine MM, Clements ML, Hughes TP, Blaser MJ.** 1988. Experimental *Campylobacter jejuni* Infection in Humans. Journal of Infectious Diseases **157:**472-479.

25. **Blaser MJ, Duncan DJ.** 1984. Human serum antibody response to *Campylobacter jejuni* infection as measured in an enzyme-linked immunosorbent assay. Infection and immunity **44:**292-298.

26. **Brimer CD, Montie TC.** 1998. Cloning and comparison of fliC genes and identification of glycosylation in the flagellin of *Pseudomonas aeruginosa* a-type strains. J Bacteriol **180:**3209-3217.

27. **Brown HL, Reuter M, Hanman K, Betts RP, van Vliet AH.** 2015. Prevention of Biofilm Formation and Removal of Existing Biofilms by Extracellular DNases of *Campylobacter jejuni.* PloS one **10:**e0121680.

28. **Brown P, Kidd D, Riordan T, Barrell RA.** 1988. An outbreak of food-borne *Campylobacter jejuni* infection and the possible role of cross-contamination. The Journal of infection **17:**171-176.

29. **Bui XT, Qvortrup K, Wolff A, Bang DD, Creuzenet C.** 2012. Effect of environmental stress factors on the uptake and survival of *Campylobacter jejuni* in *Acanthamoeba castellanii*. BMC microbiology **12:**232.

30. **Bui XT, Winding A, Qvortrup K, Wolff A, Bang DD, Creuzenet C.** 2012. Survival of *Campylobacter jejuni* in co-culture with *Acanthamoeba castellanii*: role of amoeba-mediated depletion of dissolved oxygen. Environmental microbiology **14:**2034-2047.

31. **Butty FD, Aucoin M, Morrison L, Ho N, Shaw G, Creuzenet C.** 2009. Elucidating the formation of 6-deoxyheptose: biochemical characterization of the GDP-D-glycero-d-manno-heptose C6 dehydratase, DmhA, and its associated C4 reductase, DmhB. Biochemistry **48:**7764-7775.

32. **Chelli R, Gervasio FL, Procacci P, Schettino V.** 2002. Stacking and T-shape competition in aromatic-aromatic amino acid interactions. Journal of the American Chemical Society **124:**6133-6143.

33. **Chitnis T, Khoury SJ.** 2003. 20. Immunologic neuromuscular disorders. The Journal of allergy and clinical immunology **111:**S659-668.

34. **Christendat D, Saridakis V, Dharamsi A, Bochkarev A, Pai EF, Arrowsmith CH, Edwards AM.** 2000. Crystal structure of dTDP-4-keto-6-deoxy-D-hexulose 3,5-epimerase from *Methanobacterium thermoautotrophicum* complexed with dTDP. The Journal of biological chemistry **275:**24608-24612.

35. **Cieslewicz M, Vimr E.** 1996. Thermoregulation of kpsF, the first region 1 gene in the kps locus for polysialic acid biosynthesis in *Escherichia coli* K1. J Bacteriol **178:**3212-3220.

36. **Cieslewicz M, Vimr E.** 1997. Reduced polysialic acid capsule expression in *Escherichia coli* K1 mutants with chromosomal defects in kpsF. Molecular microbiology **26:**237-249.

37. **Corcionivoschi N, Clyne M, Lyons A, Elmi A, Gundogdu O, Wren BW, Dorrell N, Karlyshev AV, Bourke B.** 2009. *Campylobacter jejuni* cocultured with epithelial cells reduces surface capsular polysaccharide expression. Infection and immunity **77:**1959-1967.

38. **Costerton JW, Lewandowski Z, Caldwell DE, Korber DR, Lappin-Scott HM.** 1995. Microbial biofilms. Annual review of microbiology **49:**711-745.

39. **Creuzenet C, Lam JS.** 2001. Topological and functional characterization of WbpM, an inner membrane UDP-GlcNAc C6 dehydratase essential for lipopolysaccharide biosynthesis in *Pseudomonas aeruginosa*. Molecular microbiology **41:**1295-1310.

40. **Creuzenet C, Urbanic RV, Lam JS.** 2002. Structure-function studies of two novel UDP-GlcNAc C6 dehydratases/C4 reductases. Variation from the SYK dogma. The Journal of biological chemistry **277:**26769-26778.

41. **Dasti JI, Tareen AM, Lugert R, Zautner AE, Gross U.** 2010. *Campylobacter jejuni*: a brief overview on pathogenicity-associated factors and disease-mediating mechanisms. International journal of medical microbiology : IJMM **300:**205-211.

42. **Davis AM, St-Gallay SA, Kleywegt GJ.** 2008. Limitations and lessons in the use of X-ray structural information in drug design. Drug discovery today **13:**831-841.

43. **Day WA, Jr., Sajecki JL, Pitts TM, Joens LA.** 2000. Role of catalase in *Campylobacter jejuni* intracellular survival. Infection and immunity **68:**6337-6345.

44. **Dirks BP, Quinlan JJ.** 2014. Development of a modified gentamicin protection assay to investigate the interaction between *Campylobacter jejuni* and *Acanthamoeba castellanii* ATCC 30010. Experimental parasitology **140:**39-43.

45. **Dong C, Major LL, Allen A, Blankenfeldt W, Maskell D, Naismith JH.** 2003. High-resolution structures of RmlC from *Streptococcus suis* in complex with substrate analogs locate the active site of this class of enzyme. Structure **11:**715-723.

46. **Dong C, Major LL, Srikannathasan V, Errey JC, Giraud MF, Lam JS, Graninger M, Messner P, McNeil MR, Field RA, Whitfield C, Naismith JH.** 2007. RmlC, a C3' and C5' carbohydrate epimerase, appears to operate via an intermediate with an unusual twist boat conformation. Journal of molecular biology **365:**146-159.

47. **Durka M, Tikad A, Perion R, Bosco M, Andaloussi M, Floquet S, Malacain E, Moreau F, Oxoby M, Gerusz V, Vincent SP.** 2011. Systematic synthesis of inhibitors of the two first enzymes of the bacterial heptose biosynthetic pathway: towards antivirulence molecules targeting lipopolysaccharide biosynthesis. Chemistry (Weinheim an der Bergstrasse, Germany) **17:**11305-11313.

48. **Escherich T.** 1886. Articles adding to the knowledge of intestinal bacteria, III. on the existence of vibrios in the intestines and feces of babies. Muench Med Wochenschr **33:**815-817.

49. **Fauchere JL, Rosenau A, Veron M, Moyen EN, Richard S, Pfister A.** 1986. Association with HeLa cells of *Campylobacter jejuni* and *Campylobacter coli* isolated from human feces. Infection and immunity **54:**283-287.

50. **Fisher M.** 1956. An unusual variant of acute idiopathic polyneuritis (syndrome of ophthalmoplegia, ataxia and areflexia). The New England journal of medicine **255:**57-65.

51. **Fomsgaard A, Freudenberg MA, Galanos C.** 1990. Modification of the silver staining technique to detect lipopolysaccharide in polyacrylamide gels. Journal of clinical microbiology **28:**2627-2631.

52. **FS Jones MO, RB Little.** 1931. *Vibrios* (*Vibrio jejuni* n.sp.) associated with intestinal disorders of cows and calves. The Journal of experimental medicine **53:** 853–864.

53. **Gerlt JA, Babbitt PC.** 1998. Mechanistically diverse enzyme superfamilies: the importance of chemistry in the evolution of catalysis. Current opinion in chemical biology **2:**607-612.

54. **Gervasio FL, Chelli R, Procacci P, Schettino V.** 2002. The nature of intermolecular interactions between aromatic amino acid residues. Proteins **48:**117-125.

55. **Giraud MF, Leonard GA, Field RA, Berlind C, Naismith JH.** 2000. RmlC, the third enzyme of dTDP-L-rhamnose pathway, is a new class of epimerase. Nature structural biology **7:**398-402.

56. **Glaser R, Brennan R, Berlin CM.** 1979. Guillain-Barre syndrome associated with Epstein-Barr virus in a cytomegalovirus-negative patient. Developmental medicine and child neurology **21:**787-790.

57. **Godschalk PC, Heikema AP, Gilbert M, Komagamine T, Ang CW, Glerum J, Brochu D, Li J, Yuki N, Jacobs BC, van Belkum A, Endtz HP.** 2004. The crucial role of *Campylobacter jejuni* genes in anti-ganglioside antibody induction in Guillain-Barre syndrome. The Journal of clinical investigation **114:**1659-1665.

58. **Godschalk PC, Kuijf ML, Li J, St Michael F, Ang CW, Jacobs BC, Karwaski MF, Brochu D, Moterassed A, Endtz HP, van Belkum A, Gilbert M.** 2007. Structural characterization of *Campylobacter jejuni* lipooligosaccharide outer cores associated with Guillain-Barre and Miller Fisher syndromes. Infection and immunity **75:**1245-1254.

59. **Grados O, Bravo N, Black RE, Butzler JP.** 1988. Paediatric campylobacter diarrhoea from household exposure to live chickens in Lima, Peru. Bulletin of the World Health Organization **66:**369-374.

60. **Graninger M, Nidetzky B, Heinrichs DE, Whitfield C, Messner P.** 1999. Characterization of dTDP-4-dehydrorhamnose 3,5-epimerase and dTDP-4-dehydrorhamnose reductase, required for dTDP-L-rhamnose biosynthesis in *Salmonella enterica serovar Typhimurium* LT2. The Journal of biological chemistry **274:**25069-25077.

61. **Guerry P, Alm RA, Power ME, Logan SM, Trust TJ.** 1991. Role of two flagellin genes in *Campylobacter* motility. J Bacteriol **173:**4757-4764.

62. **Guerry P, Ewing CP, Schirm M, Lorenzo M, Kelly J, Pattarini D, Majam G, Thibault P, Logan S.** 2006. Changes in flagellin glycosylation affect *Campylobacter* autoagglutination and virulence. Molecular microbiology **60:**299-311.

63. **Gutteridge A, Thornton JM.** 2005. Understanding nature's catalytic toolkit. Trends in biochemical sciences **30:**622-629.

64. **Hafer-Macko CE, Sheikh KA, Li CY, Ho TW, Cornblath DR, McKhann GM, Asbury AK, Griffin JW.** 1996. Immune attack on the Schwann cell surface in acute inflammatory demyelinating polyneuropathy. Annals of neurology **39:**625-635.

65. **Hall AJ, Wikswo ME, Manikonda K, Roberts VA, Yoder JS, Gould LH.** 2013. Acute gastroenteritis surveillance through the National Outbreak Reporting System, United States. Emerging infectious diseases **19:**1305-1309.

66. **Hara M, Morita A, Ichihara K, Kashima Y, Kamei S, Kuwahara M, Kusunoki S.** 2012. Miller Fisher syndrome associated with influenza A infection. Internal medicine (Tokyo, Japan) **51:**2621-2623.

67. **Hendrixson DR, DiRita VJ.** 2003. Transcription of sigma54-dependent but not sigma28-dependent flagellar genes in *Campylobacter jejuni* is associated with formation of the flagellar secretory apparatus. Molecular microbiology **50:**687-702.

68. **Hickey TE, Majam G, Guerry P.** 2005. Intracellular survival of *Campylobacter jejuni* in human monocytic cells and induction of apoptotic death by cytholethal distending toxin. Infection and immunity **73:**5194-5197.

69. **Hitchcock PJ, Brown TM.** 1983. Morphological heterogeneity among *Salmonella* lipopolysaccharide chemotypes in silver-stained polyacrylamide gels. J Bacteriol **154:**269-277.

70. **Ho N, Kondakova AN, Knirel YA, Creuzenet C.** 2008. The biosynthesis and biological role of 6-deoxyheptose in the lipopolysaccharide O-antigen of *Yersinia pseudotuberculosis*. Molecular microbiology **68:**424-447.

71. **Holst Sorensen MC, van Alphen LB, Fodor C, Crowley SM, Christensen BB, Szymanski CM, Brondsted L.** 2012. Phase variable expression of capsular polysaccharide modifications allows *Campylobacter jejuni* to avoid bacteriophage infection in chickens. Frontiers in cellular and infection microbiology **2:**11.

72. **Houliston RS, Vinogradov E, Dzieciatkowska M, Li J, St Michael F, Karwaski MF, Brochu D, Jarrell HC, Parker CT, Yuki N, Mandrell RE, Gilbert M.** 2011. Lipooligosaccharide of *Campylobacter jejuni*: similarity with multiple types of mammalian glycans beyond gangliosides. The Journal of biological chemistry **286:**12361-12370.

73. **Ica T, Caner V, Istanbullu O, Nguyen HD, Ahmed B, Call DR, Beyenal H.** 2012. Characterization of mono- and mixed-culture *Campylobacter jejuni* biofilms. Applied and environmental microbiology **78:**1033-1038.

74. **Islam D, Ruamsap N, Aksomboon A, Khantapura P, Srijan A, Mason CJ.** 2014. Immune responses to *Campylobacter* (*C. jejuni* or *C. coli*) infections: a two-year study of US forces deployed to Thailand. APMIS : acta pathologica, microbiologica, et immunologica Scandinavica **122:**1102-1113.

75. **Jauncey GE.** 1924. The Scattering of X-Rays and Bragg's Law. Proceedings of the National Academy of Sciences of the United States of America **10:**57-60.

76. **Jin S, Joe A, Lynett J, Hani EK, Sherman P, Chan VL.** 2001. JlpA, a novel surface-exposed lipoprotein specific to *Campylobacter jejuni*, mediates adherence to host epithelial cells. Molecular microbiology **39:**1225-1236.

77. **Jin S, Song YC, Emili A, Sherman PM, Chan VL.** 2003. JlpA of *Campylobacter jejuni* interacts with surface-exposed heat shock protein 90alpha and triggers signalling pathways leading to the activation of NF-kappaB and p38 MAP kinase in epithelial cells. Cellular microbiology **5:**165-174.

78. **Jones MA, Marston KL, Woodall CA, Maskell DJ, Linton D, Karlyshev AV, Dorrell N, Wren BW, Barrow PA.** 2004. Adaptation of *Campylobacter jejuni* NCTC11168 to high-level colonization of the avian gastrointestinal tract. Infection and immunity **72:**3769-3776.

79. **Jornvall H, Persson B, Krook M, Atrian S, Gonzalez-Duarte R, Jeffery J, Ghosh D.** 1995. Short-chain dehydrogenases/reductases (SDR). Biochemistry **34:**6003-6013.

80. **Joshua GW, Guthrie-Irons C, Karlyshev AV, Wren BW.** 2006. Biofilm formation in *Campylobacter jejuni*. Microbiology (Reading, England) **152:**387-396.

81. **Kaakoush NO, Castano-Rodriguez N, Mitchell HM, Man SM.** 2015. Global Epidemiology of *Campylobacter* Infection. **28:**687-720.

82. **Karlyshev AV, Champion OL, Churcher C, Brisson JR, Jarrell HC, Gilbert M, Brochu D, St Michael F, Li J, Wakarchuk WW, Goodhead I, Sanders M, Stevens K, White B, Parkhill J, Wren BW, Szymanski CM.** 2005. Analysis of *Campylobacter jejuni* capsular loci reveals multiple mechanisms for the generation of structural diversity and the ability to form complex heptoses. Molecular microbiology **55:**90-103.

83. **Karlyshev AV, Henderson J, Ketley JM, Wren BW.** 1999. Procedure for the investigation of bacterial genomes: random shot-gun cloning, sample sequencing and mutagenesis of *Campylobacter jejuni*. BioTechniques **26:**50-52, 54, 56.

84. **Karlyshev AV, Linton D, Gregson NA, Lastovica AJ, Wren BW.** 2000. Genetic and biochemical evidence of a *Campylobacter jejuni* capsular polysaccharide that accounts for Penner serotype specificity. Molecular microbiology **35:**529-541.

85. **Keegan VA, Majowicz SE, Pearl DL, Marshall BJ, Sittler N, Knowles L, Wilson JB.** 2009. Epidemiology of enteric disease in C-EnterNet's pilot site - Waterloo region, Ontario, 1990 to 2004. The Canadian journal of infectious diseases & medical microbiology = Journal canadien des maladies infectieuses et de la microbiologie medicale / AMMI Canada **20:**79-87.

86. **Kiehlbauch JA, Albach RA, Baum LL, Chang KP.** 1985. Phagocytosis of *Campylobacter jejuni* and its intracellular survival in mononuclear phagocytes. Infection and immunity **48:**446-451.

87. **Kneidinger B, Graninger M, Puchberger M, Kosma P, Messner P.** 2001. Biosynthesis of nucleotide-activated D-*glycero*-D-*manno*-heptose. The Journal of biological chemistry **276:**20935-20944.

88. **Kneidinger B, Marolda C, Graninger M, Zamyatina A, McArthur F, Kosma P, Valvano MA, Messner P.** 2002. Biosynthesis Pathway of ADP-L-*glycero*- -D-*manno*-Heptose in *Escherichia coli*. Journal of Bacteriology **184:**363-369.

89. **Kokkinidis M, Glykos NM, Fadouloglou VE.** 2012. Protein flexibility and enzymatic catalysis. Advances in protein chemistry and structural biology **87:**181-218.

90. **Konkel ME, Garvis SG, Tipton SL, Anderson DE, Jr., Cieplak W, Jr.** 1997. Identification and molecular cloning of a gene encoding a fibronectin-binding protein (CadF) from *Campylobacter jejuni*. Molecular microbiology **24:**953-963.

91. **Konkel ME, Hayes SF, Joens LA, Cieplak W, Jr.** 1992. Characteristics of the internalization and intracellular survival of *Campylobacter jejuni* in human epithelial cell cultures. Microbial pathogenesis **13:**357-370.

92. **Konkel ME, Kim BJ, Rivera-Amill V, Garvis SG.** 1999. Bacterial secreted proteins are required for the internaliztion of *Campylobacter jejuni* into cultured mammalian cells. Molecular microbiology **32:**691-701.

93. **Konkel ME, Klena JD, Rivera-Amill V, Monteville MR, Biswas D, Raphael B, Mickelson J.** 2004. Secretion of virulence proteins from *Campylobacter jejuni* is dependent on a functional flagellar export apparatus. J Bacteriol **186:**3296-3303.

94. **Konkel ME, Monteville MR, Rivera-Amill V, Joens LA.** 2001. The pathogenesis of *Campylobacter jejuni*-mediated enteritis. Current issues in intestinal microbiology **2:**55-71.

95. **Kosma P, Wugeditsch T, Christian R, Zayni S, Messner P.** 1995. Glycan structure of a heptose-containing S-layer glycoprotein of *Bacillus thermoaerophilus.* Glycobiology **5:**791-796.

96. **Krieger E, Nabuurs SB, Vriend G.** 2003. Homology modeling. Methods of biochemical analysis **44:**509-523.

97. **Krishnan VV, Rupp B.** 2001. Macromolecular Structure Determination: Comparison of X-ray Crystallography and NMR Spectroscopy, eLS. John Wiley & Sons, Ltd.

98. **Lane EM, Batchelor RA, Bourgeois AL, Burr DH, Olson JG.** 1987. Urine and faecal IgA response during naturally acquired infection with *Campylobacter jejuni*. Lancet (London, England) **1:**1141.

99. **Lau ST, Tanner ME.** 2008. Mechanism and active site residues of GDP-fucose synthase. Journal of the American Chemical Society **130:**17593-17602.

100. **Leon-Kempis Mdel R, Guccione E, Mulholland F, Williamson MP, Kelly DJ.** 2006. The *Campylobacter jejuni* PEB1a adhesin is an aspartate/glutamate-binding protein of an ABC transporter essential for microaerobic growth on dicarboxylic amino acids. Molecular microbiology **60:**1262-1275.

101. **Levinson L.** 2008. Review of Medical Microbiology and Immunology., p. 145-146. McGraw-Hill, San Francisco.

102. **Levy AJ.** 1946. A gastro-enteritis cutbreak probably due to a bovine strain of vibrio. The Yale journal of biology and medicine **18:**243-258.

103. **Liu H, Naismith JH.** 2009. A simple and efficient expression and purification system using two newly constructed vectors. Protein expression and purification **63:**102-111.

104. **Lodowska J, Wolny D, Weglarz L, Dzierzewicz Z.** 2007. The structural diversity of lipid A from gram-negative bacteria. Postepy higieny i medycyny doswiadczalnej. **61:**106-121.

105. **Logan SM, Harris LA, Trust TJ.** 1987. Isolation and characterization of *Campylobacter* flagellins. J Bacteriol **169:**5072-5077.

106. **Louwen R, Nieuwenhuis EE, van Marrewijk L, Horst-Kreft D, de Ruiter L, Heikema AP, van Wamel WJ, Wagenaar JA, Endtz HP, Samsom J, van Baarlen P, Akhmanova A, van Belkum A.** 2012. *Campylobacter jejuni* translocation across intestinal epithelial cells is facilitated by ganglioside-like lipooligosaccharide structures. Infection and immunity **80:**3307-3318.

107. **Lugert R, Gross U, Zautner AE.** 2015. *Campylobacter jejuni*: components for adherence to and invasion of eukaryotic cells. Berliner und Munchener tierarztliche Wochenschrift **128:**90-97.

108. **Malmstrom L, Goodlett DR.** 2010. Protein structure modeling. Methods in molecular biology (Clifton, N.J.) **673:**63-72.

109. **Maue AC, Mohawk KL, Giles DK, Poly F, Ewing CP, Jiao Y, Lee G, Ma Z, Monteiro MA, Hill CL, Ferderber JS, Porter CK, Trent MS, Guerry P.** 2013. The polysaccharide capsule of *Campylobacter jejuni* modulates the host immune response. Infection and immunity **81:**665-672.

110. **McCallum M, Shaw GS, Creuzenet C.** 2011. Characterization of the dehydratase WcbK and the reductase WcaG involved in GDP-6-deoxy-*manno*-heptose biosynthesis in *Campylobacter jejuni*. The Biochemical journal **439:**235-248.

111. **McCallum M, Shaw GS, Creuzenet C.** 2013. Comparison of predicted epimerases and reductases of the *Campylobacter jejuni* D-altro- and L-*gluco*-heptose synthesis pathways. The Journal of biological chemistry **288:**19569-19580.

112. **McCallum M, Shaw SD, Shaw GS, Creuzenet C.** 2012. Complete 6-deoxy-D-*altro*-heptose biosynthesis pathway from *Campylobacter jejuni*: more complex than anticipated. The Journal of biological chemistry **287:**29776-29788.

113. **McFadyean J, Stockman. S.** 1913. Report of the Departmental Committee appointed by the Board of Agriculture and Fisheries to inquire into Epizootic Abortion. III. Abortion in Sheep. London **HMSO**.

114. **McNally DJ, Jarrell HC, Khieu NH, Li J, Vinogradov E, Whitfield DM, Szymanski CM, Brisson JR.** 2006. The HS:19 serostrain of *Campylobacter jejuni* has a hyaluronic acid-type capsular polysaccharide with a nonstoichiometric sorbose branch and O-methyl phosphoramidate group. The FEBS journal **273:**3975-3989.

115. **McNally DJ, Jarrell HC, Li J, Khieu NH, Vinogradov E, Szymanski CM, Brisson JR.** 2005. The HS:1 serostrain of *Campylobacter jejuni* has a complex teichoic acid-like capsular polysaccharide with nonstoichiometric fructofuranose branches and O-methyl phosphoramidate groups. The FEBS journal **272:**4407-4422.

116. **McNally DJ, Lamoureux MP, Karlyshev AV, Fiori LM, Li J, Thacker G, Coleman RA, Khieu NH, Wren BW, Brisson JR, Jarrell HC, Szymanski CM.** 2007. Commonality and biosynthesis of the O-methyl phosphoramidate capsule modification in *Campylobacter jejuni.* The Journal of biological chemistry **282:**28566-28576.

117. **McRee DE.** 1999. Practical Protein Crystallography. Elsevier Science.

118. **Melo A, Glaser L.** 1968. The mechanism of 6-deoxyhexose synthesis. II. Conversion of deoxythymidine diphosphate 4-keto-6-deoxy-D-glucose to deoxythymidine diphosphate L-rhamnose. The Journal of biological chemistry **243:**1475-1478.

119. **Messner P, Bock K, Christian R, Schulz G, Sleytr UB.** 1990. Characterization of the surface layer glycoprotein of *Clostridium symbiosum* HB25. J Bacteriol **172:**2576-2583.

120. **Messner P, Sleytr UB.** 1988. Asparaginyl-rhamnose: a novel type of protein-carbohydrate linkage in a eubacterial surface-layer glycoprotein. FEBS letters **228:**317-320.

121. **Moens S, Vanderleyden J.** 1997. Glycoproteins in prokaryotes. Archives of microbiology **168:**169-175.

122. **Monteville MR, Yoon JE, Konkel ME.** 2003. Maximal adherence and invasion of INT 407 cells by *Campylobacter jejuni* requires the CadF outer-membrane protein and microfilament reorganization. Microbiology (Reading, England) **149:**153-165.

123. **Moran AP.** 1997. Structure and conserved characteristics of *Campylobacter jejuni* lipopolysaccharides. The Journal of infectious diseases. **2:**S115-121.

124. **Moran AP, Prendergast MM.** 2001. Molecular mimicry in *Campylobacter jejuni* and *Helicobacter pylori* lipopolysaccharides: contribution of gastrointestinal infections to autoimmunity. Journal of autoimmunity **16:**241-256.

125. **Moran AP, Prendergast MM, Appelmelk BJ.** 1996. Molecular mimicry of host structures by bacterial lipopolysaccharides and its contribution to disease. FEMS immunology and medical microbiology **16:**105-115.

126. **Moran AP, Rietschel ET, Kosunen TU, Zahringer U.** 1991. Chemical characterization of *Campylobacter jejuni* lipopolysaccharides containing N-acetylneuraminic acid and 2,3-diamino-2,3-dideoxy-D-glucose. J Bacteriol **173:**618-626.

127. **Muller A, Thomas GH, Horler R, Brannigan JA, Blagova E, Levdikov VM, Fogg MJ, Wilson KS, Wilkinson AJ.** 2005. An ATP-binding cassette-type cysteine transporter in *Campylobacter jejuni* inferred from the structure of an extracytoplasmic solute receptor protein. Molecular microbiology **57:**143-155.

128. **Myszewski MA, Stern NJ.** 1991. Phagocytosis and intracellular killing of *Campylobacter jejuni* by elicited chicken peritoneal macrophages. Avian diseases **35:**750-755.

129. **Nachamkin I, Hart AM.** 1985. Western blot analysis of the human antibody response to *Campylobacter jejuni* cellular antigens during gastrointestinal infection. Journal of clinical microbiology **21:**33-38.

130. **Novik V, Hofreuter D, Galan JE.** 2010. Identification of *Campylobacter jejuni* genes involved in its interaction with epithelial cells. Infection and immunity **78:**3540-3553.

131. **Nsahlai CJ, Silver RP.** 2003. Purification and characterization of KpsT, the ATP-binding component of the ABC-capsule exporter of *Escherichia coli* K1. FEMS Microbiol Lett **224:**113-118.

132. **Oliver JD.** 2005. The viable but nonculturable state in bacteria. Journal of microbiology (Seoul, Korea) **43 Spec No:**93-100.

133. **Olofsson J, Axelsson-Olsson D, Brudin L, Olsen B, Ellstrom P.** 2013. *Campylobacter jejuni* actively invades the amoeba *Acanthamoeba polyphaga* and survives within non digestive vacuoles. PloS one **8:**e78873.

134. **Palyada K, Threadgill D, Stintzi A.** 2004. Iron acquisition and regulation in *Campylobacter jejuni*. J Bacteriol **186:**4714-4729.

135. **Parkhill J, Wren BW, Mungall K, Ketley JM, Churcher C, Basham D, Chillingworth T, Davies RM, Feltwell T, Holroyd S, Jagels K, Karlyshev AV, Moule S, Pallen MJ, Penn CW, Quail MA, Rajandream MA, Rutherford KM, van Vliet AH, Whitehead S, Barrell BG.** 2000. The genome sequence of the food-borne pathogen *Campylobacter jejuni* reveals hypervariable sequences. Nature **403:**665-668.

136. **Parois P, Cooper RI, Thompson AL.** 2015. Crystal structures of increasingly large molecules: meeting the challenges with CRYSTALS software. Chemistry Central journal **9:**30.

137. **Pei Z, Burucoa C, Grignon B, Baqar S, Huang XZ, Kopecko DJ, Bourgeois AL, Fauchere JL, Blaser MJ.** 1998. Mutation in the peb1A locus of *Campylobacter jejuni* reduces interactions with epithelial cells and intestinal colonization of mice. Infection and immunity **66:**938-943.

138. **Petsko GA, Kenyon GL, Gerlt JA, Ringe D, Kozarich JW.** 1993. On the origin of enzymatic species. Trends in biochemical sciences **18:**372-376.

139. **Pigeon RP, Silver RP.** 1994. Topological and mutational analysis of KpsM, the hydrophobic component of the ABC-transporter involved in the export of polysialic acid in *Escherichia coli* K1. Molecular microbiology **14:**871-881.

140. **Preston A, Mandrell RE, Gibson BW, Apicella MA.** 1996. The lipooligosaccharides of pathogenic gram-negative bacteria. Critical reviews in microbiology **22:**139-180.

141. **Preston MA, Penner JL.** 1987. Structural and antigenic properties of lipopolysaccharides from serotype reference strains of *Campylobacter jejuni*. Infection and immunity **55:**1806-1812.

142. **Raetz CRH, Guan Z, Ingram BO, Six DA, Song F, Wang X, Zhao J.** 2009. Discovery of new biosynthetic pathways: the lipid A story. Journal of Lipid Research **50:**S103-108.

143. **Rahim R, Burrows LL, Monteiro MA, Perry MB, Lam JS.** 2000. Involvement of the rml locus in core oligosaccharide and O polysaccharide assembly in *Pseudomonas aeruginosa*. Microbiology (Reading, England) **146 (Pt 11):**2803-2814.

144. **Reckseidler SL, DeShazer D, Sokol PA, Woods DE.** 2001. Detection of bacterial virulence genes by subtractive hybridization: identification of capsular polysaccharide of *Burkholderia pseudomallei* as a major virulence determinant. Infection and immunity **69:**34-44.

145. **Reeser RJ, Medler RT, Billington SJ, Jost BH, Joens LA.** 2007. Characterization of *Campylobacter jejuni* biofilms under defined growth conditions. Applied and environmental microbiology **73:**1908-1913.

146. **Reuter M, Mallett A, Pearson BM, van Vliet AH.** 2010. Biofilm formation by *Campylobacter jejuni* is increased under aerobic conditions. Applied and environmental microbiology **76:**2122-2128.

147. **Rigg GP, Barrett B, Roberts IS.** 1998. The localization of KpsC, S and T, and KfiA, C and D proteins involved in the biosynthesis of the *Escherichia coli* K5 capsular polysaccharide: evidence for a membrane-bound complex. Microbiology **144:**2905-2914.

148. **Roberts IS.** 1996. The biochemistry and genetics of capsular polysaccharide production in bacteria. Annual review of microbiology **50:**285-315.

149. **Robinson DA, Jones DM.** 1981. Milk-borne campylobacter infection. British medical journal. **282:**1374-1376.

150. **Salloway S, Mermel LA, Seamans M, Aspinall GO, Nam Shin JE, Kurjanczyk LA, Penner JL.** 1996. Miller-Fisher syndrome associated with *Campylobacter jejuni* bearing lipopolysaccharide molecules that mimic human ganglioside GD3. Infection and immunity **64:**2945-2949.

151. **Samuelsson K, Lindberg B, Brubaker RR.** 1974. Structure of O-specific side chains of lipopolysaccharides from *Yersinia pseudotuberculosis*. J Bacteriol **117:**1010-1016.

152. **Sandstrom G, Saeed A, Abd H.** 2011. *Acanthamoeba*-bacteria: a model to study host interaction with human pathogens. Current drug targets **12:**936-941.

153. **Sebald M, Veron M.** 1963. Base dna content and classification of *vibrios*. Annales de l'Institut Pasteur **105:**897-910.

154. **Siegesmund AM, Konkel ME, Klena JD, Mixter PF.** 2004. *Campylobacter jejuni* infection of differentiated THP-1 macrophages results in interleukin 1 beta release and caspase-1-independent apoptosis. Microbiology **150:**561-569.

155. **Smith T, Taylor MS.** 1919. Some morphological and biological characters of the spirilla (*vibrio fetus*, n. sp.) associated with disease of the fetal membranes in cattle. The Journal of experimental medicine **30:**299-311.

156. **Smyth MS, Martin JHJ.** 2000. x Ray crystallography. Molecular Pathology **53:**8-14.

157. **Somers WS, Stahl ML, Sullivan FX.** 1998. GDP-fucose synthetase from *Escherichia coli*: structure of a unique member of the short-chain dehydrogenase/reductase family that catalyzes two distinct reactions at the same active site. Structure **6:**1601-1612.

158. **Somoza JR, Menon S, Schmidt H, Joseph-McCarthy D, Dessen A, Stahl ML, Somers WS, Sullivan FX.** 2000. Structural and kinetic analysis of *Escherichia coli* GDP-mannose 4,6 dehydratase provides insights into the enzyme's catalytic mechanism and regulation by GDP-fucose. Structure **8:**123-135.

159. **Spek AL.** 2009. Structure validation in chemical crystallography. Acta crystallographica. Section D, Biological crystallography **65:**148-155.

160. **St Michael F, Szymanski CM, Li J, Chan KH, Khieu NH, Larocque S, Wakarchuk WW, Brisson JR, Monteiro MA.** 2002. The structures of the lipooligosaccharide and capsule polysaccharide of *Campylobacter jejuni* genome sequenced strain NCTC 11168. European journal of biochemistry / FEBS **269:**5119-5136.

161. **Stahl M, Butcher J, Stintzi A.** 2012. Nutrient acquisition and metabolism by *Campylobacter jejuni.* Frontiers in cellular and infection microbiology **2:**5.

162. **Steenbergen SM, Vimr ER.** 2008. Biosynthesis of the *Escherichia coli* K1 group 2 polysialic acid capsule occurs within a protected cytoplasmic compartment. Molecular microbiology **68:**1252-1267.

163. **Stern RJ, Lee TY, Lee TJ, Yan W, Scherman MS, Vissa VD, Kim SK, Wanner BL, McNeil MR.** 1999. Conversion of dTDP-4-keto-6-deoxyglucose to free dTDP-4-keto-rhamnose by the rmlC gene products of *Escherichia coli* and *Mycobacterium tuberculosis*. Microbiology (Reading, England) **145 (Pt 3):**663-671.

164. **Sternberg MJ, Tamaddoni-Nezhad A, Lesk VI, Kay E, Hitchen PG, Cootes A, van Alphen LB, Lamoureux MP, Jarrell HC, Rawlings CJ, Soo EC, Szymanski CM, Dell A, Wren BW, Muggleton SH.** 2013. Gene function hypotheses for the *Campylobacter jejuni* glycome generated by a logic-based approach. Journal of molecular biology **425:**186-197.

165. **Szymanski CM, Burr DH, Guerry P.** 2002. *Campylobacter* protein glycosylation affects host cell interactions. Infection and immunity **70:**2242-2244.

166. **Szymanski CM, Logan SM, Linton D, Wren BW.** 2003. *Campylobacter*, a tale of two protein glycosylation systems. Trends in microbiology **11:**233-238.

167. **Szymanski CM, Michael FS, Jarrell HC, Li J, Gilbert M, Larocque S, Vinogradov E, Brisson JR.** 2003. Detection of conserved N-linked glycans and phase-variable lipooligosaccharides and capsules from *campylobacter* cells by mass spectrometry and high resolution magic angle spinning NMR spectroscopy. The Journal of biological chemistry **278:**24509-24520.

168. **Szymanski CM, Wren BW.** 2005. Protein glycosylation in bacterial mucosal pathogens. Nature reviews. Microbiology **3:**225-237.

169. **Szymanski CM, Yao R, Ewing CP, Trust TJ, Guerry P.** 1999. Evidence for a system of general protein glycosylation in *Campylobacter jejuni.* Molecular microbiology **32:**1022-1030.

170. **Taylor CM, Roberts IS.** 2005. Capsular polysaccharides and their role in virulence. Contributions to microbiology **12:**55-66.

171. **Taylor DN, Echeverria P, Pitarangsi C, Seriwatana J, Bodhidatta L, Blaser MJ.** 1988. Influence of strain characteristics and immunity on the epidemiology of *Campylobacter* infections in Thailand. Journal of clinical microbiology **26:**863-868.

172. **Tracz DM, Keelan M, Ahmed-Bentley J, Gibreel A, Kowalewska-Grochowska K, Taylor DE.** 2005. pVir and bloody diarrhea in *Campylobacter jejuni* enteritis. Emerging infectious diseases **11:**838-843.

173. **Tsukioka Y, Yamashita Y, Oho T, Nakano Y, Koga T.** 1997. Biological function of the dTDP-rhamnose synthesis pathway in *Streptococcus mutans*. J Bacteriol **179:**1126-1134.

174. **Turk D.** 2013. MAIN software for density averaging, model building, structure refinement and validation. Acta crystallographica. Section D, Biological crystallography **69:**1342-1357.

175. **Valvano MA, Messner P, Kosma P.** 2002. Novel pathways for biosynthesis of nucleotide-activated glycero-manno-heptose precursors of bacterial glycoproteins and cell surface polysaccharides. Microbiology **148:**1979-1989.

176. **Vieira A, Seddon AM, Karlyshev AV.** 2015. *Campylobacter-Acanthamoeba* interactions. Microbiology (Reading, England) **161:**933-947.

177. **Vinzio S, Andres E, Goichot B, Schlienger JL.** 2000. Guillain-Barre syndrome and *Mycoplasma pneumoniae* infection. Annales de medecine interne **151:**309-310.

178. **Wang H, Wilksch JJ, Strugnell RA, Gee ML.** 2015. Role of Capsular Polysaccharides in Biofilm Formation: An AFM Nanomechanics Study. ACS Applied Materials & Interfaces **7:**13007-13013.

179. **Wassenaar TM, Blaser MJ.** 1999. Pathophysiology of *Campylobacter jejuni* infections of humans. Microbes and infection / Institut Pasteur **1:**1023-1033.

180. **Weng YZ, Chang DT, Huang YF, Lin CW.** 2011. A study on the flexibility of enzyme active sites. BMC bioinformatics. **1:**S32.

181. **Whitfield C, Roberts IS.** 1999. Structure, assembly and regulation of expression of capsules in *Escherichia coli*. Molecular microbiology **31:**1307-1319.

182. **Whitfield C, Valvano MA.** 1993. Biosynthesis and expression of cell-surface polysaccharides in gram-negative bacteria. Advances in microbial physiology **35:**135-246.

183. **Willis LM, Whitfield C.** 2013. KpsC and KpsS are retaining 3-deoxy-D-manno-oct-2-ulosonic acid (Kdo) transferases involved in synthesis of bacterial capsules. Proceedings of the National Academy of Sciences of the United States of America **110:**20753-20758.

184. **Wong A, Lange D, Houle S, Arbatsky NP, Valvano MA, Knirel YA, Dozois CM, Creuzenet C.** 2015. Role of capsular modified heptose in the virulence of *Campylobacter jejuni.* Molecular microbiology.

185. **Wosten MM, Wagenaar JA, van Putten JP.** 2004. The FlgS/FlgR two-component signal transduction system regulates the fla regulon in *Campylobacter jejuni.* The Journal of biological chemistry **279:**16214-16222.

186. **Xiang Z.** 2006. Advances in homology protein structure modeling. Current protein & peptide science **7:**217-227.

187. **Young KT, Davis LM, Dirita VJ.** 2007. *Campylobacter jejuni*: molecular biology and pathogenesis. Nature reviews. Microbiology **5:**665-679.

188. **Yuki N, Susuki K, Koga M, Nishimoto Y, Odaka M, Hirata K, Taguchi K, Miyatake T, Furukawa K, Kobata T, Yamada M.** 2004. Carbohydrate mimicry between human ganglioside GM1 and *Campylobacter jejuni* lipooligosaccharide causes Guillain-Barre syndrome. Proceedings of the National Academy of Sciences of the United States of America **101:**11404-11409.

189. **Zhu J, Meinersmann RJ, Hiett KL, Evans DL.** 1999. Apoptotic effect of outer-membrane proteins from *Campylobacter jejuni* on chicken lymphocytes. Current microbiology **38:**244-249.

190. **Zilbauer M, Dorrell N, Boughan PK, Harris A, Wren BW, Klein NJ, Bajaj-Elliott M.** 2005. Intestinal innate immunity to *Campylobacter jejuni* results in induction of bactericidal human beta-defensins 2 and 3. Infection and immunity **73:**7281-7289.

191. **Zvelebil MJ, Sternberg MJ.** 1988. Analysis and prediction of the location of catalytic residues in enzymes. Protein engineering **2:**127-138.

APPENDICES

Appendix 1: Subcloning primers

Primer name	Sequence (5' – 3')
MlghB P2	AGGGTC**CATGG**CAATAGAATTTGATATA
MlghB P3	GCGTCG**GATCC**TTATCCTTTATTTTTAGTTGCAA
DdahB P2	GCT**GGATCC**TTATCCTTTATTTTTAGTTGCT
DdahB P3	CTCA**CATGT**CCATGGCAATAGAATTTAATATAC

Restriction sites are in **bold** and underlined

Appendix 2: SDM primers

Gene	Mutation	Primers Sequence (5' – 3')
	Epimerases	
DdahB	Asn121Ser*	**F:**GTGCCAGCAGGTTTTGGAA**AG**CGCTCATTATGTT ACT AGTG **R:**CACTAGTAACATAATGAGC**GCT**TCCAAAACCT GCTG GCAC
	His67Ala	**F:**CAATGTTATTCGCGGTATC**GCT**GGTGATGTAAA AA CTTATAAGCTTG **R:**CAAGCTTATAAGTTTTTACATCACCA**GC**GATAC CG CGAATAACATTG
	His67Asn	**F:**CAATGTTATTCGCGGTATC**A**A**T**GGTGATGTAAA AAC TTATAAGCTTG **R:**CAAGCTTATAAGTTTTTACATCACC**ATT**GATAC CGC GAATAACATTG
	Lys74Ala	**F:**CCATGGCGATGTAAAAACTTAT**GC**G**C**TTGCAAC TTG TGTTTATGG **R:**CATAAACACAAGTTGCAAG**C**GC**C**ATAAGTTTTT ACAT CGCCATGG
MlghB	Asn121Ser*	**F:**ATTACCACCAAATATGGGAA**AG**CTCTCATTATGT GAG TTCAAAG **R:**CTTTGAACTCACATAATGAGA**GCT**TCCCATATT TGGT GGTAAT
	His67Ala*	**F:**CCCATTTTAATGTTTTACGTGGAATA**GC**CGGAG ATGT GAAAACTTAC **R:**GTAAGTTTTCACATCTCCG**GCT**ATTCCACGTAA AACA TTAAAATGGG
	His67Asn	**F:**CCCATTTTAATGTTTTACGTGG**A**A**T**AAACGGAG ATG TGAAAACTTAC **R:**GTAAGTTTTCACATCTCCGTTT**ATT**CCACGTAA AACA TTAAAATGGG
	Tyr134Phe*	**F:**CAAAGGAAGCAGTGTATTAT**TT**T**T**AAACTTGCTT ATGA GGGG **R:**CCCCTCATAAGCAAGTTTA**A**A**A**ATAATACACTGC TTCC TTTG
	Tyr132Phe**	**F:**GAGTTCAAAGGAAGCAGTG**TT**T**T**TATTATAAACT TGCTTATG **R:** CATAAGCAAGTTTATAATA**A**A**A**CACTGCTTCC TTTGAACTC

	Lys74Ala	**F:**CACGGAGATGTGAAAACTTA**C<u>GC</u>**ACTTGTAACT TGTG TCTATGGAG **R:**CTCCATAGACACAAGTTACAAGT**<u>GC</u>G**TAAGTTT TCAC ATCTCCGTG
Reductases		
DdahC	His180Arg*	**F:**GACAAATTTGATCTTGAAAAATCT**C<u>G</u>T**GTATTG CCTGG AATTTTA AGAAA AATG **R:**CATTTTTCTTAAAATTCCAGGCAATACA**<u>C</u>G**AGA TTTTT CAAGATCAAA TTTGTC
	Thr110Tyr	**F:**GCTACTTTTCATAGCTTCAACT**<u>TA</u>C**GTTTATCCT AAAA ATGCAACATTG **R:**CAATGTTGCATTTTTAGGATAAAC**G<u>TA</u>**AGTTGA AGCT ATGAAAAGTA GC
	His180Arg/ Thr110Tyr*	Both His180Arg and Thr110Tyr
	Thr110Cys*	**F:**CTACTTTTTTCATAGCTTCAACT**<u>TG</u>C**GTTTAT CCTAA AAATGCAAC ATTG **R:**CAATGTTGCATTTTTAGGATAAAC**G<u>CA</u>**AGTTGA AGC TATGAAAA AAGTAG
MlghC	Cys68Ala*	**F:**GACTGCAGTCTTACCT**<u>GC</u>T**GGTGCTGCAAATGT CG **R:**CGACATTTGCAGCACCA**<u>GC</u>**AGGTAAGACTGCA GTC

*SDM done by Michael Roubakha, 2013

** SDM done by Chelsea Kubinec, 2015

F and **R** indicate forward and reverse primer respectively.

Mutated residues codons are in **bold,** and the mutated nucleotides are <u>underlined.</u>

Appendix 3: Antibodies used for Western blot

Primary antibody and dilution*	Epitope detected	Secondary antibody	Wavelength detected (nm)
Monoclonal anti-His (mouse), 1:5000	His_6 Tag	Anti-mouse (goat) 1:5000	700
Monoclonal anti-GST (rabbit), 1:3000	GST Tag	Anti-rabbit (goat) 1:2000	800

* Dilution was made in 1× PBS buffer and 0.05 % sodium azide.

Appendix 4: Integration data of the CE electropherograms for the epimerases activity on GDP-*manno*-heptose:

The table shows the means of three independent experiments (Figure 21-A2,B2). The products are represented by their order of appearance in the CE electropherograms. The data represent the area of each peak in percentage to the total area of the sugar nucleotides. The impurity and NADP+ peaks were excluded from the integration.

Enzyme	**P4γ**	**P1**	**P4β**	**P4α**
	(Percentage %)			
DdahB H67N	0.0	88.8	0.0	11.2
DdahB H67A	0.0	90.0	0.0	10.0
DdahB N121S	0.0	70.6	0.0	29.4
DdahB WT	0.0	63.7	0.0	36.3
DdahA	0.0	100.0	0.0	0.0
	(Percentage %)			
MlghB Y134F	13.0	74.4	6.4	8.3
MlghB H67N	0.0	93.1	0.0	6.9
MlghB H67A	0.0	89.2	0.0	10.8
MlghB N121S	25.0	35.7	29.0	20.0
MlghB WT	22.2	28.8	25.6	31.9
DdahA	0.0	100.0	0.0	0.0

Appendix 5: Integration data of the CE electropherograms for the epimerases activity on GDP-mannose:

The table shows the means of two independent experiments (Figure 23-B2). The products are represented by their order of appearance in the CE electropherograms. The data represent the area of each peak in percentage to the total area of the sugar nucleotides. The GDP-mannose peak was excluded from the integration.

Enzyme	**P4'**	**P1'**
	(Percentage %)	
DdahB H67N	0.0	100
DdahB H67A	0.0	100
DdahB N121S	0.0	100
DdahB WT	6.5	93.5
	(Percentage %)	
MlghB Y134F	10.1	89.9
MlghB H67N	0.0	100.0
MlghB H67A	0.0	100.0
MlghB N121S	43.0	57.0
MlghB WT	42.2	57.9

Appendix 6: Integration data for CE electropherograms shown in Figure 25

The traces and are represented in their order in the figure. The peaks are represented by their order of appearance in the CE electropherograms. For **panel A**, the dada represent the area of each peak in percentage to the total area of the sugar nucleotides. P4β peak was excluded from the integration because of the poor resolution from $NADP^+$. The impurity peak was also excluded. For **panel B**, the data for the substrates and the products peaks areas are represented in ratio to the impurity peak area (annotated as *), assuming that all traces has the same amount of the impurity. The peak of $NADP^+$ and the co-migrated P4β were included in the integration. This was done in order to evaluate the changes in the substrate specificity of the mutants. MlghB reaction trace could not be used as a control. Instead, the inactive DdahC H180R/T110Y mutant was used as a virtual control.

Trace	**Enzyme**	**P5γ**	**P4γ**	**P1**	**P5α**	**P4α**		
Panel A		(Percentage %)						
g	MlghC C68A	56.7	9.3	17.5	0.0	16.4		
f	MlghC WT	63.4	4.9	13.2	0.0	18.4		
e	DdahC H180R/T110Y	0.0	25.9	34.5	0.0	39.6		
d	DdahC H180R	0.0	21.7	24.2	35.4	18.7		
c	DdahC T110C	0.0	17.2	20.1	46.0	16.7		
b	DdahC WT	0.0	23.2	24.2	31.1	21.5		
Trace	**Enzyme**	**P5γ**	**P4γ**	**P1**	**P5α**	**$NADP^+$ P4β**	**P4α**	*****
Panel B		(Ratio to *)						
g	MlghC C68A	0.45	0.95	1.61	0.00	2.28	0.38	1.00
f	MlghC WT	0.87	0.62	1.50	0.00	2.61	0.41	1.00
e	DdahC H180R/T110Y	0.00	1.22	1.48	0.00	0.97	0.44	1.00
d	DdahC H180R	0.00	1.21	1.46	0.08	1.44	0.34	1.00
c	DdahC T110C	0.00	1.25	1.38	0.33	1.78	0.26	1.00
b	DdahC WT	0.00	1.37	1.69	0.16	1.12	0.36	1.00

HEBA BARNAWI

EDUCATION:

2013 – Present

M. Sc. Candidate
Department of Microbiology and Immunology, University of Western Ontario.
Thesis: Structural and functional studies of the heptose modifying enzymes that play a role in *Campylobacter jejuni* virulence.
Supervisor: Dr. Carole Creuzenet

2007 – 2010
Honours Bachelor of Science in Medical Laboratory Technology
Department of Applied Medical Sciences, King Abdul-Aziz University, Jeddah, Saudi Arabia.

2011 – 2012
Undergraduate courses and ESL program
Department of Microbiology and Immunology, University of Ottawa.
Language institute in Algonquin Collage, Ottawa.

SCHOLARSHIP:

The Saudi Arabian Ministry of Higher education scholarship, Department of Applied Medical Sciences, University of Hail, Saudi Arabia. 2010 – Present

RELATED FIELD EXPERIENCE:

Poster presentations:

Barnawi H, Michael Roubakha, Chelsea Kubinec, and Carole Creuzenet
Catalytic studies of *Campylobacter jejuni's* heptose modifying enzymes and their role in biofilm formation. Infection and immunity research forum. University of Western Ontario, London, ON. October 2015

Barnawi H, Michael Roubakha, Chelsea Kubinec, and Carole Creuzenet
Structural and catalytic studies of the heptose modifying enzymes that play a role in *Campylobacter jejuni* virulence. London health research day, London, ON. April 2015

Barnawi H, Michael Roubakha, Chelsea Kubinec, and Carole Creuzenet
Structural and catalytic studies of the heptose modifying enzymes that play a role in *Campylobacter jejuni* virulence. Infection and immunity research forum. University of Western Ontario, London, ON. October 2014

Barnawi H, Michael Roubakha, and Carole Creuzenet
Heptose modifying enzymes play a role in *Campylobacter jejuni* virulence. London health research day, London, ON. March 2014

Barnawi H, Rafea Alqasmy and Zahira Fathi
The bacterial contamination of the hospital laboratory worker compared to the non-hospital worker. The seventh Applied Medical Sciences Students Annual Meeting, King Abdul-Aziz University, Jeddah, Saudi Arabia

RESEARCH EXPERIENCE

M.Sc. Candidate

Supervisor: Dr. Carole Creuzenet

Structural and functional studies of the heptose modifying enzymes that play a role in *Campylobacter jejuni* virulence.

- Setting up and developing enzymatic reactions and performing kinetic studies.
- Experience in capillary electrophoresis for the analysis of sugar nucleotides detection to monitor enzymatic reactions.
- Structural modeling and structure analysis using PyMol
- Large-scale synthesis of sugar-nucleotide substrates enzymatically.
- Using the HPLC-PAD (with assistance).
- Site-directed mutagenesis, primer design, and molecular cloning.
- Protein expression and analysis by Western blotting, Coomassie Blue staining, Ponceau staining, and Bradford Protein Assays.
- Protein purification using manual and automated techniques of affinity chromatography purification.
- Experience using the ÄKTApurifier for protein purification.
- SDS-PAGE analysis of protein and capsular polysaccharide
- Microaerobic growth techniques (liquid and plates).
- Biofilm formation assay.

2009 – 2010

Fourth Year Honours Project (Department of Applied Medical Sciences, King Abdul-Aziz University, Jeddah, Saudi Arabia)

Supervisor: Zahira Fathi

The bacterial contamination of the hospital laboratory worker compared to the non-hospital worker.

- Aerobic growth techniques (liquid and plates)
- Colony forming unit counting.
- Research subjects' samples and data collection.

TRAINING EXPERIANCE

2010 – 2011

Undergraduate Internship

Microbiology Laboratory, King Abdul-Aziz University Hospital, Jeddah, Saudi Arabia.

- Diagnosis of patients' bacterial culture of body fluids samples.
- Preparing different media for culturing patients' samples.
- Body fluids samples collection and preanalytical processing.

Hematology Laboratory, King Fahad Armed Forces Hospital, Jeddah, Saudi Arabia.

- Diagnosis of patients blood films using light microscopy.
- Using flow cytometry for complete blood count.
- Collecting blood and body fluids samples.

Genomic medicine Unit, Center of Excellence In Genomic Medicine Research, King Fahad Research Center, Jeddah, Saudi Arabia.

- DNA and RNA extraction from peripheral blood, PCR analysis, and gel electrophoresis
- Chromosome extraction and karyotype analysis

SUPERVISORY EXPERIENCE

6/2011 – 12/2011

Teaching Assistant

Medical Laboratory, Department of Applied Medical Sciences, University of Hail, Saudi Arabia.

- Overseeing laboratory periods.
- Tutoring in the tutorial sessions.
- Putting exams' multiple-choice questions and correcting answers.